**Defense & Security** Oude Waalsdorperweg 63 2597 AK The Hague P.O. Box 96864
2509 JG The Hague

www.tno.nl

T +31 88 866 10 00

**TNO report**

**TNO 2021 R10471**

# Effect of the Whiswall at long range: simulations with FEM-PE and a calculation rule for SRM2

| | |
|---|---|
| Date | May 2022 |
| Author(s). | Erik Salomons<br>Sandra Blaak<br>Rafal Kurylek<br>Frits van der Eerden<br>Tessel van der Laan<br>Ad van Heijningen |
| Number of pages | 100 (including appendices) |
| Number of appendices | 6 |
| Clients | Rijkswaterstaat, ProRail, RIVM |
| Project name | Whiswall phases 4-6 |
| Project numbers | 060.46488, 060.46489, 060.46491, 060.49105 |

# Summary

This report describes calculations of noise reduction by a Whiswall along a traffic road or railroad line. A Whiswall consists of a diffractor on a noise barrier, with which in principle a greater noise reduction can be than with an equally high noise barrier without diffractor. This study concerns the extra noise reduction provided by the diffractor, in addition to the 'normal' screen effect provided by the noise barrier.

The numerical simulation method FEM-PE was used for the calculations. This is a hybrid calculation method, using FEM for the noise field near the Whiswall and PE for the noise propagation to long distances, up to a maximum of 600 m in this case. The FEM model has been validated in previous studies based on measurements in situations with a Whiswall along a traffic road and a railroad line. Calculations with FEM-PE were performed in this for 42 different situations, varying source position, screen height, and soil type, among others.

Based on the results of the calculations with FEM-PE, a calculation rule was developed with which the noise reduction by the diffractor can be determined. The calculation rule is suitable for addition to calculation method SRM2 from the Dutch calculation and measurement regulations for road and rail traffic noise. The calculation rule is based on the results of FEM-PE and also on measured 'product properties' of the Whiswall.

For 8 of the 42 situations, the calculations were repeated with an alternative diffractor, which provides better noise reduction of low-frequency components of traffic noise. The developed calculation rule was tested against these new results. It was also investigated whether the calculation rule could be further optimized.

# Table of contents

# 1 In leadership

A diffractor is a noise-reducing object that can be used to reduce noise from road and rail traffic. The noise reduction results from the resonant action of trenches with different depths in the diffractor. In recent studies, measurements and calculations were performed on a diffractor in the verge of a road (see Figure 1.1 [1]. Based on the results, TNO developed a calculation rule [2] that has since been added to the RMG [3]. The diffractor in the verge is referred to by the commercial name *Whisstone*[4].

Figure 1.1 Illustration of a diffractor on the shoulder of a road (Whisstone).

A diffractor can also be placed on top of a noise barrier along a road or rail line (see Figure 1.2). The diffractor is expected to increase the screen effect. The combination of diffractor and noise barrier is referred to by the commercial name Whis *wall*[5].

Figure 1.2 Illustration of a diffractor on a screen along a road (Whiswall).

Commissioned by Rijkswaterstaat, ProRail and RIVM, a calculation rule is also being developed for the effect of the Whiswall diffractor, which can be added to the RMG. For this purpose, a study has been set up, consisting of the following six phases.

**Phase 1**. Conducting noise measurements at the Whiswall, with two measurement setups:

- A setup to determine the "product properties "[6] (diffraction test),
- An arrangement along a traffic road.

[1] F. van der Eerden, E. Brouns, B. Binnerts, A. Eisses, A. Kruyen, "Development of computational rule diffractor phase 1," TNO Report R10198, March 2018.
[2] F. van der Eerden, E. Brouns, A. Eisses, "Development of computational rule diffractor phase 2," TNO Report R11565, March 2019.
[3] Noise Calculation and Measurement Regulations 2012 (RMG2012), Government Gazette No. 11810, June 27, 2012.
[4] The Whisstone was developed by the company 4Silence, in collaboration with the University of Twente. See www.4silence.com/whisstone/.
[5] The Whiswall was developed by the company 4Silence, in collaboration with the University of Twente. See www.4silence.com/whiswall/.
[6] By product properties here is meant a representative spectrum of noise reduction by "the product" (the diffractor in this ), averaged over different positions of the noise source and observer relative to "the product.

**Phase 2**. A comparison of measurement results from Phase 1 with results of calculations with a numerical model.

**Stage 3**. A comparison of results from measurements along a railroad line with results from calculations with a numerical model.

**Phase 4**. Calculating the effect of the Whiswall for road and rail traffic noise with a numerical model, for different geometries with distances up to 600 m.

**Phase 5**. The development of a computational rule for the effect of the Whiswall diffractor suitable for the RMG for road and rail traffic noise.

**Phase 6**. Further analysis of the computational rule, including testing against results for An alternative diffractor that is more tuned to low frequencies ("LF diffractor").

This report describes the results of phases 4, 5 and 6. The results of phase 2 (road traffic) and phase 3 (rail traffic) are described in previous reports and [7,8].

The calculations in phases 2 and 3 were performed with a FEM [model9]. This involved the effect of the Whiswall diffractor at small distances, up to a maximum of 25 m. For road traffic, good agreement was found between measurement and calculation results. For rail traffic, the agreement was good for 7.5 m distances and less good for 15 and 25 m. The latter was attributed to an underestimation of the effect of the diffractor in the measurements.

In the study described here, calculations were performed of the effect of the Whiswall at greater distances, up to a maximum of 600 m behind the screen. The calculations were performed with the hybrid calculation model FEM-PE, using FEM up to 15 m behind the Whiswall and PE for noise propagation to greater [distances10]. The calculations with FEM-PE are described in Chapter 2.

Chapter 3 the development of the computational rule for the effect of Whiswall diffractor. The development is based on two elements.
1 The results of the measurements from phase 1 (diffraction test).
2 The results of the calculations from Chapter 2.
The calculation rule can be added to the RMG. The calculation rule provides a correction term to the screen effect, as calculated using the 's Standard Calculation Method 2 (SRM2). The correction term is similar to the correction term for a screen top, or T-top, already included in the RMG.

---

[7] F. van der Eerden, R. Kurylek, T. van der Laan, "Comparison of measurement and calculation results for the Whiswall," TNO Report R11645, January 2021.
[8] R. Kurylek, F. van der Eerden, E. Salomons, A. Eisses, T. van der Laan, "Comparison of measurement and calculation results for the Whiswall along the track near Susteren," TNO Report 2021 R10470, March 2021.
[9] FEM = Finite Element Method, the English name for the finite element method for numerically solving differential equations, in this case the wave equation for noise in the atmosphere.
[10] PE= Parabolic Equation, the English name for an approximate wave equation that can be used to calculate sound propagation in the atmosphere over long distances.

The calculation rule described in Chapter 3 was developed based on the results for the Whiswall diffractor. The "product properties" of the diffractor, as obtained from a so-called diffraction test, are used as input parameters of the calculation rule. One question is whether the computational rule also works well for a similar diffractor with slightly different product properties. To answer this question, an analysis was performed for alternative diffractor, which is more tuned to low frequencies than the original *diffractor11*. The alternative diffractor is referred to as "LF diffractor "*12* in this report. The analysis is described in Chapter 4. This also examined whether the calculation rule could be slightly optimized further.

*11* The dimensions of the LF diffractor were defined by the company 4Silence[5].

*12* A potential advantage of the LF diffractor over the original diffractor is that the broadband noise reduction of the LF diffractor may greater. This is especially true for situations with a high noise shield (i.e., a high Whiswall), in which low-frequency components of traffic noise are stronger than in situations without shielding.

# 2 Simulations with FEM- PE

The effect of the Whiswall at distances up to 600 m was calculated with the hydride calculation model FEM-PE, for 42 different scenarios (situations). The influences of the atmosphere and soil on noise propagation were taken into account. The calculations can be regarded as simulations of noise propagation in practice.

The results of the calculations are used in Chapter 3 to develop the computational rule.

## 2.1 The effect of the diffractor on the Whiswall

A Whiswall between a source and an observer reduces the sound level at the observer through two effects:

- shielding of sound (screen effect),
- noise reduction due to the resonant effect of the diffractor.

We are particularly interested here in the second effect.

The noise reduction due to the diffractor is defined as (minus) the difference in noise level between two situations (see Figure 2.1):

- the situation with the Whiswall,
- The situation with an equally high screen without diffractor.

Because of the height of the diffractor, the screen in the second situation is slightly higher than the (buckled) screen of the Whiswall. The height of the diffractor is about 20 cm.

Therefore, two calculations with FEM-PE are performed for all scenarios, for the two situations mentioned. To also get an impression of the shielding of the noise for some scenarios, a third calculation is performed, for the situation without a screen or Whiswall (flat bottom).

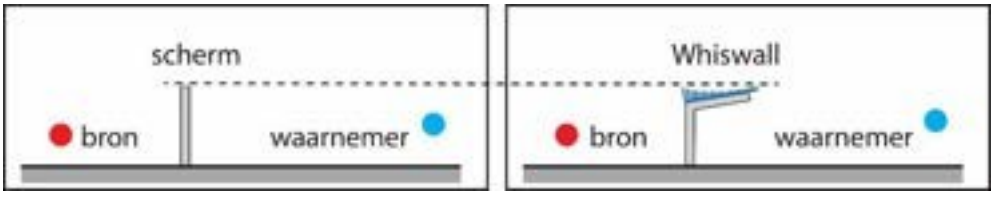


Figure 2.1 The noise reduction due to the diffractor (the blue portion at the top of the Whiswall) is defined as (minus) the difference in noise level between the situation with the Whiswall (right) and the situation with an equally high screen without a diffractor (left).

## 2.2 Setup of calculations with FEM- PE

This study uses a FEM-PE model that has also been used in previous studies. The FEM model was developed in the studies at the [Whiswall7,8]. The coupling with the PE model was performed in the same manner as in the studies at the [Whisstone1,2].

The FEM-PE model is a two-dimensional model, which is applied in a vertical plane by a point source (above a line of travel of a road, or a railroad line) and an observer. This plane is referred to as a sector plane in SRM2. Figure 2.2 shows a sector plane for a situation with the Whiswall. The angle θ between the line of travel and the sector plane varies between 0° and 180°. At 90°, the sector plane is perpendicular to the driving line and the screen. At other angles, distances are increased by a factor of $1/\sin\theta$. This also applies to the width of the diffractor and the width of the slots in the diffractor.

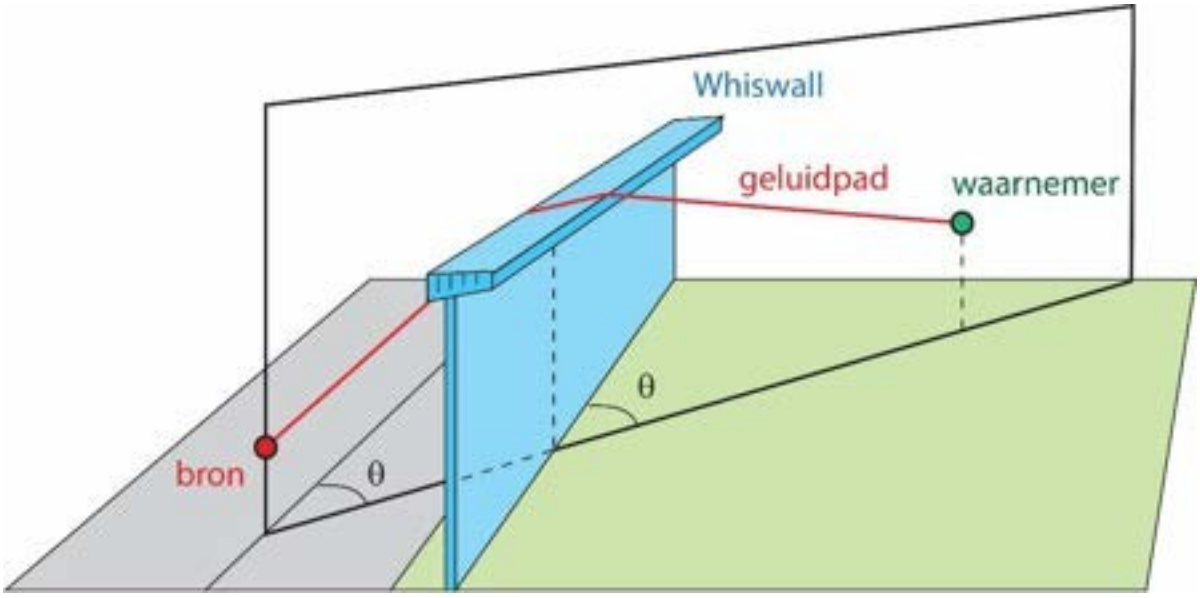


Figure 2.2 Illustration of the vertical plane (thick black line) through a point source above a driving line and an observer. The red line is the noise path across the Whiswall. Angle θ between the vertical plane and the screen (or driving line) is indicated.

Figure 2.3 shows the geometry of the calculations with FEM-PE in a sector plane. FEM is in a region around the source and the Whiswall. The sound pressure at the vertical right edge of the FEM domain, 15 m behind the Whiswall, is used as the starting vector for the calculation with PE. With PE, calculations are made over a distance of 600 m, taking into account tailwind, i.e. wind from the source to the *observer*[13].

The soil is divided into three areas (see Figure 2.3):

- road/track: road surface or ballast bed,
- bottom 1: the bottom for the Whiswall,
- bottom 2: the bottom behind the Whiswall.

This study assumed a hard soil for the first soil area (unless otherwise stated), and a hard soil or grass *soil*[14] for the other two areas. For "soil 1," a strip with a width of 2 m was assumed; in other , the Whiswall is placed 2 m away from the edge of the road or ballast bed.

[13] With PE, a logarithmic wind profile is computed, with 4.6 m/s wind at 10 m height (unless otherwise stated). SRM2 also assumes a situation with a tailwind.

[14] For soil, a boundary condition is imposed in FEM and PE. For a grass soil, the impedance model of Delany & Bazley (Applied Acoustics **3** (1970) 105-116) is assumed, with a flow resistance of 200 kN s $m^{-4}$.

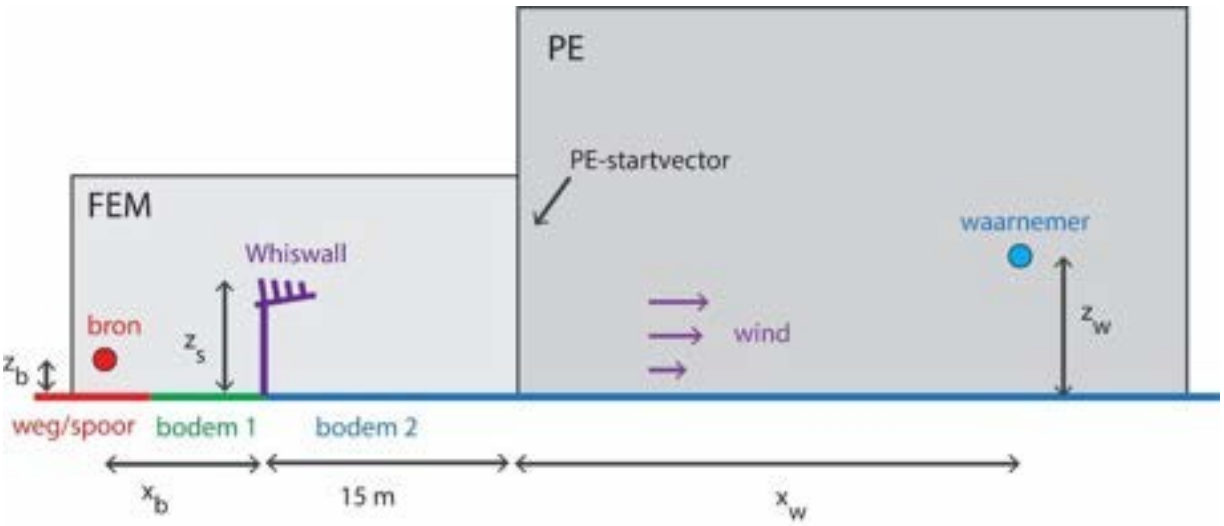


Figure 2.3 Illustration (not to ) of the geometry for calculations with FEM-PE. With FEM, the noise in the left domain (light gray) is calculated. The sound pressure at the vertical right edge, 15 m behind the Whiswall, is used as a starting vector for a calculation with PE of the sound in the right domain (dark gray), over a distance of 600 m.

FEM calculations are performed using the software package *Comsol*[15]. Near the diffractor, a highly refined
FEM grid, so that the complex shape of the diffractor is well represented. The total FEM domain is typically 32 m wide and 13 m high. For the source, a point source is assumed with emission equal for all directions and frequencies. For the soil, a boundary condition is imposed for a grass soil or a hard soil (as described above). At the other edges of the domain, an absorbing *layer*[16] is used avoid reflections. In previous studies[7,8] the FEM model has been optimized through comparison with *measurement* results[17].

The calculations with PE are performed using a computer program developed by TNO, based on the GFPE *method*[18]. The PE domain is 620 m wide and 62 m high. At the bottom, a boundary condition is imposed for a grass soil or a hard soil. An absorbing layer is used at the top of the domain to avoid reflections. The calculation with PE assumes a PE start vector from the FEM *calculation*[19] and proceeds in steps to the observers up to 620 m. Figure 2.3 shows only a single observer, but in fact the whole PE domain is filled with calculation results, for the following distances and heights:

- $_{xw}$= 1, 2, ..., 620 m,
- $_{sw}$= 0.5, 1, ..., 62 m.

*15* Comsol Multiphysics ®. See www.comsol.com.
*16* PML= Perfectly Matched Layer.
*17* Here, the depth and coverage of the front slot in the diffractor was adjusted. In addition, it was that an empirical correction of 2.5 dB is needed for the 400 Hz third band. This correction was retrospectively applied to the FEM-PE results in this study.
*18* GFPE = Green's Function Parabolic Equation. See: E.M. Salomons, "Improved Green's function parabolic equation method for atmospheric sound propagation" J. Acoust. Soc. Am. 104, 100-111 (1998). See also: E.M. Salomons, "Computational atmospheric acoustics"(Kluwer, Dordrecht, 2001). *19* Since the PE domain is higher than the FEM domain, the PE start vector from FEM is extrapolated to the height of the PE domain.

Calculations are made for 72 frequencies, obtaining results for third-bands 50-2500 Hz and octave bands 63-2000 Hz. Here four frequencies per third-band are used.

The diffractor is designed for noise reduction at frequencies of about 400 Hz and above. The calculation rule in Chapter 3 considers the five octave bands 125-2000 Hz. The effect of the diffractor is assumed equal to zero outside this frequency range.

## 2.3 Scenarios

Calculations with FEM-PE were performed for 42 different scenarios, with parameters given in Table 2.1. Parameter θ is the angle of the sector plane, shown in Figure 2.2. The other parameters are shown in Figure 2.3.

Initial calculations were made for 24 scenarios (upper part of Table 2.1):
- 10 scenarios with θ=0° (A-J),
- 14 scenarios with θ=45° (C45-U45).

For θ=0°, we calculate for distances $x_b$ of 3.5, 7, and 15 m. Distance 3.5 m represents the line of travel on a road closest the screen. Distances 7 and 15 m represent more distant driving lines. For θ=45°, calculation is made for distances $x_b$ of 5 and 10 m. These (oblique) distances correspond to the perpendicular distances of 3.5 and 7 m (since 3.5/sin45° = 5 and 7/sin45° = 10). Calculations were made for two screen heights, 1.1 m and 5 m, and four source heights, 0.1, 0.5, 2 and 4 m. Source height 0.1 m is relevant for road traffic noise, the portion of noise generated by the interaction of the tires and the road surface. For rail traffic noise, all four source heights are relevant.

Based on the results for the first 24 scenarios, 18 scenarios were then added (bottom portion of Table 2.1). In doing so, the following elements were added:
- source height of 1.1 m,
- ballast bed for the soil area road/rail,
- screen height 3 m,
- weaker wind, 2.3 m/s instead of 4.6 m/s,
- no wind, 0 m/s (neutral atmosphere).

The ballast bed was modeled using an appropriate impedance [20]. The scenarios with weaker wind and no wind were added in light of the new European calculation model Cnossos-EU, which averages over two wind situations (windward and no wind).

[20] An impedance model of Zwikker and Kosten was used for this purpose (rigid-skeleton model), with flow resistance 30 kN s $m^{-4}$, porosity 0.08, structure factor 1, and layer thickness 330 mm.

Table 2.1 Parameters of FEM-PE scenarios.

| height of source $z_b$ (m) | screen height $z_s$ (m) | soil road/rail | soil 1 | soil 2 | distance from source to screen xb (m) 3.5 | 5 | 7 | 10 | 15 | 25 | corner θ (gr) | wind (m/s) | number |
|---|---|---|---|---|---|---|---|---|---|---|---|---|---|
| 0.1 | 1.1 | hard | grass | grass | C | | F | | I | | 0 | 4.6 | 3 |
| 0.5 | | | | | H | | G | | J | | | | 3 |
| 2 | | | | | | | | | | | | | |
| 4 | | | | | | | | | | | | | |
| 0.1 | 1.1 | hard | grass | grass | | C45 | | F45 | | | 45 | 4.6 | 2 |
| 0.5 | | | | | | H45 | | G45 | | | | | 2 |
| 2 | | | | | | K45 | | | | | | | 1 |
| 4 | | | | | | L45 | | | | | | | 1 |
| 0.1 | 5 | hard | grass | grass | | M45 | | R45 | | | 45 | 4.6 | 2 |
| 0.5 | | | | | | N45 | | S45 | | | | | 2 |
| 2 | | | | | | P45 | | T45 | | | | | 2 |
| 4 | | | | | | Q45 | | U45 | | | | | 2 |
| 0.1 | 1.1 | hard | hard | grass | B | | E | | | | 0 | 4.6 | 2 |
| | | | | hard | A | | D | | | | | | 2 |
| | | | | | | | | | | | | | 24 |
| 1.1 | 1.1 | hard | grass | grass | V | | W | | Y | | 0 | 4.6 | 3 |
| | | | | | | V45 | | W45 | | | 45 | | 2 |
| 0.1 | 1.1 | ballast bed | grass | grass | CB | | | | | | 0 | 4.6 | 1 |
| 1.1 | | ballast bed | | | VB | | | | | | | | 1 |
| 0.1 | 3 | hard | grass | grass | | MM45 | | | | XX45 | 45 | 4.6 | 2 |
| | | | | hard | | MMH45 | | | | XXH45 | | | 2 |
| 0.1 | 5 | hard | grass | grass | | | | | | X45 | 45 | 4.6 | 1 |
| | | | | hard | | MH45 | | | | XH45 | | | 2 |
| 0.5 | 1.1 | hard | grass | grass | HW | | GW | | | | 0 | 2.3 | 2 |
| | | | | | HZ | | GZ | | | | | 0 | 2 |
| | | | | | | | | | | | | | 42 |

## 2.4 Results of FEM- PE

In the next section, results from FEM-PE in octave bands are to a computational rule. In this section, some results from FEM-PE are presented as (A-weighted) broadband noise reductions by the diffractor. Appendix C presents broadband results from all calculations.

A spectrum of road traffic noise according to European standard EN [21] (see Appendix A and B) is used to calculate broadband noise reductions. This spectrum is intended to determine the broadband noise reduction by an object, such as a noise barrier along a road.

[21] European standard prEN 1793-3, "Road traffic noise reducing devices - Test method for determining the acoustic performance - Part 3 : Normalized traffic noise spectrum".

Figure 2.4 shows an example of the broadband noise reduction by the diffractor, for scenario C45 ($z_b$ = 0.1 m, $z_s$ = 1.1 m, $x_b$ = 5 m). The noise reduction below the line of sight is approximately 2 dB. Numerical values at twelve positions are shown in the graph.

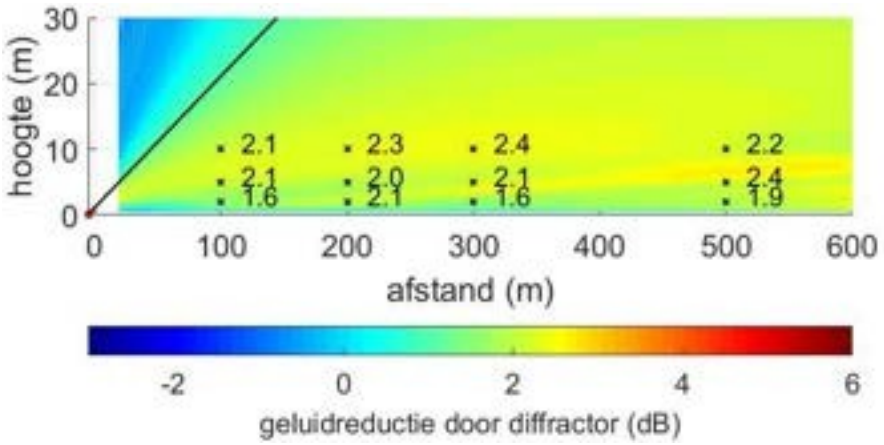


Figure 2.4 Example of the result of a calculation with FEM-PE, for scenario C45 ($z_b$= 0.1 m, $z_s$= 1.1 m, $x_b$= 5 m). The color represents the A-weighted broadband noise reduction due to the Whiswall diffractor. The black line is the line of sight through the source (red dot) and the screen top.

The FEM-PE results for the screen and Whiswall include not only the effect of the diffractor, but also the effect of shielding by the screen or Whiswall. Due to shielding, high frequencies from the traffic spectrum are suppressed more than low frequencies. This is illustrated by the following example.

Figure 2.5 shows graphs of the noise reduction due to the diffractor calculated with FEM-PE for scenarios M45, N45, P45, and Q45, with source heights 0.1, 0.5, 2 and 4 m, and screen heights 5 m, respectively. The value of the noise reduction varies greatly with the source height. For example, for the observer at distance 100 m and height 10 m applies:

- noise reduction -1.4 dB for source height 0.1 m,
- noise reduction 3.8 dB for source height 0.5 m,
- noise reduction 0.2 dB for source height 2 m,
- noise reduction 1.5 dB for source height 4 m.

The calculation of these four numbers through the A-weighted traffic spectrum is also illustrated in the figure. This shows that for source height 0.1 m, the noise reduction is determined by the octave band 250 Hz, while for source height 0.5 m the octave bands 500 and 1000 Hz make the largest contributions.

This shift in the spectrum is a result of interference on the source side of the screen or Whiswall. This is the path length difference between direct sound and sound through the ground, from the source to the top of the screen. This path length difference is exactly half a wavelength at 250 Hz for source height 0.5 m, resulting in a minimum in sound transmission at that . Figure 2.6 shows transmission spectra for the four source heights. The minimum at 250 Hz for source height 0.5 m is clearly visible. For comparison, the transfer spectrum according to SRM is also shown, which is the same for the four source heights.

Thus, the interference for source height 0.5 m causes a spectral shift to higher frequencies than 250 Hz. For other source heights and other distances between source and screen, this interference generally does not occur. For these situations, the contribution at 250 Hz is greater than, or approximately equal to, the contributions at 500 and 1000 Hz. This limits the broadband noise reduction provided by the diffractor. The large noise reductions at 500 and 1000 Hz are not reflected in the broadband noise *reduction22*.

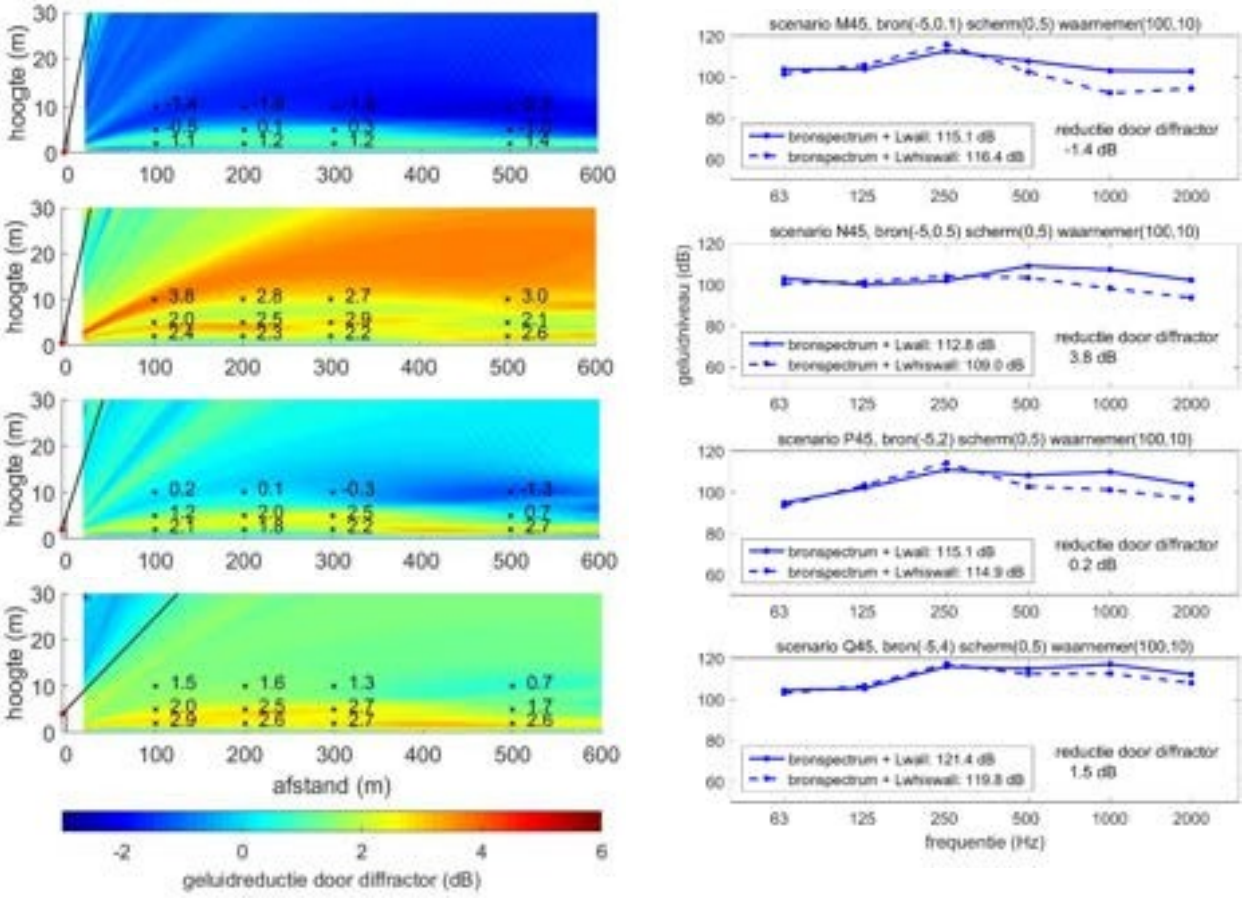


Figure 2.5 The graphs on the left show the broadband noise reduction by the diffractor calculated with FEM-PE for scenarios M45, N45, P45, Q45 (from top to bottom). The broadband noise reduction was determined based on octave band levels from FEM-PE (Lwall, Lwhiswall) and a typical A-weighted octave band spectrum of road traffic noise (see Appendix A and B). The graphs on the right show the octave band levels and illustrate the broadband noise reduction calculation, for observer position (100,10).

[22] The noise reduction effect of the diffractor is limited to the frequency range 400-2500 Hz. This is evident, for example, from spectra presented in Chapter 3.

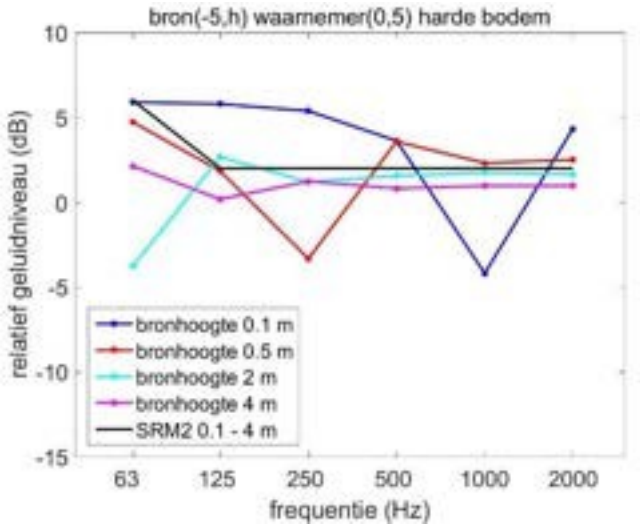


Figure 2.6 Analytically calculated transfer spectra from the source to an observer at the screen top (5 m away from the source, height 5 m), for four source heights. Also shown are the transfer spectra according to SRM2.

# 3 Calculation rule for SRM2

As described in Chapter 1, a goal of this study is to develop a calculation rule for the Whiswall diffractor. The calculation rule should suitable for calculation method SRM2 of the RMG, both for road and rail traffic.

The development is based on the following two elements.

- Measured product properties of the Whiswall diffractor, as determined in a diffraction test7.
- The results of the calculations with FEM-PE, described in Chapter 2. This chapter the development of the calculation rule step by step.

## 3.1 Screen effect according to SRM2

The screen effect $\Delta L_{SWN}$ at SRM2 is calculated using the following formula3,[23]:

$$\Delta L_{SWN} = HF(N)_f + C_T - C_p \quad (3.1)$$

with

- $H$: The effectiveness of the screen,
- $F(_{NF})$: a function of the Fresnel number $_{NF}$,
- $_{CT}$: a correction term for a screen top (T-top),
- $_{Cp}$: a correction term for the profile of the screen.

For a thin vertical screen without a screen top, $_{CT}$= 0 and $_{Cp}$= 0. For rail traffic, $_{CT}$ is not applied.

The screen effect depends on frequency via the magnitudes $H$ and $_{NF}$. Calculations are made for eight octave bands, from 63 Hz to 8 kHz.

Figure 3.1 shows an example of the screen effect at 125 Hz and 1000 Hz, for a situation with a source at height 0.75 m and a 5 m high screen 10 m away. Also shown are the line of sight and five lines of constant Fresnel number ($_{NF}$ = -0.2, -0.1, 0, 0.1, 0.2). The Fresnel number increases as the observer moves from top to bottom into the sound shadow. The screen effect also increases, from zero far above the line of sight to a value of 10-25 dB deep in the shadow. The transition is more gradual at low frequency than at high frequency.

Figure 3.2 shows for this situation the value of the correction term $_{CT}$ for T-peaks. The correction term $_{CT}$ is zero far above the line of sight and increases to 5 dB deep in the shadow.

[23] If a median screen is present then a correction $_{Cmbs}$ is calculated for this, and the total screen effect is calculated as follows: $\Delta L_{SW} = \Delta L_{SWN} + C_{mbs}$ . The screen effect $\Delta L_{SWN}$ is calculated from the Fresnel number, which is indicated by subscript 'SWN' (SW = screen effect). The Fresnel number is also used in calculating the Whiswall correction term, as defined in Section 3.2.
A correction $_{Cdiff}$ for the Whisstone was also recently added: $\Delta L_{SW} = \Delta L_{SWN} + C_{mbs} + C_{diff}$.

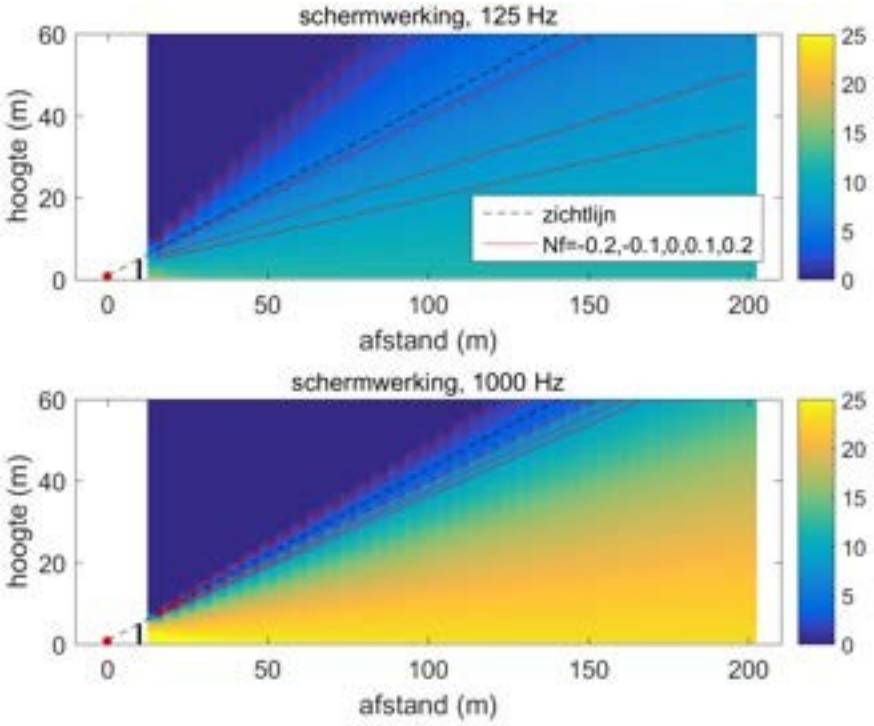


Figure 3.1 Screen effect at 125 Hz (top) and 1000 Hz (bottom), for a situation with a source at height 0.75 m (red dot) and a 5 m high screen 10 m away. Also shown are the line of sight and the lines with $_{NF}$ = -0.2, -0.1, 0, 0.1, 0.2.

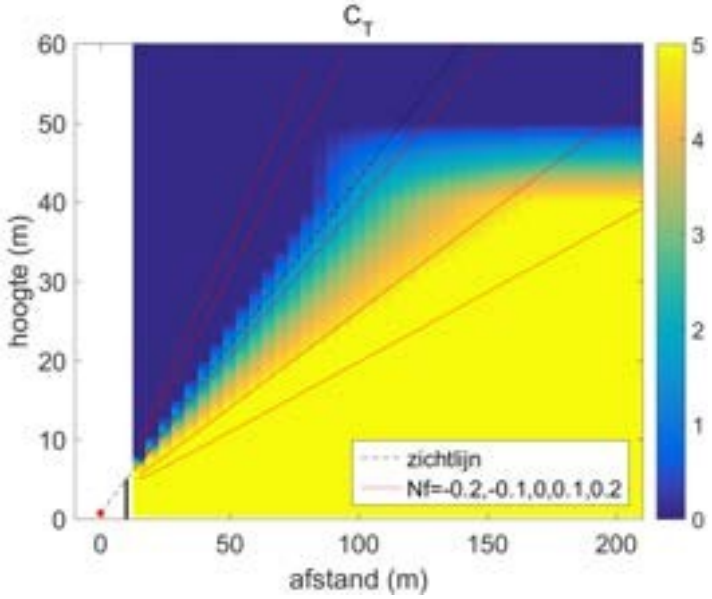


Figure 3.2 Value of correction term $_{CT}$ for T-peaks, in the situation of Figure 3.1.

## 3.2 Structure of the calculation rule

For the effect of the diffractor of the Whiswall, we add a correction term $_{CW}$ added to the formula of SRM2:

$$\Delta L_{SWN} = HF(N_f) + C_T - C_W - C_p$$

(3.2) The correction term $_{CW}$ is a function of:

- the frequency,
- geometric parameters of *source*[24], screen, and observer,
- 'product features' of the Whiswall diffractor.

In principle, $_{CW}$ also depends on soil properties. This dependence is negligible, as will be shown in the following paragraphs. It will also be shown that the dependence on geometric parameters can be formulated via the Fresnel number. With this, the correction term satisfies the acoustic principle of *reciprocity*[25].

The calculation rule applies to the noise propagation in the vertical plane through the source (point source above driving line/track line) and the observer. This plane was also considered in simulations with FEM-PE described in Chapter 2 (see Figure 2.2). The plane is called the sector plane in SRM2.

No distinction is made between the two situations shown in Figure 3.3, in which the sector plane makes different angles with the Whiswall (angle $\vartheta$ in Figure 2.2). This is an approximation. The computational rule basically represents an average over different directions of the sector planes. The same is true for the computational rule for a T-top.

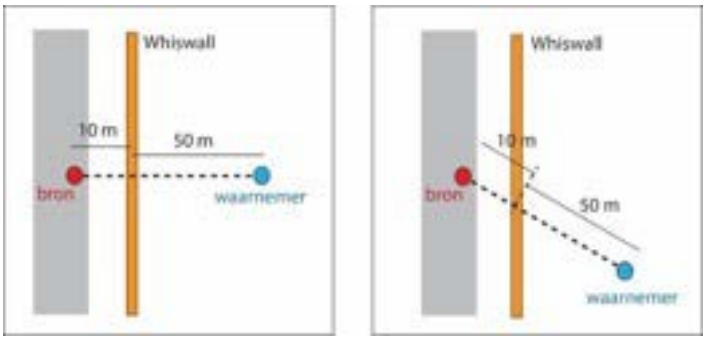


Figure 3.3 Top view of two situations where the sector plane (broken line) is perpendicular to the Whiswall (left) and at 60 degrees (right). The calculation rule does not distinguish between the two situations.

[24] In SRM2 for road traffic noise, a vehicle is modeled by a point source at height 0.75 m above the road surface. From a physical point of view, a source height of about 0.1 m is more realistic, especially for passenger cars. For the diffractor calculation rule, it is preferable to choose the source height as realistic as possible, so for example 0.1 m.

[25] Reciprocity in acoustics means that sound transmission from a source to an observer remains the same if source and observer are swapped positions. This principle applies in general to systems with no preferred direction. It also applies to a system with wind in a given , if the influence of wind is represented by a profile of the effective speed of sound.

### 3.3 Product Features of the Whiswall

For the product properties, we assume the result of the so-called diffraction test. The idea is that the computational rule for the Whiswall should also valid for a similar kind of diffractor on a screen, with (slightly) different product properties. Thus, the product properties are parameters of the computational rule.

Measurements and calculations of the Whiswall diffraction test are described in a previous report from [20217]. The measurement procedure in the diffraction test is described in NEN-EN standard [1793-426]. The measurement setup is shown in Figure 3.4, with three source heights, five microphone heights, and two angles (0° and 45°). The source height 0 m (i.e., the height of the screen top) is added here; the NEN-EN standard lists only the source heights -0.15 m and -0.5 m.

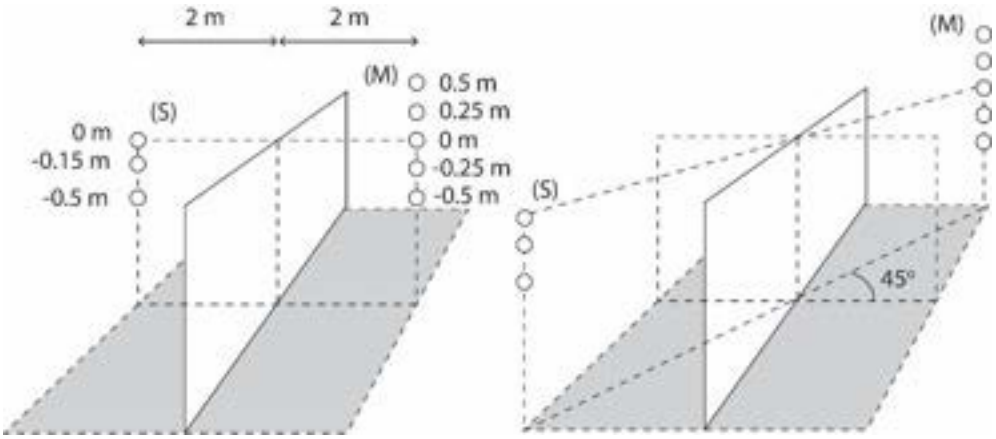


Figure 3.4 Geometry of the diffraction test, with three source positions (S), five microphone positions (M), and two angles: 0 degrees (left) and 45 degrees (right). Sources and microphones are located 2 m away from the screen (white plane). Measurements are taken with and without a diffractor at the top of the screen (shown here is the situation without a diffractor). Heights are measured relative to the highest point of the diffractor and the top of the screen, respectively.

The measurements are made for two situations:

- The situation with the diffractor on the screen (Whiswall),
- The situation with only the screen (reference).

For both situations, a noise spectrum in third bands is determined (normalized with respect to the free ). This spectrum is referred to as:

- diffraction index *DI*.

Here the normalized levels are averaged (energetically) over the 10 microphone positions for the two angles. The difference between the spectra of *DI* for the two situations is denoted as:

- diffraction index difference *ΔDI*.

This quantity is a measure of the effect of the diffractor. The spectrum of *ΔDI* can be converted to a broadband value of *ΔDI*, weighted by the traffic noise spectrum according to standard EN-1793-3 (see Appendix B).

[26] NEN-EN 1793-4:2015 "Traffic noise reduction structures - Test methods for determination of acoustic performance - Part 4: Intrinsic characteristics - In situ values of sound diffraction."

Figure 3.5 shows the measured third-band spectrum of *ΔDI*, for the three source heights, and also the energetic average spectrum over the three source heights (energetic or linear averaging makes no significant difference in this case). The influence of source height is limited. Around 800 Hz, where the effect of diffractor is greatest, the value of *ΔDI* increases slightly with decreasing source height. A larger value of *ΔDI* corresponds to greater noise reduction by the diffractor. On the other hand, the value of *ΔDI* around 250 Hz is more negative at lower source height; that is, there is more amplification of the sound by the diffractor around this frequency.

Figure 3.6 shows the individual contributions of the two angles for the three source heights. Especially around 400 Hz, the difference between the spectra for the two angles is significant.

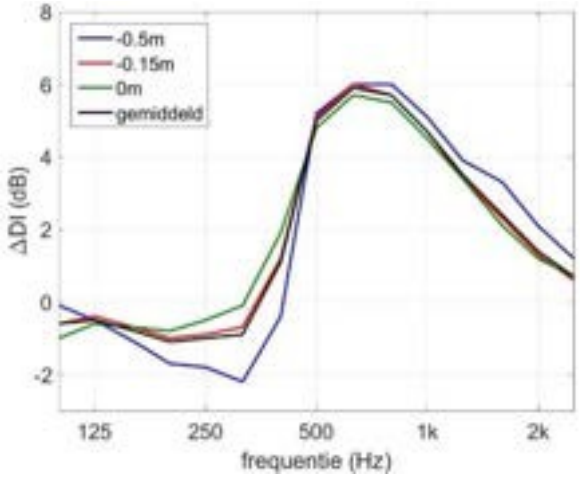


Figure 3.5 Tertiary band spectrum of the diffraction index difference *ΔDI*, for the three source heights, and also the average spectrum over the three source heights.

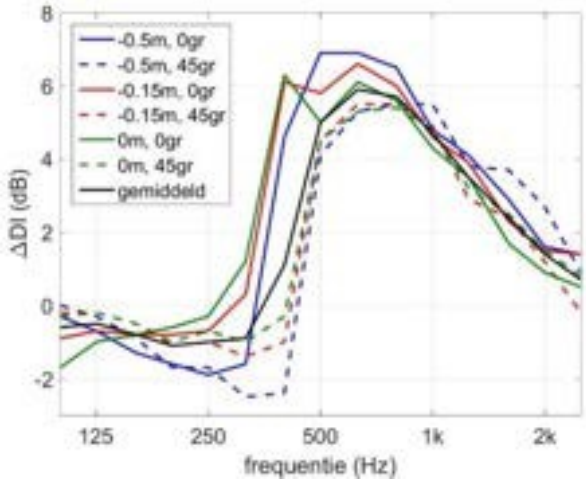


Figure 3.6 As Figure 3.5, but now the spectra for the three source heights at the two angles 0° and 45° are shown separately. The black line (average) is the same as in Figure 3.5.

Figure 3.7 shows octave band spectra of *ΔDI* calculated in two ways from the average third-band spectrum from Figure 3.5:

- by energetic averaging,
- by weighted energetic averaging with the traffic noise spectrum from standard EN 1793-3.

The values for the octave bands 125-2000 Hz are respectively:

- -0.6, -1.0, 3.4, 4.5, 1.4 dB,
- -0.7, -1.0, 3.9, 4.6, 1.6 dB.

The difference is at most 0.5 dB. For the further analysis described here, we assume the octave band spectrum without weighting (see Sections 3.6-3.10).

Figure 3.8 is like Figure 3.6, but now in octaves. Especially at 500 Hz, the difference in *ΔDI* between the two angles 0° and 45° is significant.

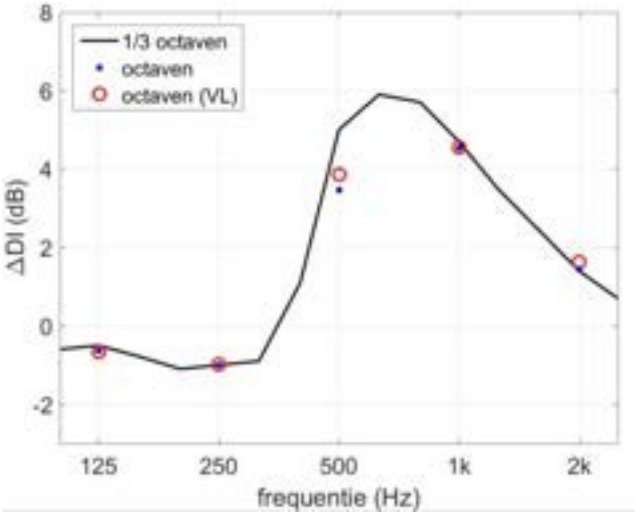


Figure 3.7 Third-band spectrum from Figure 3.5 (average), and corresponding octave band spectra calculated by energetic averaging (blue) and weighted energetic averaging with the traffic noise spectrum from EN 1793-3 (red).

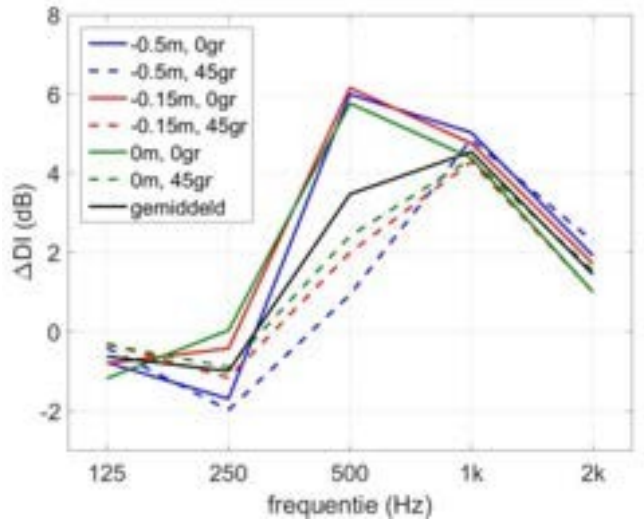


Figure 3.8 As Figure 3.6, but now in octaves.

### 3.4 Effect of a screen at large distance

Figure 3.9 shows results from FEM-PE and SRM2 for the effect of a screen (without diffractor) at 1000 Hz, for scenario B, with source height 0.1 m, screen height 1.1 m, source screen distance 3.5 m, 'soil 1' = hard and 'soil 2=grass (see Chapter 2).

The graphs on the left show three FEM-PE results:
i) situation without a screen,
ii) situation with screen,
iii) the difference between (i) and (ii): the noise reduction by the screen.
The levels in the top two graphs are direct results of FEM-PE. The PE calculation assumes a starting vector calculated with FEM (at distance $_{xw}$ = 0 in the graphs). The levels depend on the source strength selected in FEM. The level difference shown in the bottom graph is independent of the chosen source strength.
The levels lower than -20 dB in the upper left corner of the top two graphs should be ignored. This is because PE is not valid for elevation angles greater than typical 45 degrees.
The bottom graph shows that the screen effect mainly occurs below the line of sight (broken line). This is as expected.

The graphs to the right show four SRM2 results:
i) situation without a screen,
ii) situation with screen,
iii) the difference between (i) and (ii): the noise reduction by the screen,
iv) The screen effect (without the effect of soil).
The difference between (i) and (ii) is sometimes referred to as "insertion loss" or "intermediate link weakening. Two effects come play here:
- screen operation,
- change in soil attenuation.

The change in ground attenuation is a result of a secondary source on the screen top, which is higher than the real source. In particular, near the bottom, the screen effect (iv) is greater than the noise reduction by the screen (iii). Apparently, here the noise reduction by the screen is somewhat reduced by the influence of the soil.

FEM-PE and SRM2 give slightly different results for noise reduction due to the screen (third graph from top). For FEM-PE, the noise reduction is higher at some locations and lower at others than for SRM2.

The calculation rule for the diffractor (see following paragraphs) is based on the difference in FEM-PE results between two situations:
i) situation with screen,
ii) Situation with screen with diffractor (Whiswall).
The approach here is that this difference can be added to the screen effect according to SRM2 (see formula 3.2), although SRM2 and FEM-PE do not give exactly the same results for the noise reduction due to the screen without diffractor.

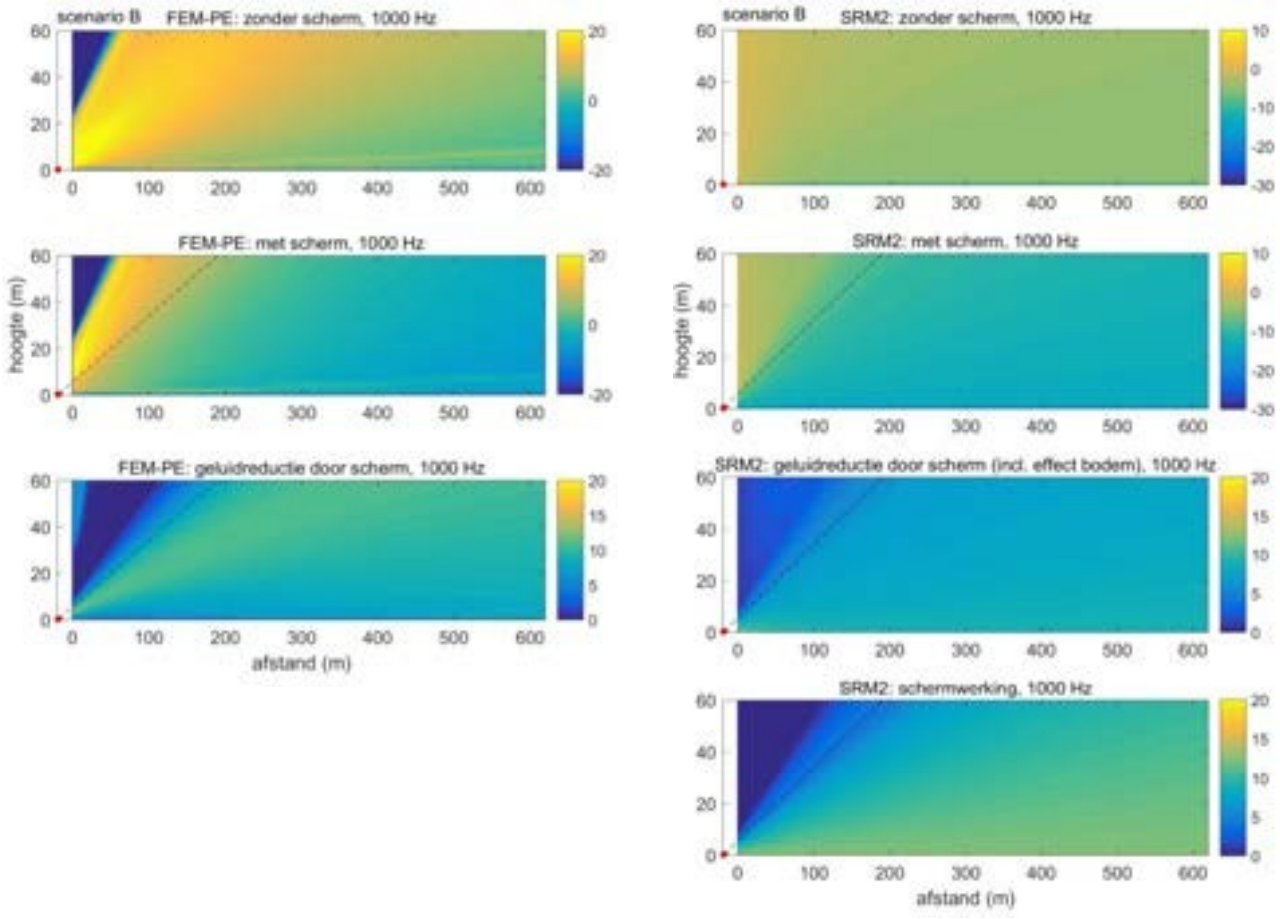


Figure 3.9 Results of FEM-PE (left) and SRM2 (right) for relative noise levels at 1000 Hz without screen and with screen, and the difference (noise reduction due to the screen), for scenario B. For SRM2, the screen effect is also separately. The broken line is the line of sight through the source (red dot) and the screen top.

## 3.5 Effect of the Whiswall at large distance

Figure 3.10 shows FEM-PE results for the effect of the diffractor at 1000 Hz for scenario A ($z_b$= 0.1 m, $z_s$= 1.1 m, $x_b$= 3.5 m; see Chapter 2).

The graphs show three FEM-PE results:

i) result for the situation with screen,
ii) result for the situation with Whiswall (screen with diffractor),
iii) the difference between i) and ii): the noise reduction by the diffractor.

The upper left region should again be disregarded because PE is only valid for elevation angles up to typical 45 degrees. The noise reduction due to the diffractor is approximately zero above the line of sight and increases to about 5 dB below the line of sight.

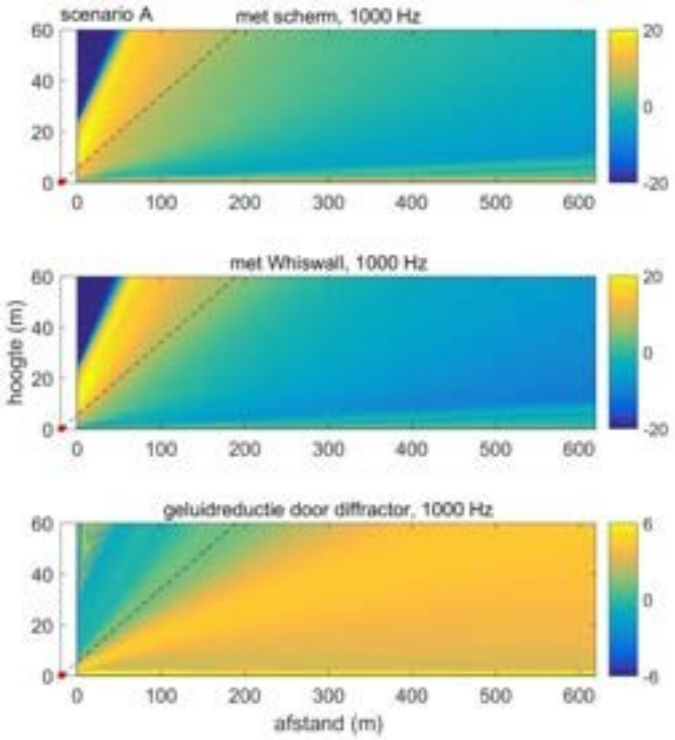


Figure 3.10 FEM-PE results for the relative sound level at 1000 Hz for scenario A ($z_b$ = 0.1 m, $z_s$ = 1.1 m, $x_b$ = 3.5 m), without diffractor (top) and with diffractor (middle), and the difference, i.e., the noise reduction due to the diffractor (bottom).

Figure 3.11 shows the course of the reductions by screen and by diffractor as a function of frequency, for a fixed position of the observer (distance 200 m, height 10 m). For clarity, the narrow-band results from FEM-PE are shown here, for the 72 frequencies described in Section 2.2. The effect of the diffractor is small between 100 and 350 Hz, and increases sharply at 350 Hz. Also shown is the screen effect according to SRM2 for this observer. In this situation (hard ground), in SRM2 the reduction due to the screen is equal to the screen effect.

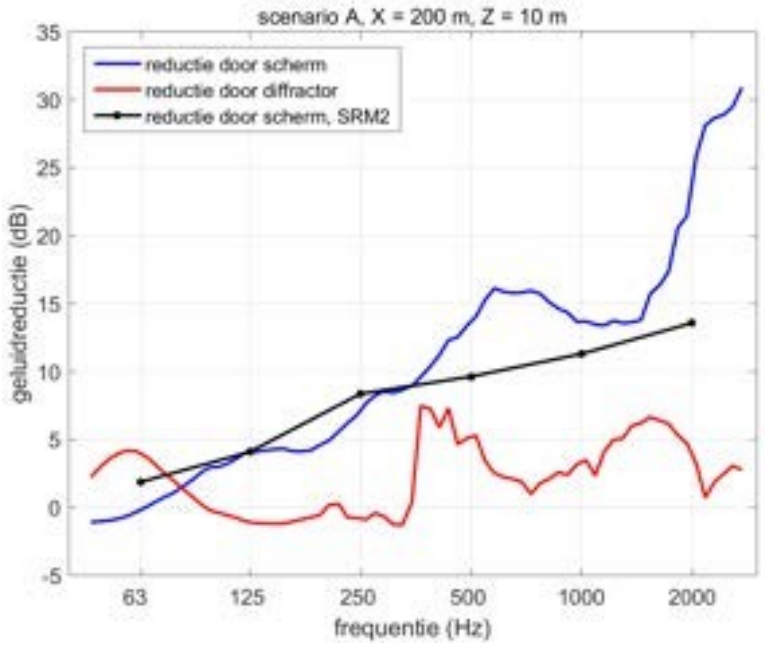


Figure 3.11 FEM-PE results for the reductions due to screen and diffractor, for scenario A, for an observer at distance 200 m and height 10 m. Also shown is the screen effect according to SRM2.

Figure 3.12 shows results from FEM-PE for noise reduction by the diffractor at 1000 Hz for scenarios A-J.

The difference between scenarios A and B is the soil behind the screen. In scenario A the soil is hard and in scenario B the soil consists of grass. The graphs show that the effect of the diffractor is only slightly affected by the soil behind the screen.

The influence of the soil hardness of the 2 m wide strip in front of the screen is also small. This is evident from a comparison of the graphs for scenarios B and C, and scenarios E and F.

The distance from the source to the screen is an important parameter. This distance is 3.5 m (left), 7 m (center), and 15 m (right) for the graphs in the figure. The noise reduction due to the diffractor is greater for distance 3.5 m than for distances 7 and 15 m. Thus, the calculation rule must include the distance from the source to the screen as a parameter. This can be done through the line of sight, or through the Fresnel number (which is always calculated in screen operation; see Sections 3.1 and 3.2).

The effect of the diffractor is approximately limited to the area below the line of sight. The line of sight depends on the position of the source relative to the screen top. This is visible in the figure: the line of sight is less steeply upward for greater distance between source and screen and for greater source height.

Figure 3.13 shows results from FEM-PE for noise reduction by the diffractor at 1000 Hz for scenarios C45-U45. Most striking in these graphs is the influence of the screen height. For the 5 m high screen, the noise reduction by the diffractor is greater than for the 1.1 m high screen.

Figure 3.14 shows FEM-PE results for noise reduction by the diffractor at 1000 Hz, for scenarios V-HZ. These are the 18 scenarios in the bottom section of Table 2.1. These graphs were used to examine the influence of acoustic ground hardness at the source (red in Figure 2.3) and atmospheric wind speed.

The influence of soil hardness at source is small. This is illustrated by the that the differences are small between the graphs for scenarios CB and VB (ballast bed) and scenarios C and V (hard soil).

The influence of wind speed in the atmosphere is also small. This is evident from a comparison of the results for scenarios H and G (wind speed 4.6 m/s), HW and GW (wind speed 2.3 m/s), and HZ and GZ (wind speed 0 m/s). The refraction due to the wind gradients in windy conditions does show up in the graphs in Figure 3.12 and Figure 3.14.

For mutual comparability, the color scale was chosen the same for all graphs, running from -6 to + 6 dB. This limits the largest noise reductions. The following sections will show that the noise reductions increase to a maximum of about 10 dB at 1000 Hz.

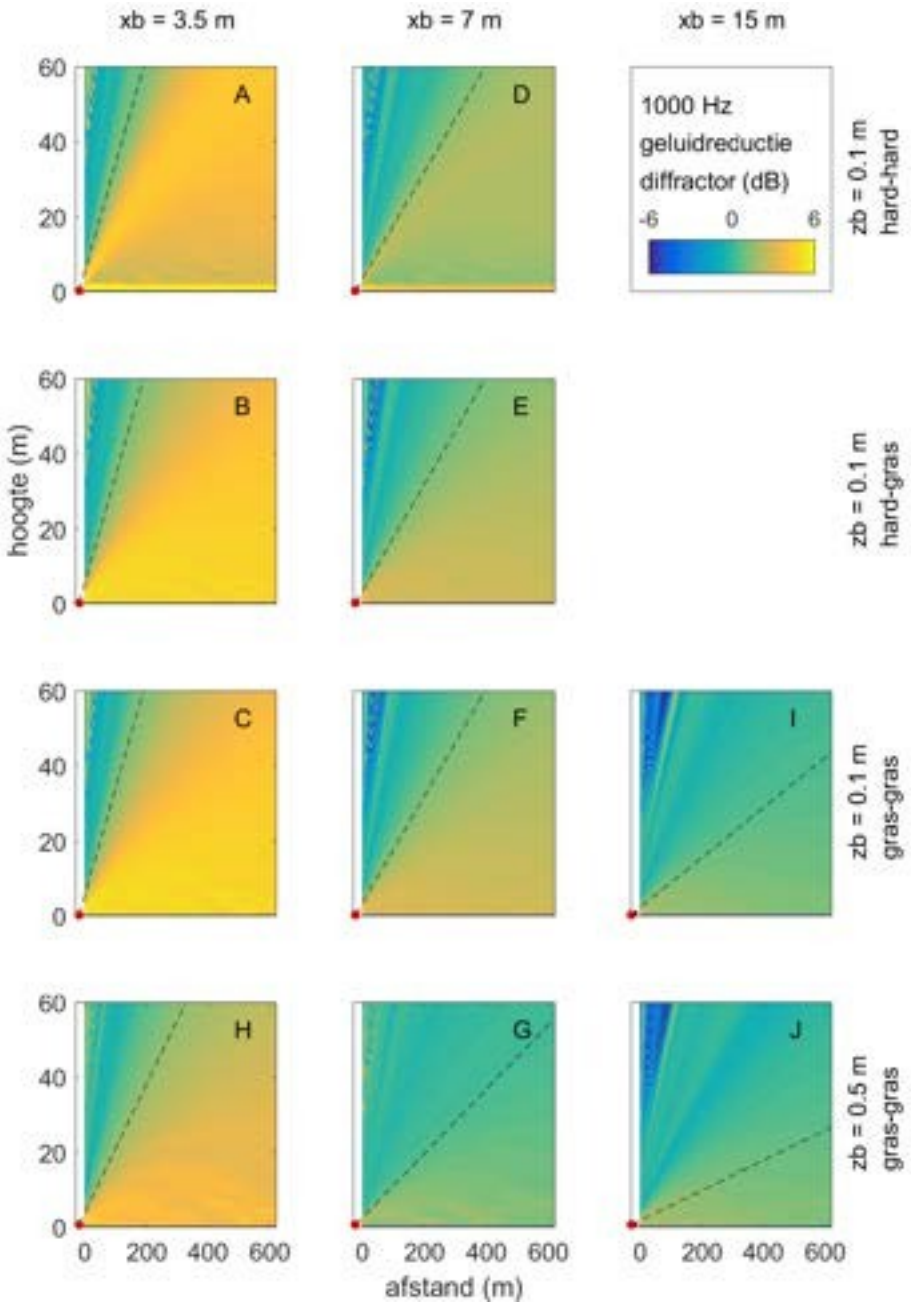


Figure 3.12 FEM-PE results for noise reduction by the diffractor at 1000 Hz, for scenarios A-J.

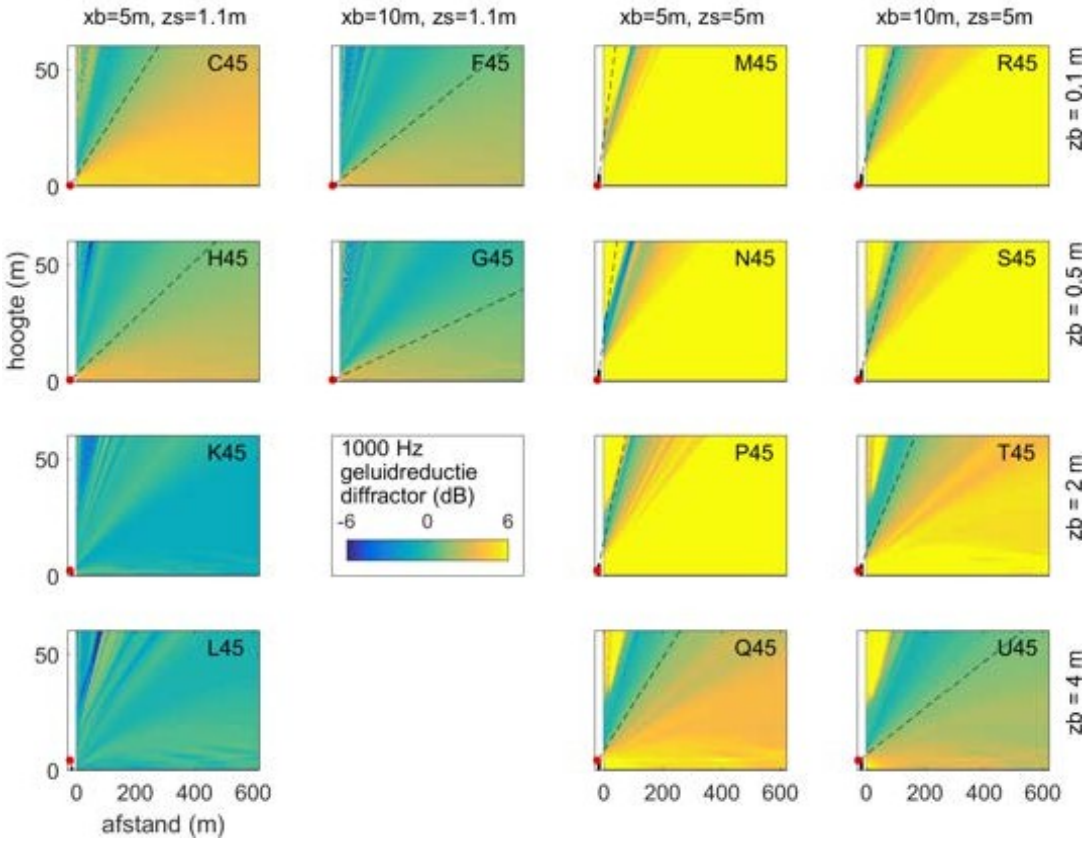


Figure 3.13 FEM-PE results for noise reduction by the diffractor at 1000 Hz, for scenarios C45-U45. Note: For M45-P45, apparently large reductions occur near the line of sight, up to 20 dB, due to the angular constraint of the PE model.

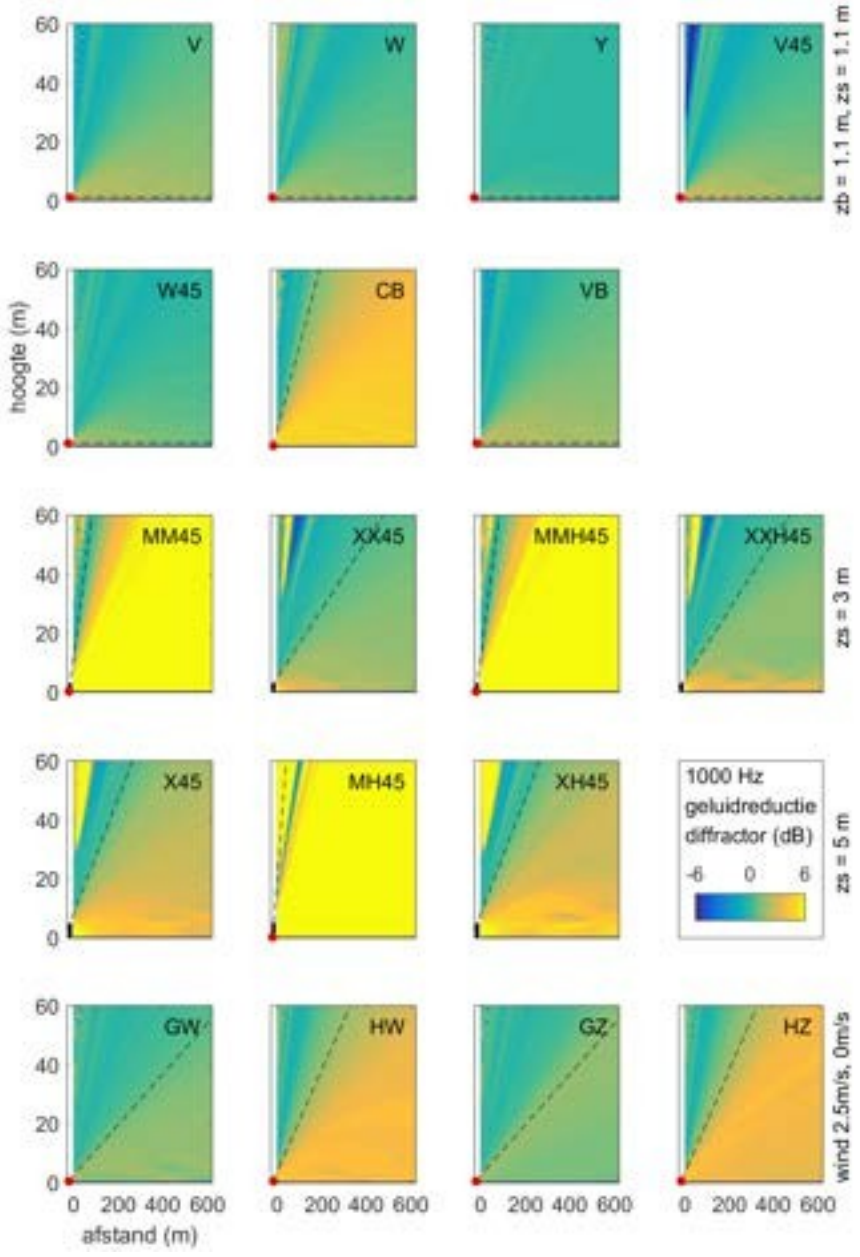


Figure 3.14 FEM-PE results for noise reduction by the diffractor at 1000 Hz, for scenarios V-HZ (18 scenarios in the lower part of Table 2.1).

## 3.6 Calculation Rule, version 1

Figure 3.16 shows FEM-PE results for the noise reduction due to the screen, Whiswall, and diffractor at 1000 Hz, for scenarios A and M45. Also shown are SRM2 results for the screen effect and the corresponding Fresnel number used to calculate the screen effect. The goal is to develop a computational rule that properly approximates the FEM-PE results for diffraction noise reduction. For this purpose, the Fresnel number is a useful parameter.

To develop the computational rule, we consider FEM-PE results on a grid of 12 observer positions (see Figure 3.15), with:

- four distances to the screen: 100, 200, 300, and 500 m,
- three heights: 2, 5, and 10 m.

The four distances correspond to $_{xw}$= 85, 185, 285, and 485 m in Figure 2.3.

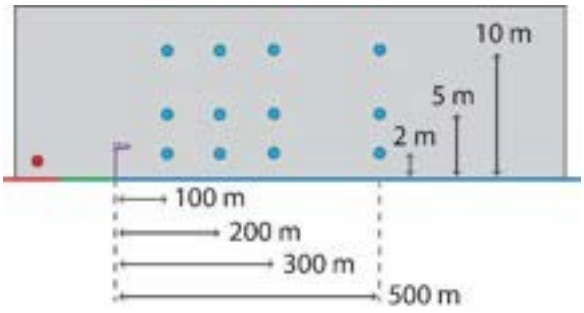


Figure 3.15 Grid of twelve observer positions.

Figure 3.17 shows FEM-PE results on this grid as a function of Fresnel number. The graphs show

- The noise reduction by the screen (dark circles),
- The noise reduction by the Whiswall (light rounds).

The green lines in the graphs represent the screen effect according to Maekawa's formula for screen *effect*[27]:

$$D_{screen} = 10 \log_{10} [\max(1, 20 N_F + 3)], \quad (3.3)$$

where $N_F$ is the Fresnel number. For $N_F < -0.1$, the screen effect is zero. The screen effect at SRM2 is calculated using a formula that gives similar values to Maekawa's formula in good approximation, up to a maximum of 25 dB of screen effect (see Figure 3.18). For SRM2, the screen effect does not exceed 25 dB.

The FEM-PE results for screen noise reduction show a significant spread, but show an average trend consistent with Maekawa's formula. Some FEM-PE results are significantly greater than 25 dB.
Especially at 1000 and 2000 Hz, the FEM-PE results for the Whiswall are on average higher than for the screen. This means that a higher noise reduction is achieved with the diffractor than with the screen without the diffractor. In other , the noise reduction by the diffractor here is positive on average.

[27] The formula is based on scale model measurements performed by Maekawa in 1968 (Applied Acoustics **1**, 157-173).

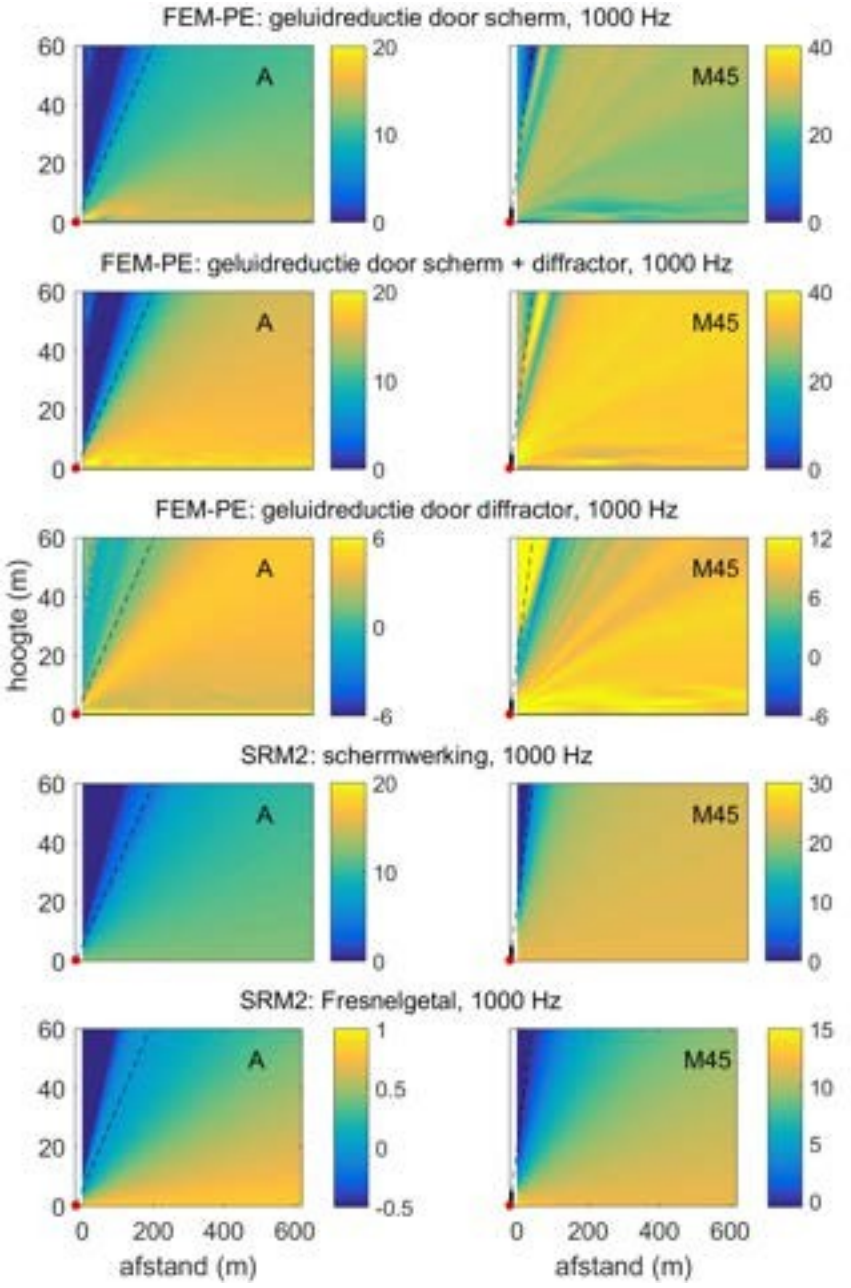


Figure 3.16 FEM-PE results for noise reduction due to the screen, Whiswall (screen and diffractor), and diffractor at 1000 Hz for scenarios A and M45, and SRM2 results for the screen effect and Fresnel number.

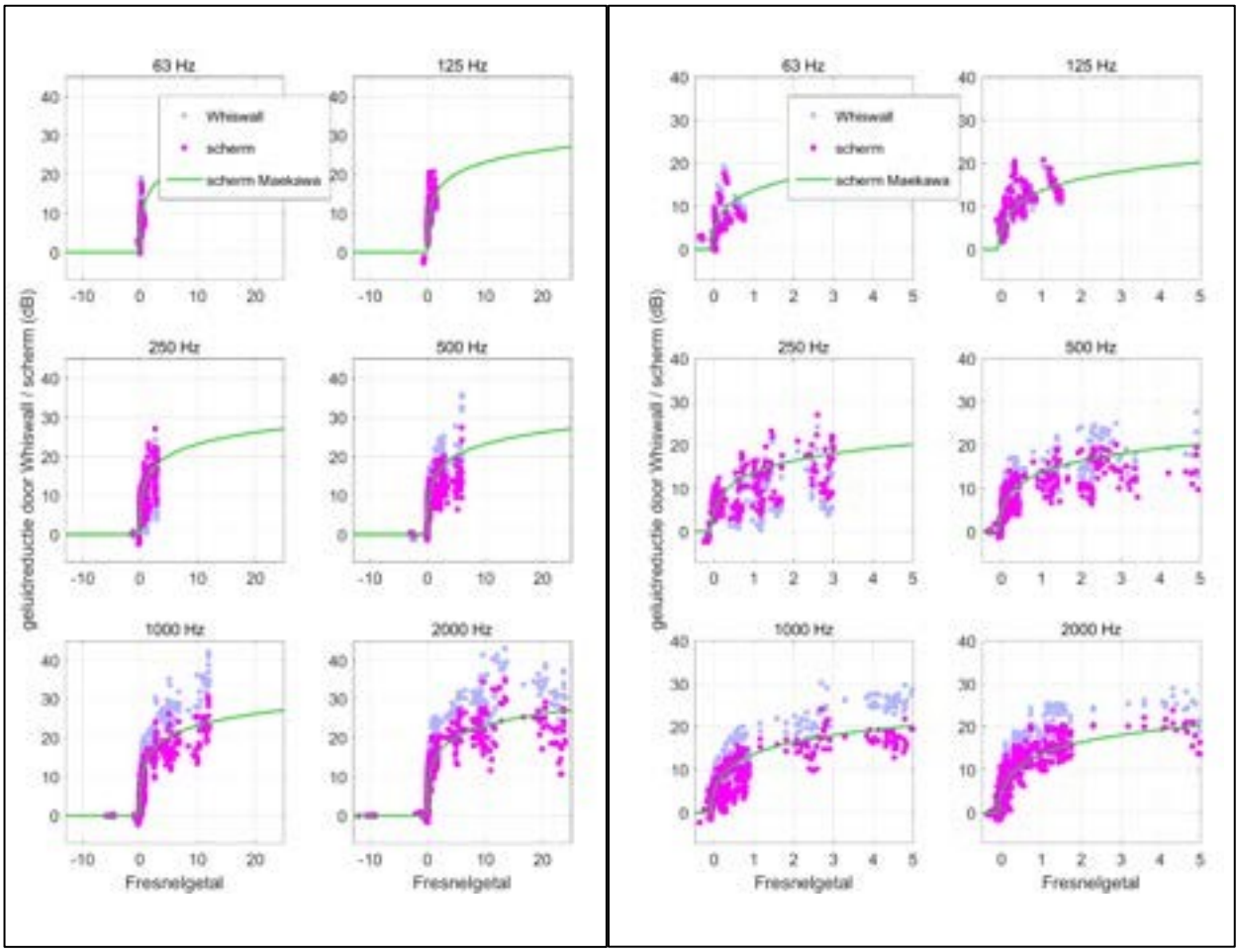


Figure 3.17 FEM-PE results for noise reduction by Whiswall / screen as a function of Fresnel number, for the 42 scenarios, with observers at distances of 100, 200, 300 and 500 m and heights of 2, 5 and 10 m. Left: all results. Right: zoomed in on Fresnel numbers between -0.5 and 5. Also shown is the screen effect according to Maekawa's formula.

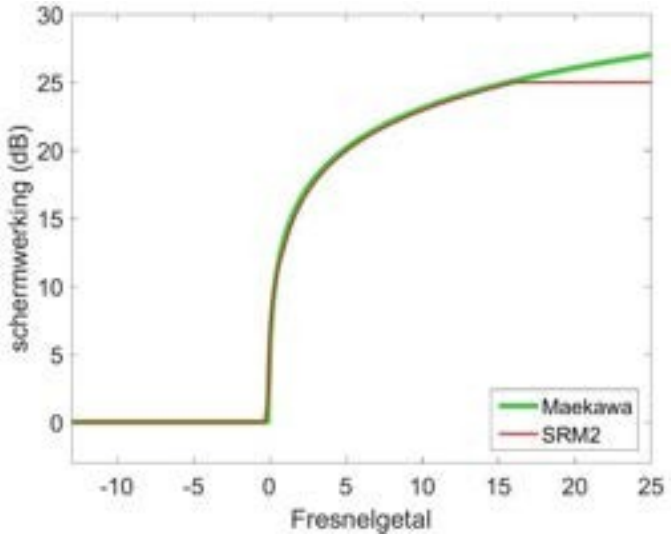


Figure 3.18 Screen effect as a function of Fresnel number according to SRM2 and Maekawa's formula.

Figure 3.19 shows FEM-PE results for noise reduction by the diffractor as a function of Fresnel number, for the 42 scenarios. Results for which the noise reduction by the screen or Whiswall are greater than 25 dB are shown as open circles. Also shown are $_{Adif}$ values from the diffraction test.

Figure 3.20 is as Figure 3.19, but now with version 1 of the calculation rule (green line):

$$_{CW} = 0.1\ _{Adif}\ D_{scherm}(NF), \qquad (3.4)$$

with

- $_{CW}$ the noise reduction by the diffractor (see Section 3.2),
- $D_{screen}(NF)$ the screen effect according to formula (3.3) of Maekawa,
- $_{Adif}$ the value of the "diffraction index difference" $\Delta DI$ [28].

This means that $_{CW}$ is calculated by scaling the screen effect according to Maekawa's formula with the value of $_{Adif}$ from the diffraction test, and a factor of 0.1. The values of $_{Adif}$ are in Figure 3.7 (blue circles).

As indicated earlier, the diffractor was developed for noise reduction at frequencies of about 400 Hz and above. In this study, the computational rule is limited to the five octave bands 125 - 2000 Hz. The results of the diffraction test are limited to this same frequency range. Thus, for 63, 4000, and 8000 Hz, $_{CW} = 0$.

The calculation rule describes the FEM-PE results reasonably well up to 1000 Hz, but at 2000 Hz the calculation rule gives lower values than calculated with FEM-PE. Interestingly, the noise reduction calculated with FEM-PE increases with the Fresnel number to values much larger than $_{Adif}$, at 1000 and 2000 Hz.

The next section describes an improvement (version 2) of the calculation rule.

[28] The notation $_{Adif}$ is used here because the notation $\Delta DI$ is confusing in mathematical formulas. In the scientific literature, the use of compound symbols like $\Delta DI$ for physical quantities is not recommended, to avoid confusion with multiplication.

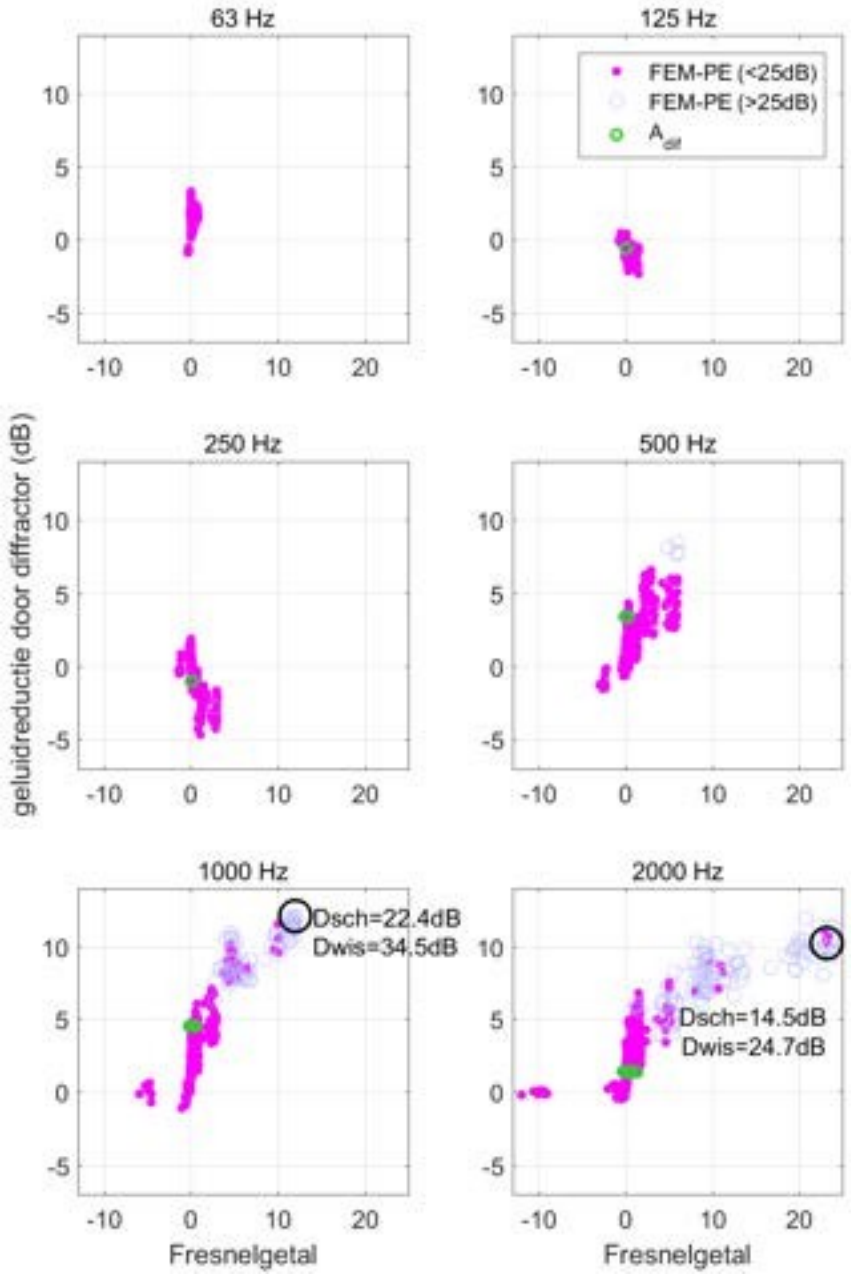


Figure 3.19 FEM-PE results for noise reduction by the diffractor as a function of Fresnel number, for the 42 scenarios. Results for which the noise reduction by the screen (Dsch) or the Whiswall (Dwis) are greater than 25 dB are shown as open purple circles. With the black circles, values of reductions by screen (Dsch) and Whiswall (Dwis) are given for scenario M45 (screen height 5 m), at distance 100 m and height 2 m. Also shown are the values of $_{Adif}$ from the diffraction test.

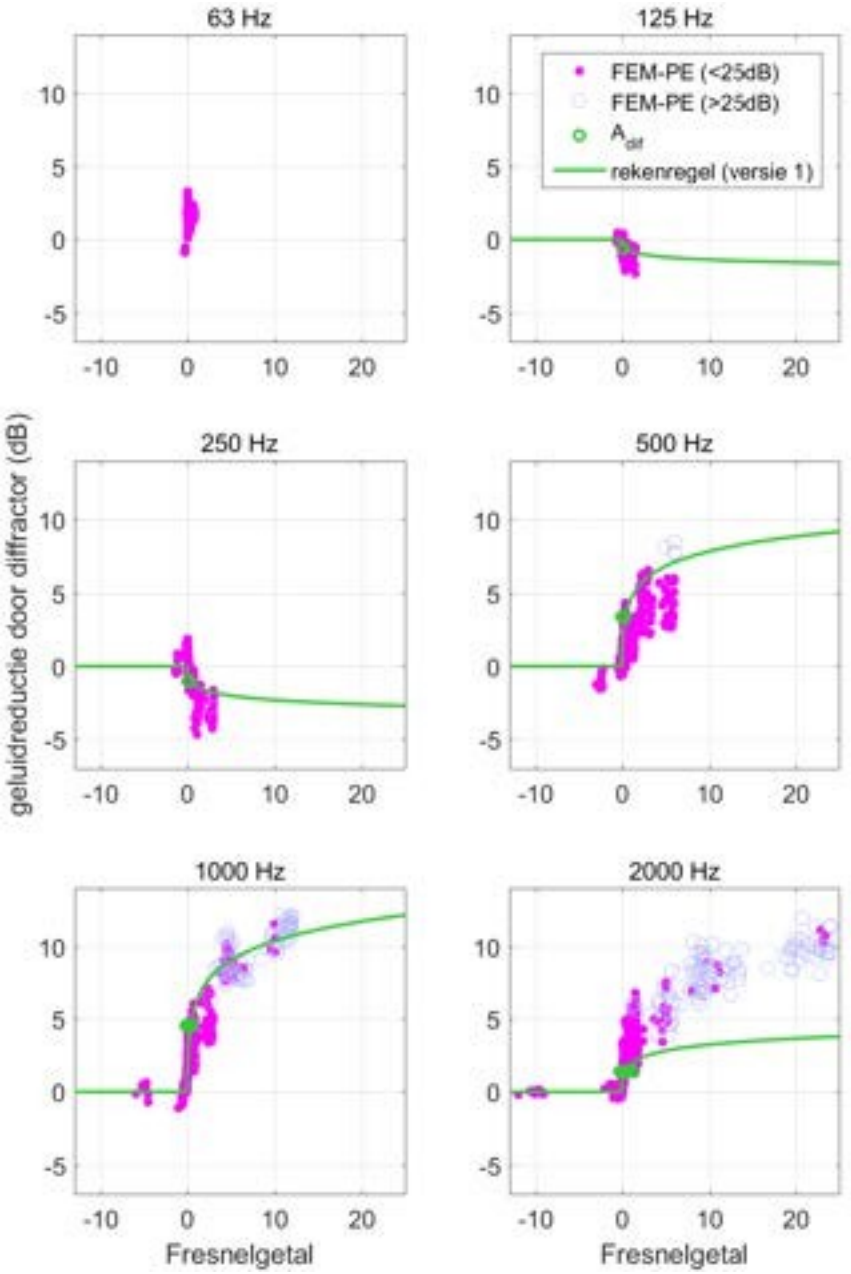


Figure 3.20 As Figure 3.19, but now with version 1 of the calculation rule (green line).

## 3.7 Diffraction test: linear means

To improve on the calculation rule from the previous section, we consider the diffraction test again. Instead of the *energetic* mean value $A_{dif}$, we now derive a *linear* mean value $A_{dif,lin}$ from the measurement results. The value of $A_{dif,lin}$ is used in Section 3.8 for version 2 of the calculation rule.

Figure 3.21 shows results of the measurements according to the diffraction test, as described in Section 3.3. This *does not include* averaging across the three source heights, five observer heights, and two angles. All results for the different combinations of source and observer are shown separately.

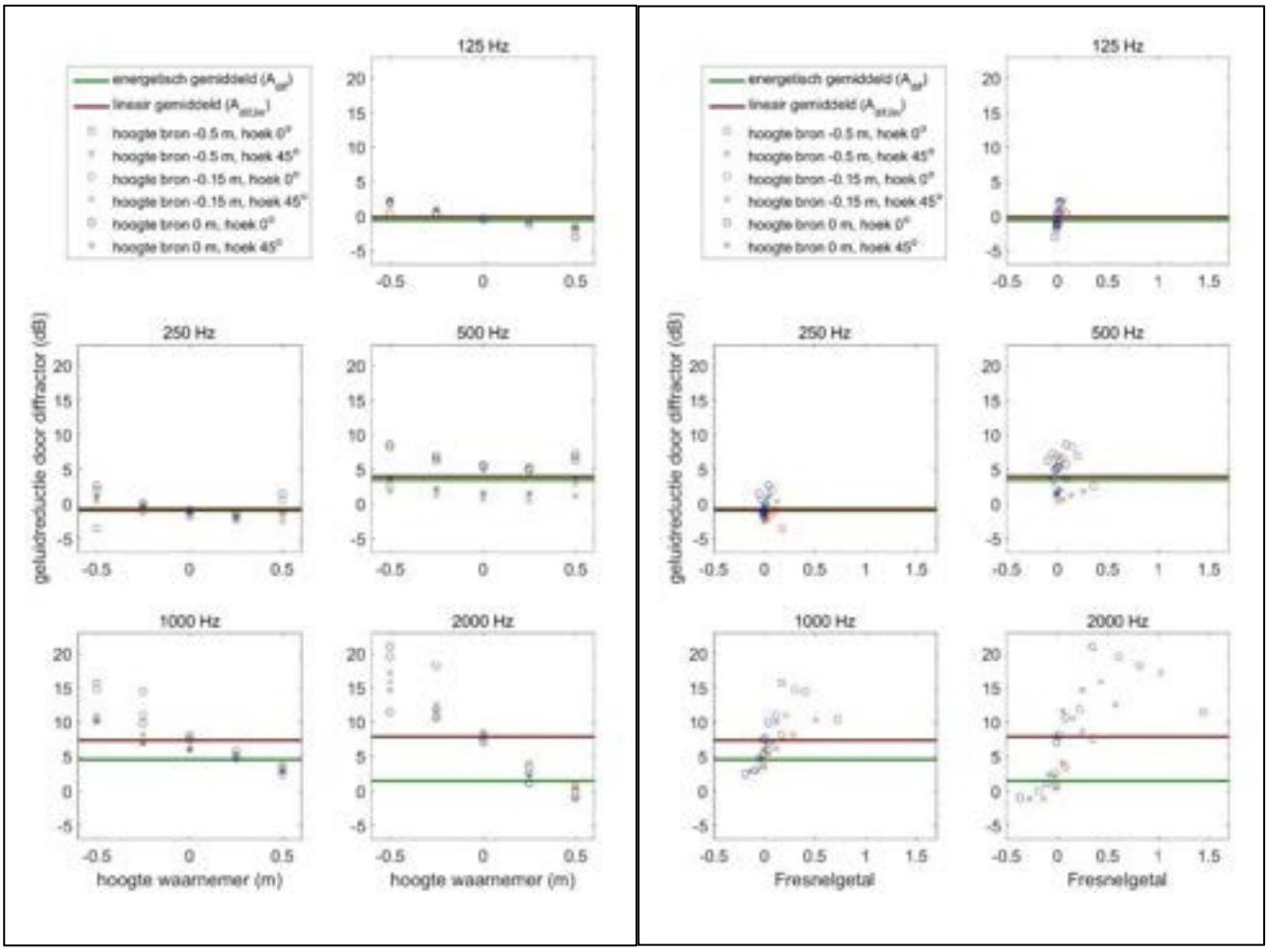


Figure 3.21 Measurement results for noise reduction by the diffractor in the diffraction test, as a function of observer height (left) and Fresnel number (right). Also shown are the energetic mean values ($A_{dif}$) and linear mean values ($A_{dif,lin}$).

The graphs on the left show the noise reduction by the diffractor as a function of observer height, for the three source heights and two angles. The graphs on the right show the noise reduction by the diffractor as a function of the Fresnel number.

This shows that also in the diffraction test, values of noise reduction by the diffractor occur that are significantly larger than the energetic mean value $A_{dif}$, represented by horizontal green lines in the graphs. This is particularly true for the frequencies 1000 and 2000 Hz.

The red horizontal lines in the graphs represent *linearly* averaged values of noise reduction by the diffractor, denoted as $A_{dif,lin}$. We calculate this quantity by linearly averaging the noise reductions for all 3x5x2=30 combinations of source and observer positions.

For frequencies 1000 and 2000 Hz, the value of $A_{dif,lin}$ is significantly larger than the value of $A_{dif}$. Table 3.1 gives the values, and also values calculated with FEM described in Section 3.9.

Table 3.1 Values of $A_{dif}$ and $A_{dif,lin}$, based on the results of measurements and calculations according to the diffraction test.

| frequency (Hz) | 125 | 250 | 500 | 1000 | 2000 |
|---|---|---|---|---|---|
| **measurement** | | | | | |
| energetic average, $A_{dif}$ (dB) | -0.6 | -1.0 | 3.4 | 4.5 | 1.4 |
| linear average, $A_{dif,lin}$ (dB) | -0.2 | -0.8 | 4.0 | 7.3 | 7.8 |
| **calculation** | | | | | |
| energetic average, $A_{dif}$ (dB) | -0.9 | -1.0 | 3.3 | 4.3 | 1.5 |
| linear average, $A_{dif,lin}$ (dB) | -0.6 | -0.7 | 3.6 | 7.6 | 7.8 |

## 3.8 Calculation Rule, version 2

In Section 3.6, we presented version 1 of the computational rule. The graphs in Figure 3.20 showed that version 1, based on $A_{dif}$, provides reasonable agreement with the FEM-PE results. In this section, we present version 2 of the computational rule, based on $A_{dif,lin}$ described in Section 3.7.

Figure 3.22 is as Figure 3.20, but now version 2 of the calculation rule is used (green line):

$$_{CW} = 0.05\ A_{dif,lin}\ D_{scherm}(N_F). \qquad (3.5)$$

So we replaced $A_{dif}$ with $A_{dif,lin}$ and replaced the coefficient 0.1 with 0.05.

Version 2 of the calculation rule gives a good representation of the results from FEM-PE for the frequencies 500, 1000, and 2000 Hz. At 125 and 250 Hz, the negative values are slightly less well represented according to FEM-PE than with version 1 of the calculation rule.

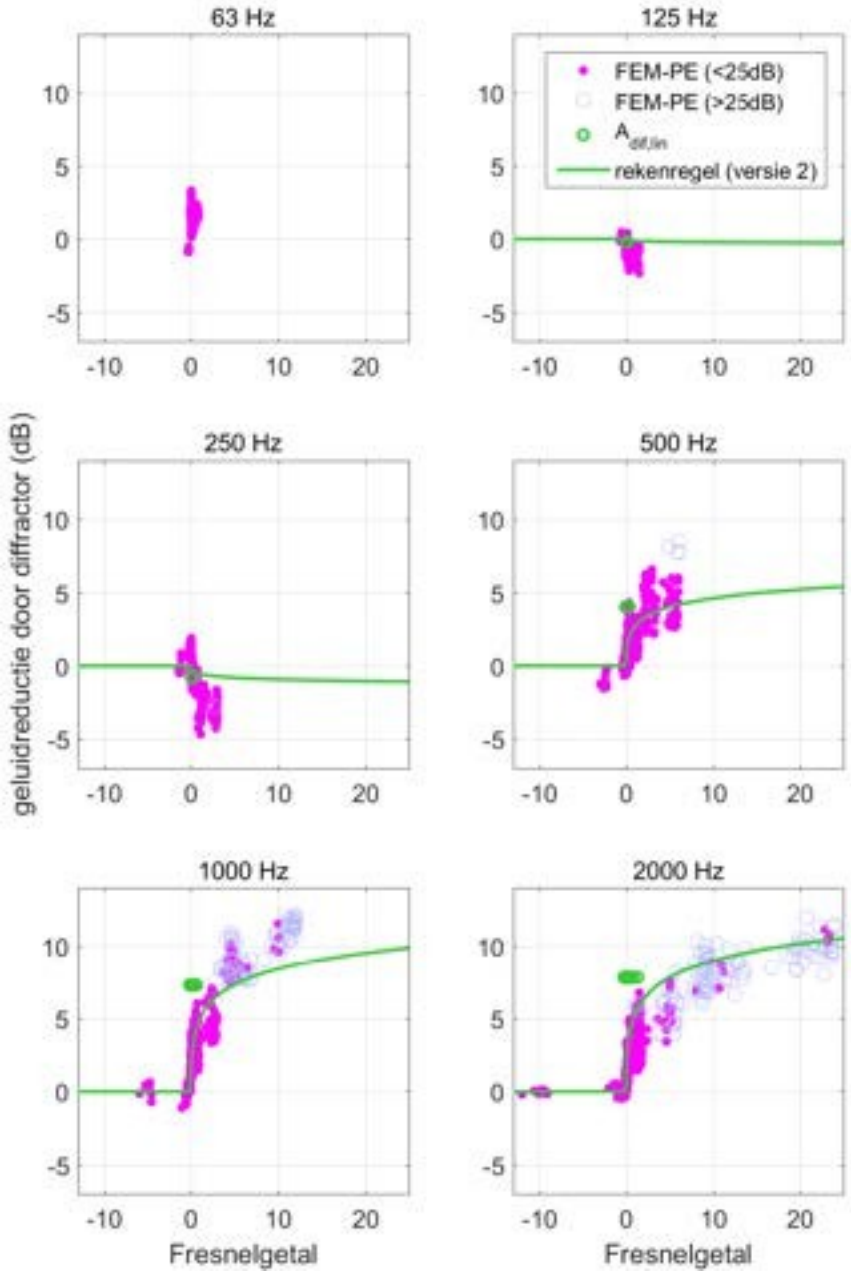


Figure 3.22 As Figure 3.20 but now with version 2 of the calculation rule.

## 3.9 Calculations with FEM for the diffraction test

The previous two sections have shown that using the linear mean quantity $A_{dif,lin}$ leads to an improved computational rule. To gain more insight into the diffraction test of the Whiswall, here we consider results of calculations with FEM for the diffraction test, and compare them with the measurement results.

As already indicated in Section 3.3, in a previous [study7] we analyzed measurements and calculations of the Whiswall diffraction test. This found good agreement between the energetically averaged measurement and calculation results.

Figure 3.23 shows the FEM results from this earlier study, now shown as a function of Fresnel number, in the same way as in Figure 3.21 with measurement results. The calculation results show approximately the same progression with frequency and Fresnel number as the measurement results. The energetic and linear mean values are given in Table 3.1. The values differ at most 0.4 dB off from the values according to the measurements.

Figure 3.24 shows the measurement results versus the calculation results for the 3x5x2=30 combinations of source and observer positions. Also shown are the energetic and linear mean values. The graphs show that the points lie around the diagonal, meaning that there is good agreement between the measurement results and the computational results. For octave band 500 Hz, the deviations from the diagonal are the largest.

The right section of Figure 3.23 shows FEM results for a more extensive collection of microphone heights in the diffraction test:

-3.5, -3.25, -3.0, ..., 2.75, 3.0 m

instead of

-0.5, -0.25, 0.0, 0.25, and 0.5 m.

In this way we get a better impression of the gradient with Fresnel number at 250 and 125 Hz. At 250 Hz, the noise reduction by the diffractor varies between -3 and +5 dB. At 125 Hz, the noise reduction varies between -2 and +7 dB.

The long-range FEM-PE results (see Figure 3.22) show mostly negative noise reductions for 125 and 250 Hz. At 250 Hz, the noise reduction ranges between -4 and +1 dB, and at 125 Hz between -2 and 0 dB.

A relevant question here is what values of the Fresnel number occur in practice. The answer to this question is shown in Figure 3.22, which shows which Fresnel numbers occur for the different scenarios, with the restriction to the grid of twelve observer positions shown in Figure 3.15.
For clarity, Figure 3.25 shows the values of the Fresnel number at 250 and 1000 Hz, for four scenarios. The Fresnel number scales linearly with frequency, so values at other frequencies can be easily derived from the graphs.

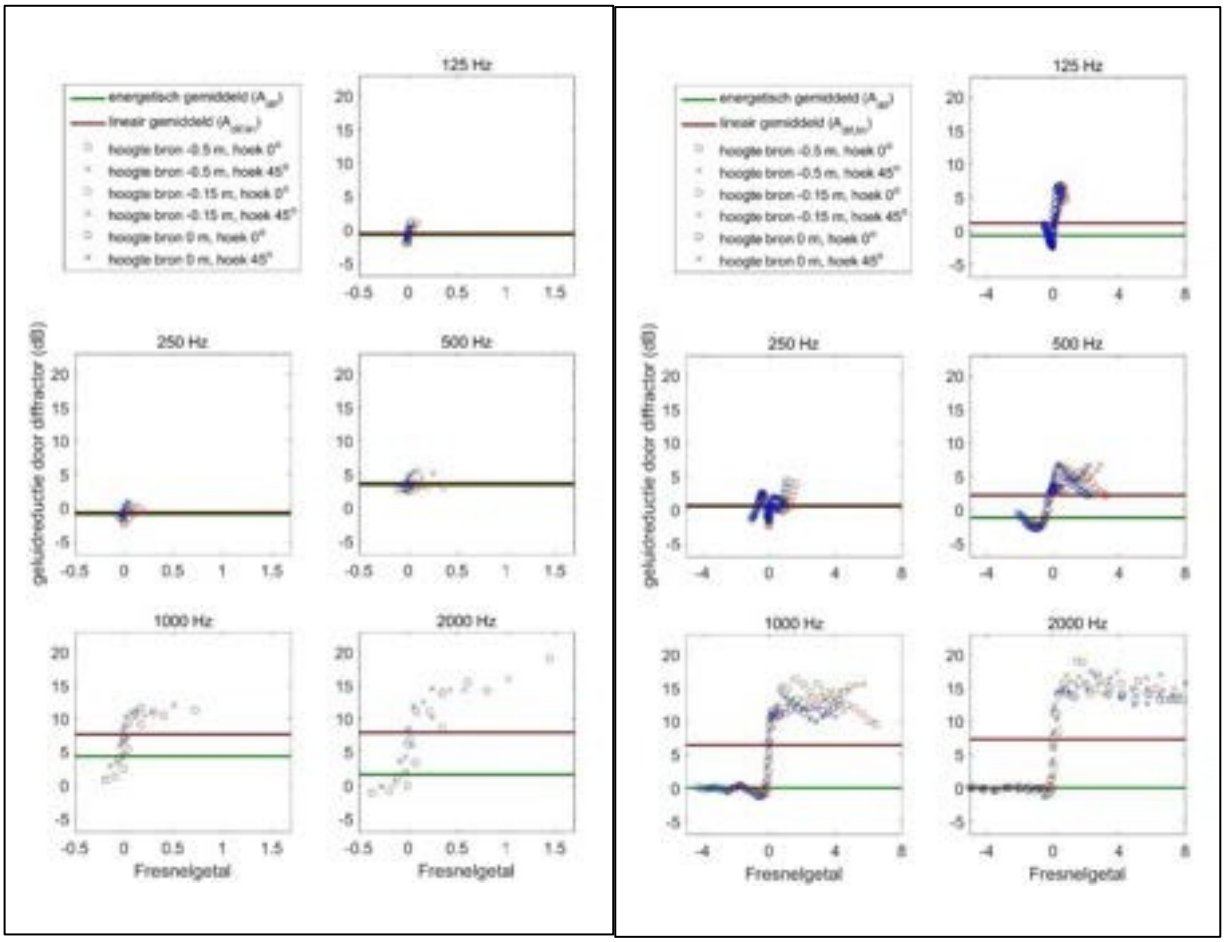


Figure 3.23 Left: as Figure 3.21 but now based on the results of the calculations with FEM for the diffraction test. Right: same, but now with microphone heights of -3.5, -3.25, ..., 3.5 m instead of -0.5, -0.25, ..., 0.5 m.

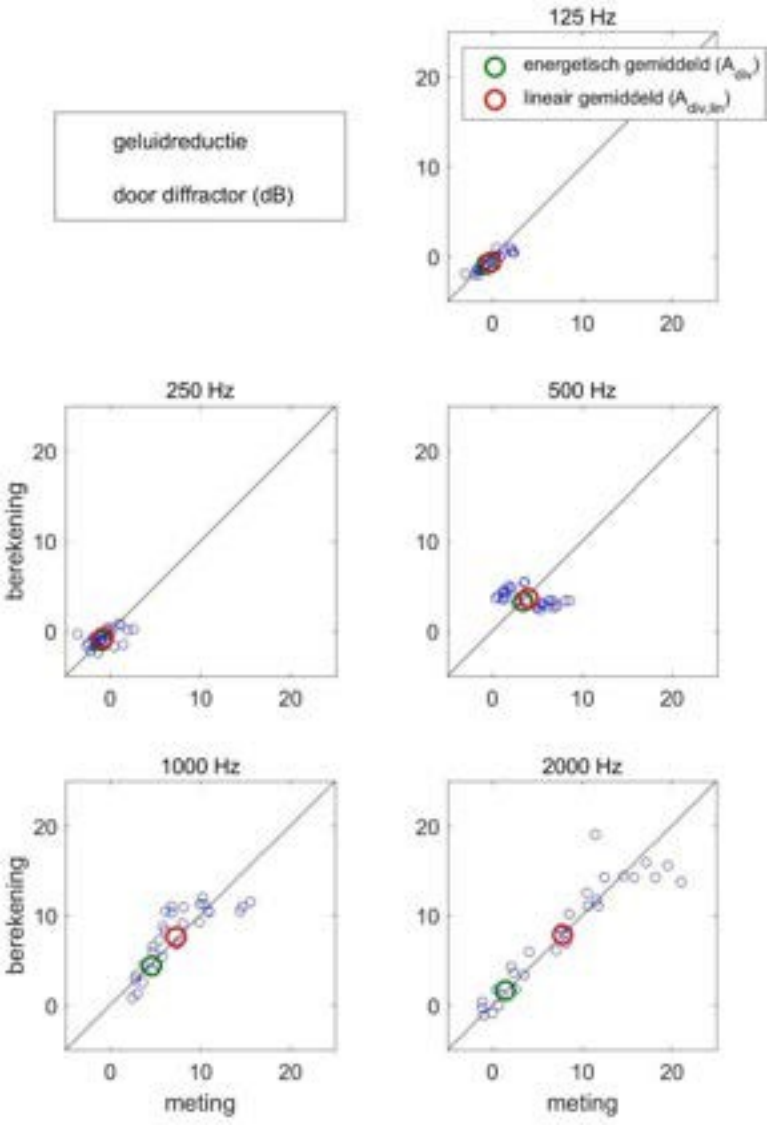


Figure 3.24 Measurement results versus calculation results for noise reduction by the diffractor in the diffraction test, for the 3x5x2=30 combinations of source and observer positions (blue circles). Also shown are the energetic mean values ($A_{dif}$) and linear mean values ($A_{dif,lin}$).

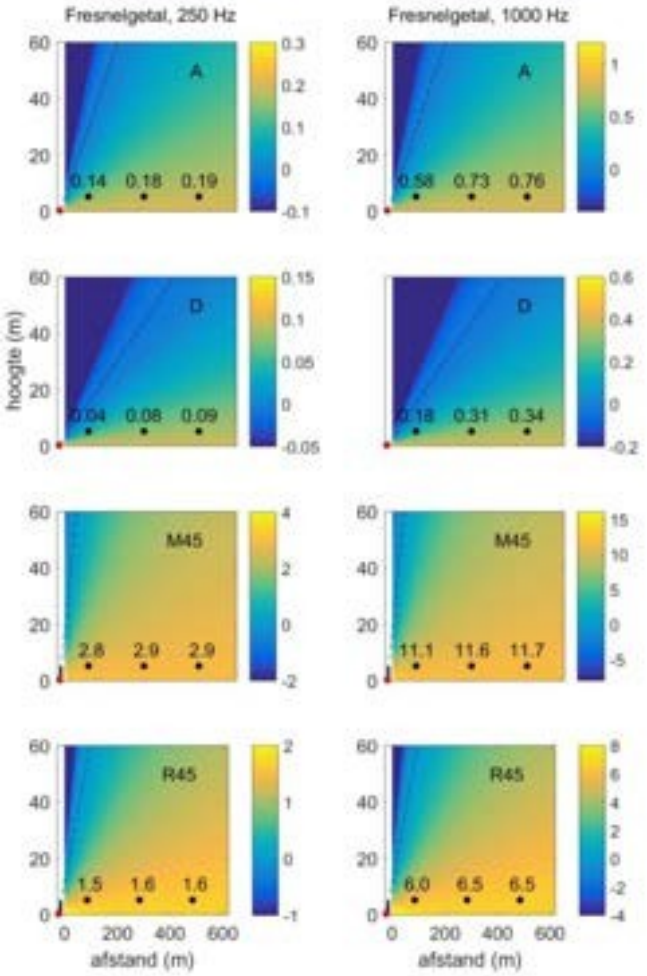


Figure 3.25 Fresnel number values at 250 Hz (left) and 1000 Hz (right), for scenarios A, D, M45, and R45. Numerical values at 5 m height and distances 100, 300, and 500 m are shown.

## 3.10 Calculation Rule, version 3

Version 2 of the calculation rule underestimates the *gain* due to the diffractor at 250 Hz, and to a lesser extent at 125 Hz (see Figure 3.22). This is undesirable, especially since the noise at 250 Hz often determines broadband levels behind noise barriers (see Section 2.4). The problem at 250 Hz does not occur with version 3 of the computational rule:

$$C_W = \begin{cases} 0.2_{A(dif,lin)} D_{scherm}(N)_f & \text{for 125 and 250 Hz} \\ 0.05_{A(dif,lin)} D_{scherm}(N)_f & \text{for 500, 1000, 2000 Hz} \end{cases} \quad (3.6)$$

Thus, a different coefficient is used here for 125 and 250 Hz than for 500-2000 Hz. Figure 3.26 is as Figure 3.22, but now with version 3 of the calculation rule (green line). The agreement with the FEM-PE results is now better for 250 Hz.

Version 3 of the calculation rule can also be formulated in a different way:

$$C_W = \begin{cases} 0.2 A di_{f,lin} D_{scherm}(N)_f & \text{if } A_{dif,lin} < 0 \\ 0.05 A di_{f,lin} D_{scherm}(N_f) & \text{as } A_{dif,lin} \geq 0 \end{cases} \quad (3.6a)$$

This formulation has the advantage that in principle it also works for a diffractor with more and/or deeper resonant slots, so that the noise reduction effect of the diffractor is not limited to 500-2000 Hz but also occurs at 250 Hz (i.e., if $A_{dif} > 0$ at 250 Hz). In Chapter 4, we describe the analysis of such a low-frequency diffractor. Results of the computational rule are compared with results of calculations with FEM-PE for the low-frequency diffractor.

Appendix D presents some additional graphs comparing results from FEM-PE with results from version 3 of the computational rule. This also shows that there is good agreement between FEM-PE and version 3 of the calculation rule.

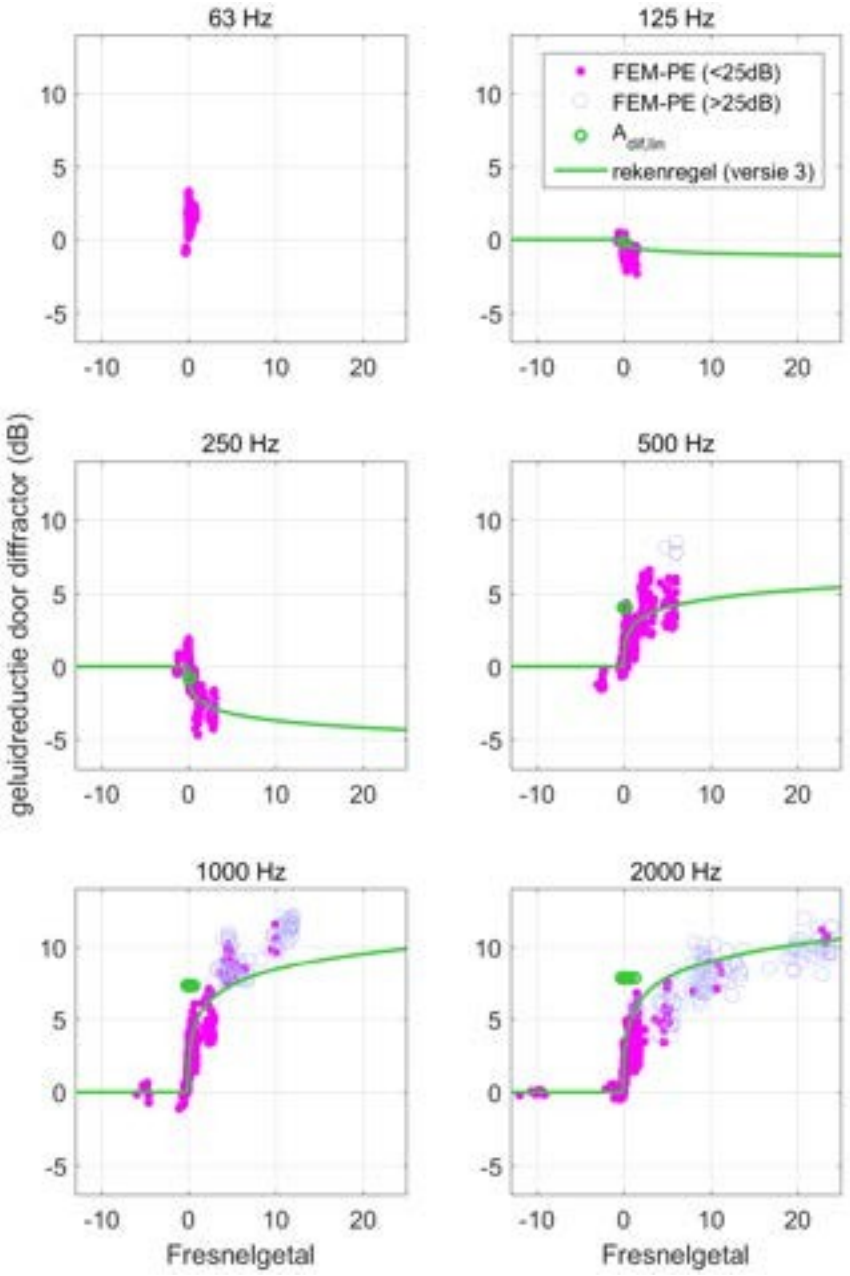


Figure 3.26 As Figure 3.22, but now with version 3 of the calculation rule.

### 3.11 Calculation Rule, version 4

For even better agreement with FEM-PE results, one can further adjust the coefficients of the calculation rule. This was done in version 4 of the calculation rule:

$$C_W = K A_{dif,lin} D_{scherm} (N)_f \tag{3.7}$$

with coefficient $K$ varying with frequency as follows:

- *K*= 0.7 for 125 Hz,
- *K*= 0.2 for 250 Hz,
- *K*= 0.05 for 500 and 1000 Hz,
- *K*= 0.04 for 2000 Hz.

Figure 3.27 is as Figure 3.22, but now with version 4 of the calculation rule (green line). The agreement with the FEM-PE results is good for all octave bands.

The values of *K* were determined by "" the computational rule per octave band to the FEM-PE results. In Chapter 4, the values are determined via numerical minimization of the difference between FEM-PE results and the computational rule. The values found are also compared with those above.

Version 4 has the disadvantage that, in principle, it is valid only for the diffractor for which the computational rule was developed. For an alternative diffractor, with different values of $A_{dif,lin}$, different values of coefficient *K* are needed. This aspect is considered in more detail in Chapter 4.

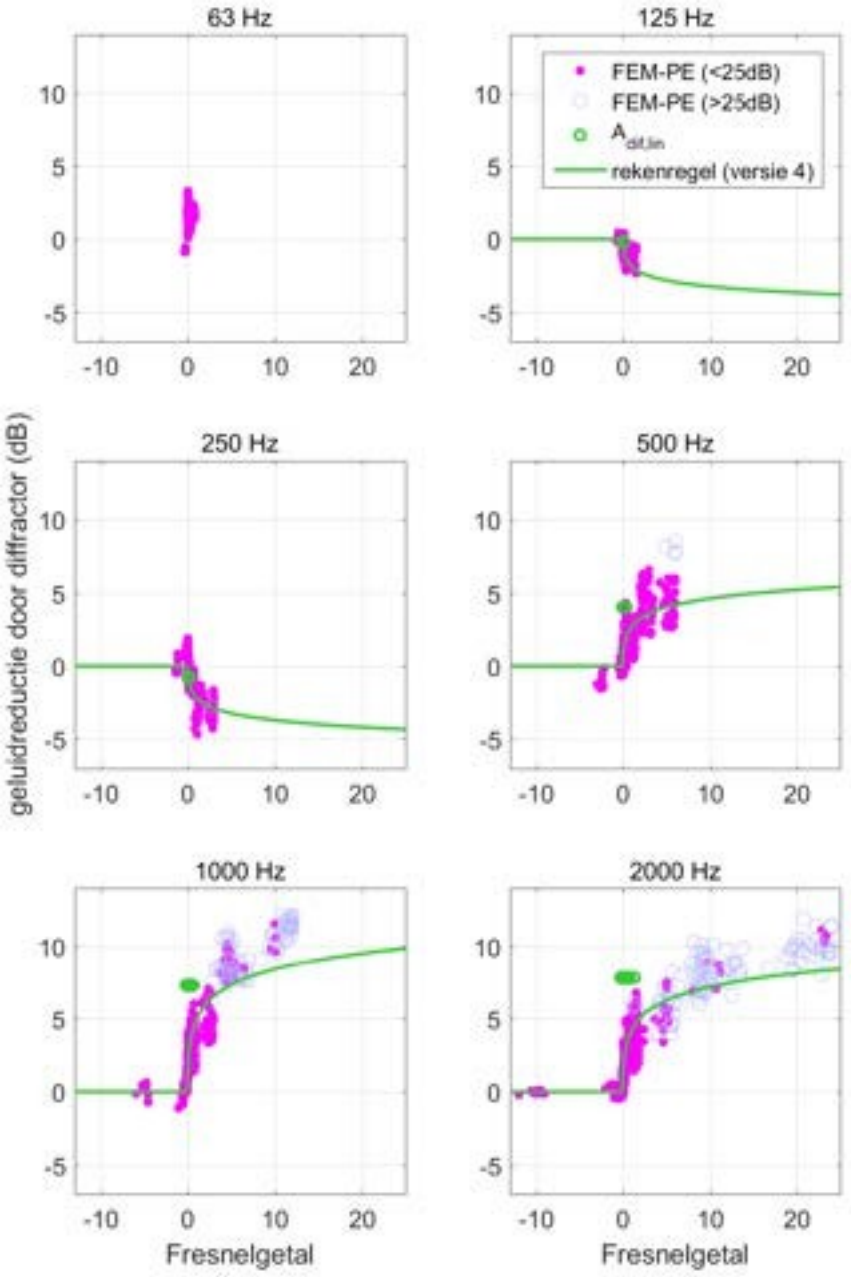


Figure 3.27 As Figure 3.22, but now with version 4 of the calculation rule.

## 3.12 Conclusions of chapter 3

Based on results of numerical calculations with FEM-PE for a large number of scenarios, we have developed a calculation rule with which the noise reduction due to the Whiswall diffractor can be calculated. The calculation rule is suitable for method SRM2 of the Noise Calculation and Measurement Regulations. In the with FEM-PE, observer distances up to 600 m behind the Whiswall were considered.

We have developed four versions of the computational rule, versions 1-4, with increasing accuracy. Version 3 has the advantage of being formulated in such a way that, in principle, it is also valid for diffractors with other product properties. Version 4 is slightly more accurate for the Whiswall diffractor.

The computational rule is formulated as a product of two quantities:
- a quantity representing the product properties of the diffractor,
- The screen effect according to Maekawa's formula.

Maekawa's formula gives the screen effect as a function of the Fresnel number, which is determined by the positions and heights of the source, diffractor, and observer. As a result, the computational rule satisfies the acoustic principle of reciprocity.

The product properties of the diffractor are represented in the four different versions of the calculation rule by two quantities, $A_{dif}$ and $A_{dif,lin}$. These quantities are determined from measurements according to the diffraction test.
Magnitude $A_{dif}$ is hereby determined according to the usual way of energetic averaging, while for magnitude $A_{dif,lin}$ is linearly averaged over the different positions of source and microphone in the diffraction test.

The calculation rule works in octave bands, as calculation method SRM2 works in octave bands. We also converted the results of the calculations with FEM-PE to broadband noise reductions, weighted by a typical
A-weighted traffic noise spectrum. This showed that the broadband noise reduction is often limited, due to a spectral shift caused by the screen effect. While the A-weighted traffic noise spectrum has a maximum around 1000 Hz, that maximum behind a noise screen is often lower, typically at 250 Hz. At 250 Hz, however, the noise reduction effect of the diffractor is negative for most of the scenarios studied.

It would therefore be beneficial to develop a Whiswall with a diffractor that has a noise-reducing effect even at 250 Hz. In the course of this research, company 4Silence created a design of such a low-frequency diffractor (LF diffractor). The slots in the diffractor have been modified to expect greater noise reduction at 250 Hz.

In Chapter 4, we describe an analysis of this LF diffractor. Results from FEM-PE are used to investigate whether the computational rule (version 3 or 4) also works for the LF diffractor.

# 4 LF diffractor; further analysis and optimization

In this section we describe results of calculations with FEM and FEM-PE for a low-frequency diffractor (LF diffractor). The results are used for further analysis and optimization of the calculation rule (versions 3 and 4) from chapter 3.

## 4.1 Dimensions of the LF- diffractor

The LF diffractor was designed by company *4Silence*[29]. It consists of 15 slots with different depths and widths, as shown in Figure 4.1. Figure 4.2 shows schematically how the LF diffractor is placed at a $13^{o}$ angle on a screen, with the original diffractor on the screen (Whiswall) also shown for comparison. The original diffractor consists of 38 slots.

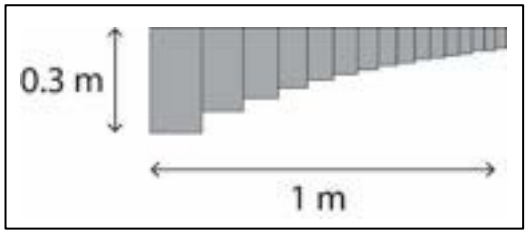


Figure 4.1 Dimensions of the 15 slots of the LF diffractor.

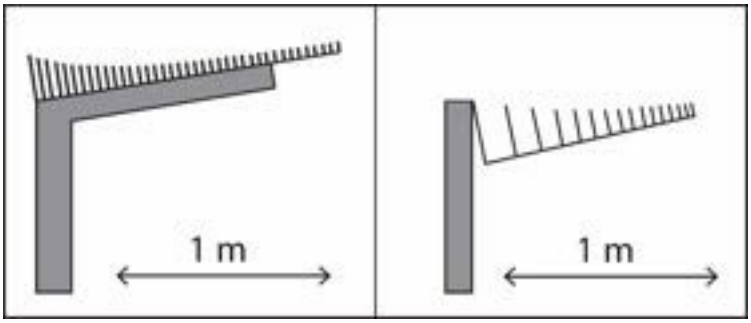


Figure 4.2 Schematic representation of the Whiswall showing the 38-slot diffractor (left), and the 15-slot LF diffractor on a vertical screen (right).

## 4.2 Calculations with FEM for the diffraction test of the LF- diffractor

Calculations for the LF diffractor were performed with FEM to simulate the diffraction test. Figure 4.3 shows as an example the sound field around the LF diffractor as calculated with FEM at 325 Hz. The computational grid with the finite elements of the FEM model is also shown. Figure 4.4 shows the calculated sound field at
345 Hz, represented in two ways: by the sound pressure in Pascal and by the sound pressure level in dB. The shielding by the screen and diffractor is visible.

[29] No physical design has been made so far. The design is still only a specification of dimensions.

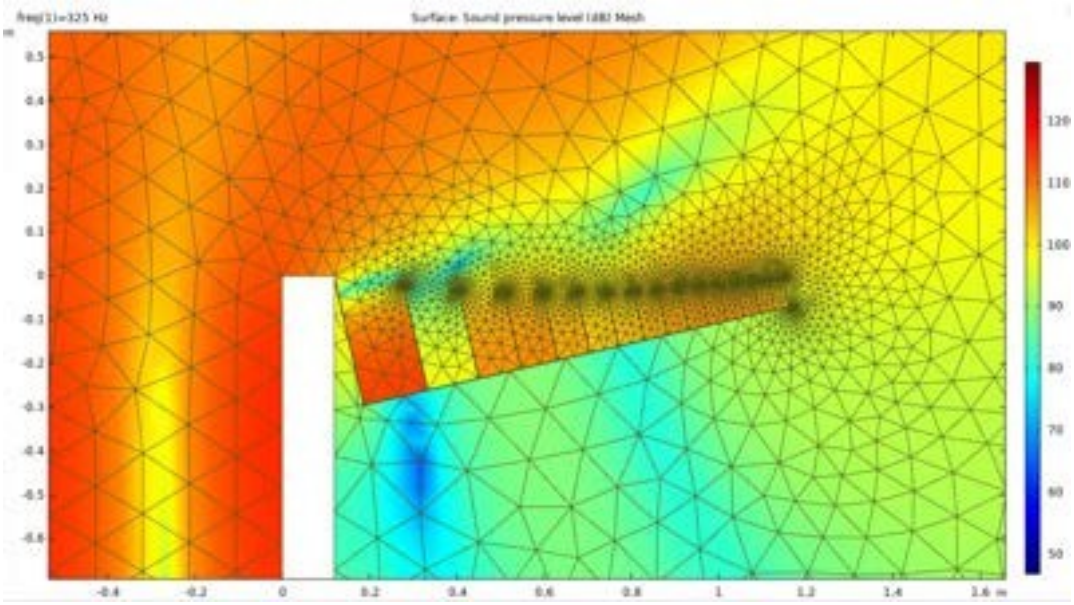

Figure 4.3 Sound level at 325 Hz calculated with FEM for the LF diffractor. The FEM calculation grid is also shown.

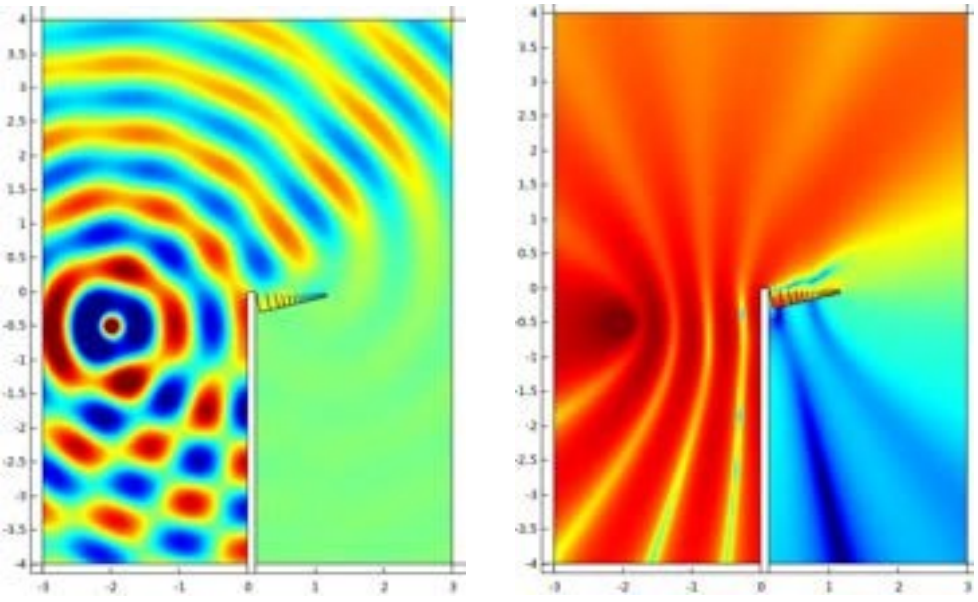

Figure 4.4 Result of calculation with FEM for the LF diffractor, at 345 Hz. On the left the sound pressure in Pascal, on the right the sound pressure level in dB. The source is located 2 m to the left of the diffractor.

Figure 4.5 shows the result of the FEM calculation of the diffraction test for both the original Whiswall diffractor and the LF diffractor. Shown are third-band spectra of the diffraction index difference $\Delta DI$ (relative to a straight screen). The points in the graphs represent the results for the 3x2x5=30 combinations of source and receiver positions. The lines represent the average values $A_{dif}$, energetically averaged in the manner according to the NEN-EN standard 1793-4 and as described in section 3.3. The graphs show that at the third band 250 Hz, $A_{dif}$ is negative for the original diffractor and positive for the
LF diffractor.

Figure 4.6 shows the octave band spectra of the diffraction index difference ΔDI. The value of $_{Adif}$ at the octave band 250 Hz is negative for the original diffractor and positive for the LF diffractor. The values for the original diffractor correspond to the values in Table 3.1 ("Calculation, energetically averaged").

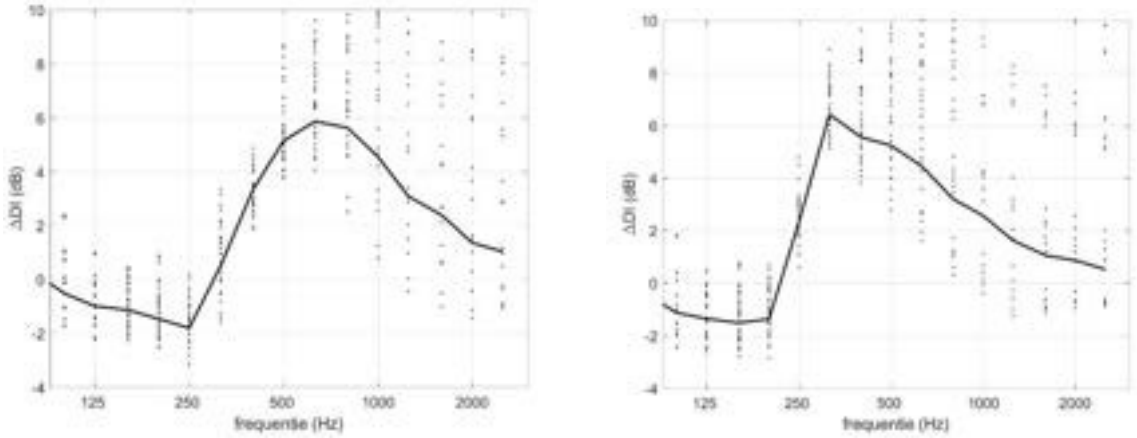


Figure 4.5 Results of calculations with FEM for the diffraction test, for the original Whiswall diffractor (left) and the LF diffractor (right). Shown are third-band spectra of the diffraction index difference ΔDI. The lines represent the energetic mean values $_{Adif}$.

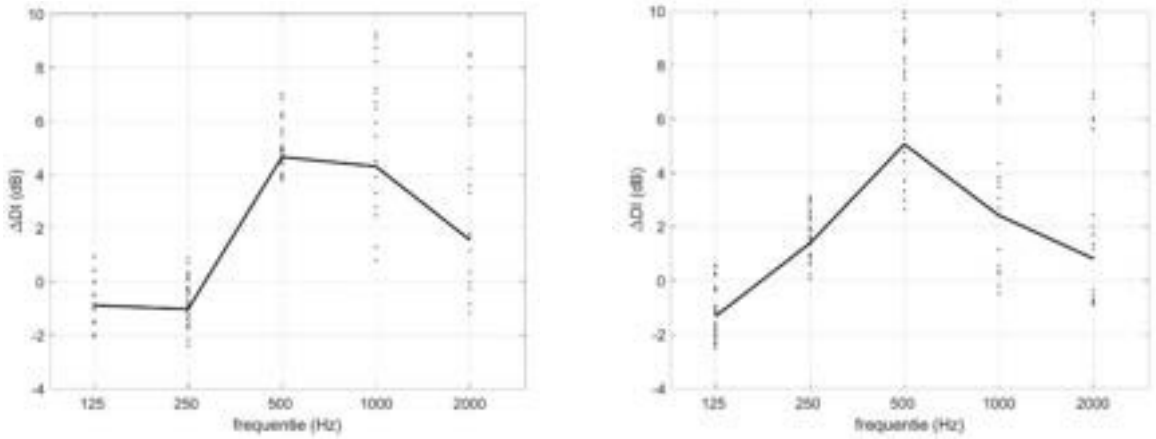


Figure 4.6 Octave band spectra corresponding to the third-band spectra in Figure 4.5.

For the analysis and optimization of the computational rule, described later in this chapter, we values of $_{Adif,lin}$. The values of $_{Adif,lin}$ are calculated by linear averaging over the 30 combinations of source and receiver positions (see Section 3.7). The resulting values are given in Table 4.1, in thirds and in octaves, both for the original diffractor and for the
LF diffractor.

Table 4.1 Values of $_{Adif,lin}$ calculated with FEM for the original diffractor and the LF diffractor. The values are based on results for three source heights (-0.5, -0.15, and 0 m), two angles (0° and 45°), and five receiver heights (-0.5 -0.25, 0, 0.25, 0.5 m). Negative values are in blue, positive values in red.

| frequency (Hz) | 125 | 250 | 500 | 1000 | 2000 |
|---|---|---|---|---|---|
| **original diffractor** | | | | | |
| $_{Adif,lin}$ (dB), octaves | -0.6 | -0.7 | 3.6 | 7.6 | 7.8 |
| $_{Adif,lin}$ (dB), thirds | -0.2/-0.7/-0.9 | -1.1/-1.5/0.9 | 0.9/5.8/6.9 | 7.3/8.2/7.9 | 8.1/7.7/7.9 |
| **LF diffractor** | | | | | |
| $_{Adif,lin}$ (dB), octaves | -1.0 | 1.7 | 6.5 | 6.8 | 6.2 |
| $_{Adif,lin}$ (dB), thirds | -0.8/-1.1/-1.2 | -1.0/2.5/6.8 | 6.4/6.6/6.6 | 6.6/7.0/7.1 | 6.7/6.3/5.7 |

As indicated in Section 3.3, the source height 0 m was added in the diffraction test, in addition to the source heights -0.5 and -0.15 m according to the standard. To the influence of this on $_{Adif,lin}$, we present in Table 4.2 the values of $_{Adif,lin}$ calculated from the two source heights -0.5 and -0.15 m. The differences from the values in Table 4.1 are small (typically 0 to 0.3 dB). For further analysis, we assumed the values in Table 4.1.

Table 4.2 As Table 4.1, but now with values of $_{Adif,lin}$ calculated from results for **two** source heights (-0.5 and -0.15 m), two angles (0° and 45°), and five receiver heights (-0.5 -0.25, 0, 0.25, 0.5 m).

| frequency (Hz) | 125 | 250 | 500 | 1000 | 2000 |
|---|---|---|---|---|---|
| **original diffractor** | | | | | |
| $_{Adif,lin}$ (dB), octaves | -0.6 | -0.9 | 3.6 | 7.9 | 8.3 |
| $_{Adif,lin}$ (dB), thirds | -0.2/-0.7/-0.9 | -1.2/-1.7/0.7 | 0.7/6.0/7.2 | 7.6/8.5/8.2 | 8.6/8.1/8.6 |
| **LF diffractor** | | | | | |
| $_{Adif,lin}$ (dB), octaves | -1.0 | 1.5 | 6.7 | 7.0 | 6.4 |
| $_{Adif,lin}$ (dB), thirds | -0.8/-1.1/-1.2 | -1.2/2.3/7.0 | 6.6/6.9/6.9 | 6.6/7.2/7.3 | 7.0/6.6/5.8 |

## 4.3 Calculations with FEM-PE for 8 scenarios with the LF- diffractor

In section 2.3, we described 42 scenarios for calculations with FEM-PE up to 600 m distance. For 8 of the 42 scenarios, we repeated the calculations for the LF diffractor. These are the following 8 scenarios from Table 2.1:

C, F, M45, R45, V, W, MM45, and XX45.

These scenarios are shown in Table 4.3. The 8 scenarios have differences in the following parameters: source height, screen height, source-screen distance, and angle θ (0 or 45°).

Table 4.3 Copy of Table 2.1, showing the 8 scenarios for which calculations were made with FEM-PE for the LF diffractor are implemented.

| hoogte bron $z_s$ (m) | hoogte scherm $z_s$ (m) | bodem weg/spoor | bodem 1 | bodem 2 | afstand van bron naar scherm $x_s$ (m) 3.5 | 5 | 7 | 10 | 15 | 25 | hoek $\theta$ (gr) | wind (m/s) | aantal |
|---|---|---|---|---|---|---|---|---|---|---|---|---|---|
| 0.1 | 1.1 | hard | gras | gras | C | | F | | I | | 0 | 4.6 | 3 |
| 0.5 | | | | | H | | G | | J | | | | 3 |
| 2 | | | | | | | | | | | | | |
| 4 | | | | | | | | | | | | | |
| 0.1 | 1.1 | hard | gras | gras | | C45 | | F45 | | | 45 | 4.6 | 2 |
| 0.5 | | | | | | H45 | | G45 | | | | | 2 |
| 2 | | | | | | K45 | | | | | | | 1 |
| 4 | | | | | | L45 | | | | | | | 1 |
| 0.1 | 5 | hard | gras | gras | | M45 | | R45 | | | 45 | 4.6 | 2 |
| 0.5 | | | | | | N45 | | S45 | | | | | 2 |
| 2 | | | | | | P45 | | T45 | | | | | 2 |
| 4 | | | | | | Q45 | | U45 | | | | | 2 |
| 0.1 | 1.1 | hard | hard | gras | B | | E | | | | 0 | 4.6 | 2 |
| | | | | hard | A | | D | | | | | | 2 |
| | | | | | | | | | | | | | 24 |
| 1.1 | 1.1 | hard | gras | gras | V | | W | | Y | | 0 | 4.6 | 3 |
| | | | | | | V45 | | W45 | | | 45 | | 2 |
| 0.1 | 1.1 | ballastbed | gras | gras | CB | | | | | | 0 | 4.6 | 1 |
| 1.1 | | hallenbed | | | VB | | | | | | | | 1 |
| 0.1 | 3 | hard | gras | gras | | MM45 | | | | XX45 | 45 | 4.6 | 2 |
| | | | | hard | | MMH45 | | | | XXH45 | | | 2 |
| 0.1 | 5 | hard | gras | gras | | | | | | X45 | 45 | 4.6 | 1 |
| | | | | hard | | MH45 | | | | XH45 | | | 2 |
| 0.5 | 1.1 | hard | gras | gras | HW | | GW | | | | 0 | 2.3 | 2 |
| | | | | | HZ | | GZ | | | | | 0 | 2 |
| | | | | | | | | | | | | | 42 |

## 4.4 Analysis and optimization of the computational rule

Based on the results of the calculations for the original diffractor and the LF diffractor, we performed a further analysis and optimization of version 3 of the calculation rule described in Chapter 3. In doing so, we created a large number of graphs, which are included in Appendices E and F. Below we provide a brief summary of the results and conclusions.

Appendix E contains graphs for an analysis of noise reduction by the *screen* (without diffractor). These graphs show the spread of results from FEM-PE around the prediction according to Maekawa and SRM2. Here we again use the results of FEM-PE for 12 receivers, at distances 100, 200, 300, 500 m, and heights 2, 5, 10 m. We find a significant spread of FEM-PE around Maekawa and SRM2.
We also examined whether the dispersion becomes smaller if we assume receiver heights of 5, 10, and 15 m instead of 2, 5, and 10 m. The idea was that the soil would then a less disturbing influence. This turns out not to be significantly the case: the dispersion remains about the same. Here the dispersion is represented by the deviation of Maekawa and SRM2, in two ways:

- $\delta_{rms}$= the rms value of the difference in noise reduction between FEM-PE and Maekawa or SRM2,
- $\delta$= the noise reduction according to Maekawa or SRM2 minus the noise reduction according to FEM-PE.

The values of $\delta_{rms}$ and $\delta$ are given in the graphs.

Appendix F contains graphs for an analysis of the noise reduction by the diffractor, for both the original diffractor and the LF diffractor. In doing so, we are also

assumed the two choices for receiver heights: i) 2, 5, 10 m, and ii) 5, 10, 15 m. In each case, the graphs also show the prediction of the computational rule (green lines). We initially assumed version 3 of the calculation rule, with fixed values of 0.2 and 0.05 for the coefficient; see formula (3.6a). The coefficient (or factor) is denoted by the symbol F. For version 3:

- F= 0.2 for $A_{dif,lin} < 0$,
- F= 0.05 for $A_{dif,lin} \geq 0$.

We compared the FEM-PE results with the computational rule both for third-band and octave bands. We again represented the deviation from the arithmetic rule in two ways:

- $\delta_{rms}$= the rms value of the difference in diffractor effect between FEM-PE and the computational rule,
- $\delta$= the diffractor effect according to the calculation rule minus the diffractor effect according to FEM-PE.

The values of $\delta_{rms}$ and $\delta$ are given in the graphs.

We then also performed equations optimizing the coefficients F of the calculation rule for each third-band such that the value of $\delta_{rms}$ is minimal. The optimized values of F are shown in Figures 4.7 and 4.8. The values of F, $\delta_{rms}$ and $\delta$ are also shown in tables in the Appendix.

Figures 4.7 and 4.8 show that one could slightly modify the calculation rule (version 3) from Chapter 3, by choosing the coefficient for $A_{dif,lin} < 0$ slightly smaller, for example:

- F= 0.15 for $A_{dif,lin} < 0$,
- F= 0.05 for $A_{dif,lin} \geq 0$.

In this way, the computational rule remains "generally" valid, that is, for both the original diffractor and the LF diffractor, with values of F depending only on the sign of $A_{dif,lin}$.

If one prefers a computational rule with values of F that vary with the octave band (as in version 4 in Chapter 3), one could choose a value lower than 0.05 for the octave bands 1000 and 2000 Hz, for example, 0.04 for 1000 Hz and and and 0.03 for 2000 Hz[30].

Appendix F also contains graphs illustrating that for distances of 30-50 m instead of 100-500 m, the agreement between FEM-PE and the calculation rule is similar. Here, for the calculation rule with optimization of F, the interval 100-500 m was assumed for optimization.

We also conclude that the choice between receiver heights 2, 5, 10 m and 5, 10, 15 m yields no significant difference. Furthermore, the advantage of computing via the thirds appears to be nil.

[30] The values of 0.04 and 0.03 are 20% and 40% smaller than 0.05, respectively. These differences are significantly larger than the differences in $A_{dif,lin}$ that occur when using only two source heights in the diffraction test instead of three source heights (see Section 4.2).

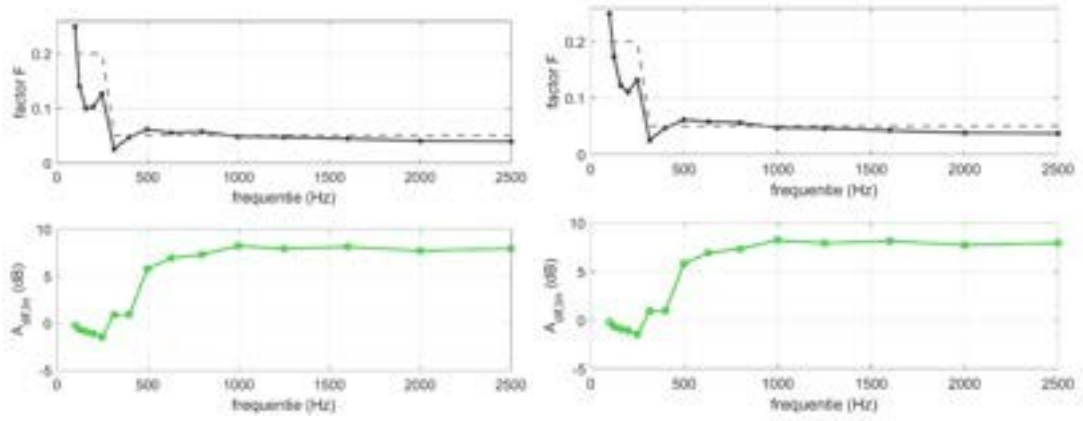


Figure 4.7 Values of the coefficients F determined via optimization (see Figure F.2 in Appendix F), for the original diffractor. The broken lines represent the values 0.2 and 0.05 from Chapter 3. Also shown (green line) are the corresponding values of $A_{dif,lin}$.

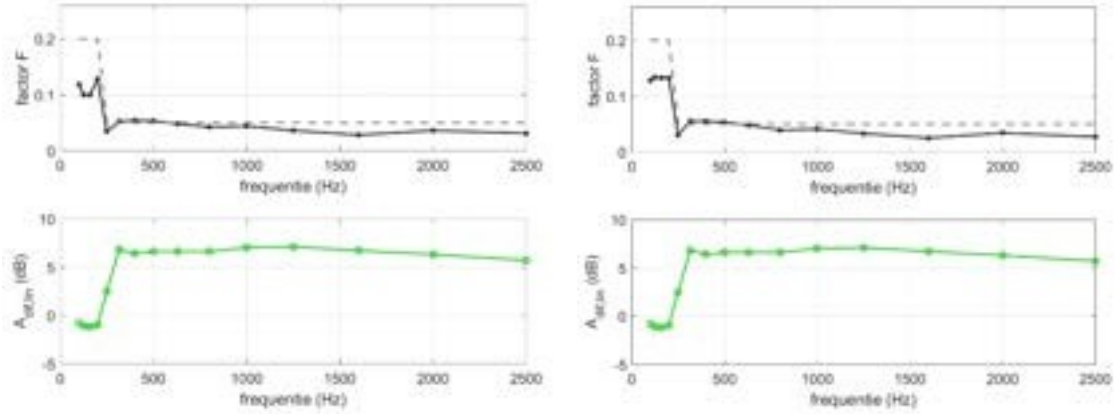


Figure 4.8 As Figure 4.7, for the LF diffractor.

## 4.5 Conclusions of chapter 4

Based on the analysis in this chapter, we conclude that the computational rule (version 3) developed for the original diffractor also works well for the LF diffractor. Based on an optimization, we found that the coefficient for $A_{dif,lin} < 0$ could be slightly smaller: 0.15 instead 0.2. With this, the computational rule becomes as follows:

$$C_W = \begin{cases} 0.15 A_{dif,lin} D_{scherm}(N_f) & \text{as } A_{dif,lin} < 0 \\ 0.05 A_{dif,lin} D_{scherm}(N_f) & \text{as } A_{dif,lin} \geq 0 \end{cases} \quad (4.1)$$

If one prefers a calculation rule with values of F that vary with the octave band (version 4), one choose a value lower than 0.05 for the octave bands 1000 and 2000 Hz, for example, 0.04 for 1000 Hz and and 0.03 for 2000 Hz.

The calculation rule works well for the original diffractor and for the LF diffractor. The calculation rule is formulated for octave bands. A calculation via third-bands yields no significant improvement in accuracy. The calculation rule also appears to

work well for smaller distances, 30 to 50 m, rather than the distances 100-500 m on which the development of the calculation rule is based.

# 5 Conclusions

In this study, we developed a calculation rule that can be used to calculate the noise reduction provided by the Whiswall diffractor. The calculation rule also works well for an alternative diffractor, which provides greater noise reduction at the low frequency 250 Hz (LF diffractor). The mathematical form of the calculation rule is given in Section 4.5 of this report.

The development is based on results of calculations with the numerical calculation model FEM-PE. The calculations with FEM-PE considered observer distances from 30 to 600 m behind the Whiswall.

The computational rule is formulated as a product of two quantities:

- a quantity representing the product properties of the diffractor,
- The screen effect according to Maekawa's formula.

Maekawa's formula gives the screen effect as a function of the Fresnel number, which is determined by the positions and heights of: i) the source, ii) the diffractor, and
(iii) the observer. The product properties of the diffractor are represented by quantity $A_{dif,lin}$. This quantity is determined from measurements according to the diffraction test. This involves linear averaging over the different positions of source and microphone. In this study, three source heights were assumed, while the noise standard for the diffraction test assumes two source heights. The effect of this difference is small.

The calculation rule is suitable for the standard SRM2 calculation method of the Noise Calculation and Measurement Regulations. The calculation rule works in octave bands, as SRM2 is formulated in octave bands. We investigated whether a calculation via third-band results in a more accurate calculation rule, since the effect of the diffractor varies greatly with frequency. This was found to be the case; the computational rule did not become significantly more accurate by a calculation via third-bands.

# A Broadband noise reduction through the diffractor

To calculate the A-weighted broadband noise reductions, we use a spectrum of road traffic noise described in Appendix B. We use here the spectrum expressed in octave bands, for 63-2000 Hz. This spectrum is intended to determine the broadband noise reduction by an object (such as a noise barrier along a road).

The broadband noise reduction due to the diffractor, denoted $_{Ddiffractor}$, is calculated as follows:

$$D_{diffractor}=L_{\ scherm}-L_{\ Whiswall}$$

with

$$L_{scherm}= 10log_{\ 10}(\sum_{i=1}^{6} 10^{(\Delta Lsc_{herm,i}+L_{\ verkeer,i})/10})$$

$$L_{Whiswall}= 10log_{\ 10}(\sum_{i=1}^{6} 10^{(\Delta_{LWhiswall,i}+L_{\ verkeeer,i})/1010})$$

Herein is

- *Ltraffic*$_{,i}$ the octave band spectrum for traffic noise,
- *ΔLscreen*$_{,i}$ the noise level calculated with FEM-PE for the situation with the screen,
- *ΔLWhiswall*$_{,i}$ the sound level calculated with FEM-PE for the situation with the Whiswall.

Summing is performed over the six octave bands from 63 Hz ($i$= 1) to 2000 Hz ($i$ = 6).

The noise levels *ΔLshield*$_{,i}$ and *ΔLWhiswall*$_{,i}$ calculated with FEM-PE represent all influences of propagation on the traffic noise spectrum: screen effect, ground attenuation, and refraction. In the situation with the Whiswall, the effect of the diffractor is also represented. The calculations with FEM-PE assume an omni-directional source with a flat spectrum.

# B Spectrum of road traffic noise

In calculating the A-weighted broadband noise reductions (see Appendix A), a representative spectrum of road traffic noise is used.

A third-band spectrum of road traffic noise according to European standard EN [1793-331] is assumed for this purpose. This is shown in Figure B.1 (blue line), with all levels increased by 120 dB.

From this spectrum we determined an octave band spectrum, which is also shown in the graph (red line). Here, the value for 63 Hz was determined by extrapolation. The octave band spectrum is also given in Table B.1.

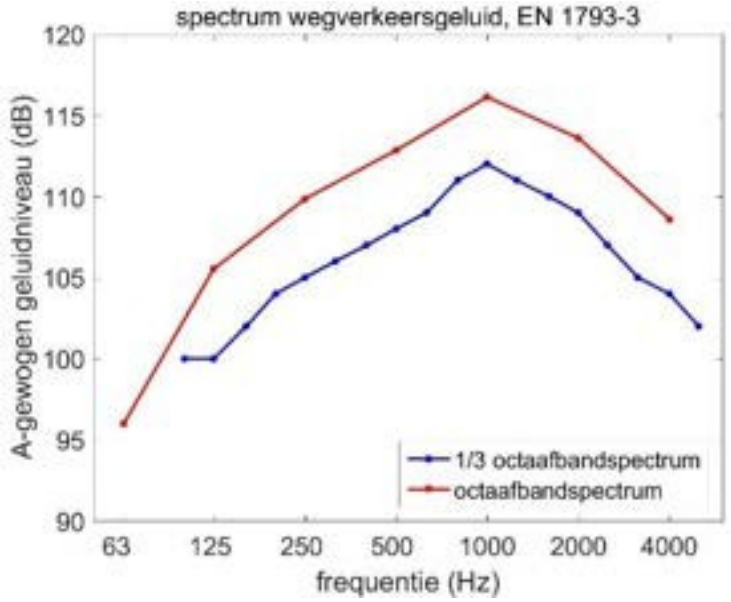


Figure B.1 Spectrum of road traffic noise, based on EN 1793-3.

Table B.1 Octave band spectrum of road traffic noise, based on EN 1793-3.

| Frequency (Hz) | 63 | 125 | 250 | 500 | 1000 | 2000 | 4000 |
|---|---|---|---|---|---|---|---|
| A-weighted sound level (dB) | 96.0 | 105.5 | 110.0 | 112.8 | 116.0 | 113.6 | 108.6 |

[31] European standard prEN 1793-3, "Road traffic noise reducing devices - Test method for determining the acoustic performance - Part 3 : Normalized traffic noise spectrum".

# C Broadband results from FEM-PE

This appendix presents broadband FEM-PE results for all the 42 scenarios.

The graphs show the broadband A-weighted noise reduction by the diffractor. Here, the A-weighted spectrum of traffic noise from Appendix B was used. The calculation is described in Section 2.4 and Appendix A.

The 42 graphs are in the order described in Section 2.4:

- 10 scenarios A-J,
- 14 scenarios C45-U45,
- 18 scenarios V-GZ.

In the graphs, the line of sight is shown as a black line. Above each graph, the parameters from Table 2.1 are given (with distance $x_b$ between source and screen, source height $z_b$, and screen height $z_s$).

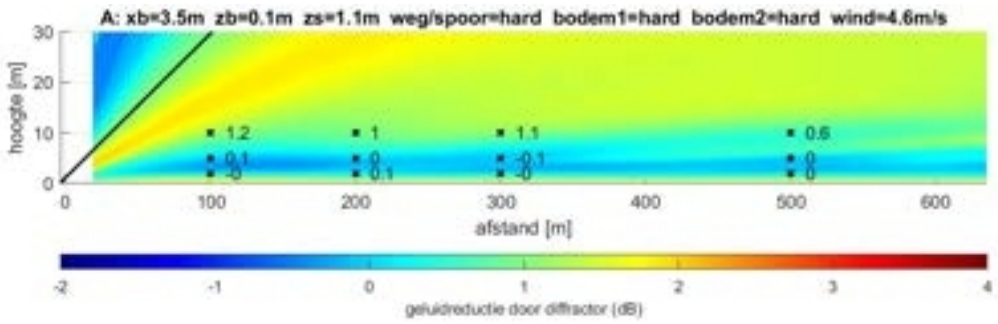
A: xb=3.5m zb=0.1m zs=1.1m weg/spoor=hard bodem1=hard bodem2=hard wind=4.6m/s
hoogte [m]
afstand [m]
geluidreductie door diffractor (dB)

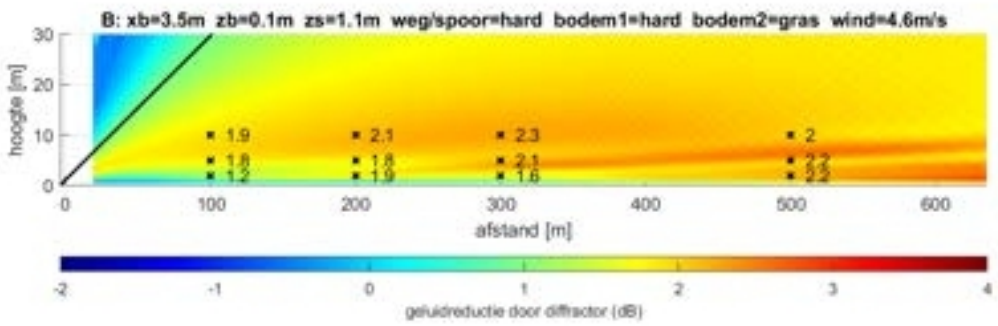
B: xb=3.5m zb=0.1m zs=1.1m weg/spoor=hard bodem1=hard bodem2=gras wind=4.6m/s
hoogte [m]
afstand [m]
geluidreductie door diffractor (dB)

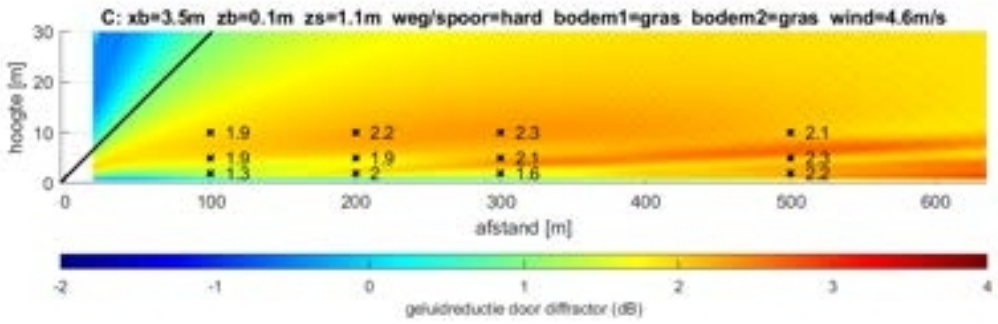
C: xb=3.5m zb=0.1m zs=1.1m weg/spoor=hard bodem1=gras bodem2=gras wind=4.6m/s
hoogte [m]
afstand [m]
geluidreductie door diffractor (dB)

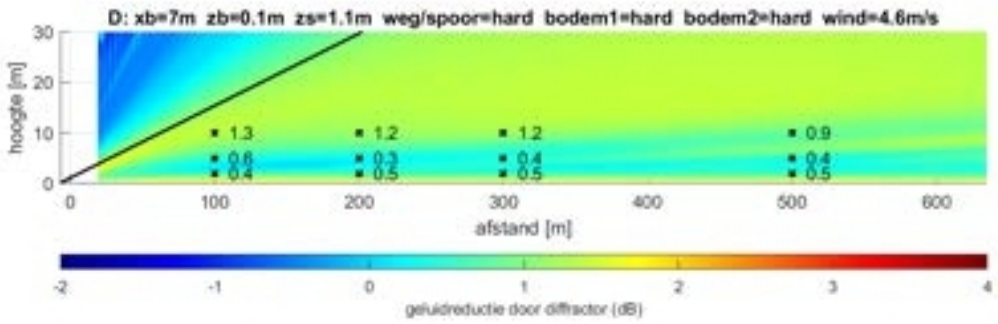
D: xb=7m zb=0.1m zs=1.1m weg/spoor=hard bodem1=hard bodem2=hard wind=4.6m/s
hoogte [m]
afstand [m]
geluidreductie door diffractor (dB)

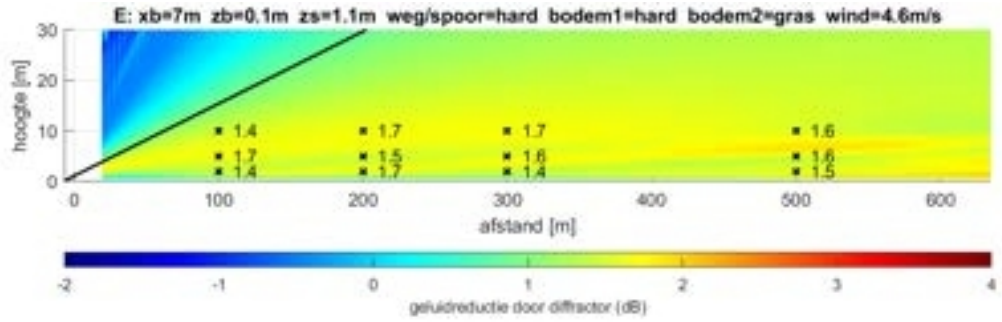
E: xb=7m zb=0.1m zs=1.1m weg/spoor=hard bodem1=hard bodem2=gras wind=4.6m/s
hoogte [m]
afstand [m]
geluidreductie door diffractor (dB)

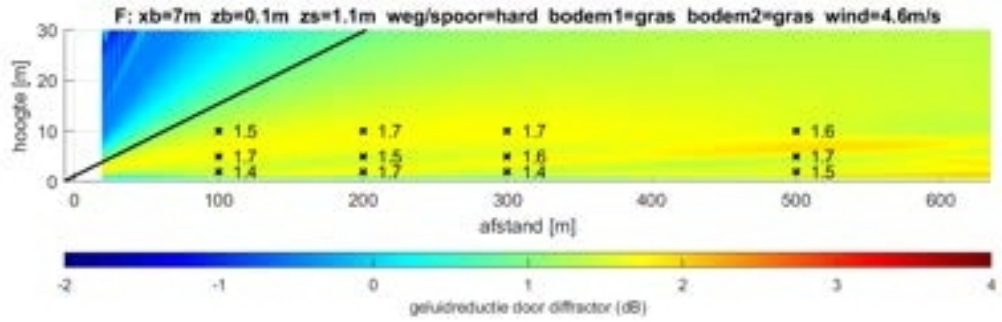
F: xb=7m zb=0.1m zs=1.1m weg/spoor=hard bodem1=gras bodem2=gras wind=4.6m/s
hoogte [m]
afstand [m]
geluidreductie door diffractor (dB)

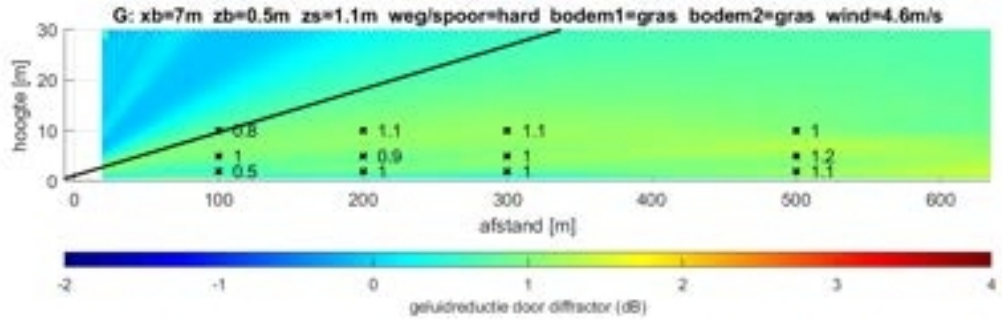
G: xb=7m zb=0.5m zs=1.1m weg/spoor=hard bodem1=gras bodem2=gras wind=4.6m/s
hoogte [m]
afstand [m]
geluidreductie door diffractor (dB)

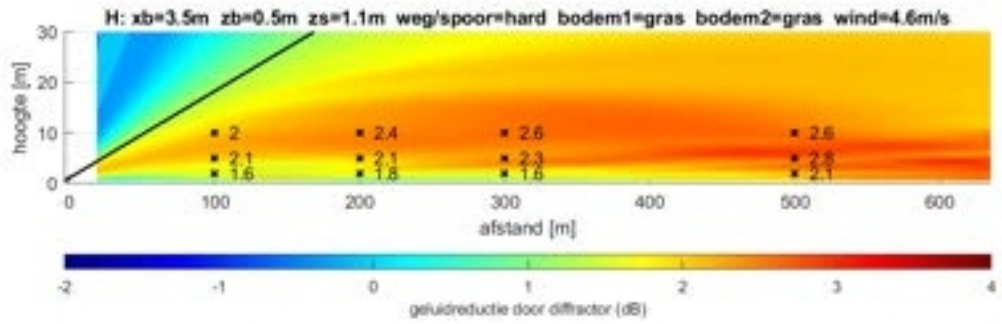
H: xb=3.5m zb=0.5m zs=1.1m weg/spoor=hard bodem1=gras bodem2=gras wind=4.6m/s
hoogte [m]
afstand [m]
geluidreductie door diffractor (dB)

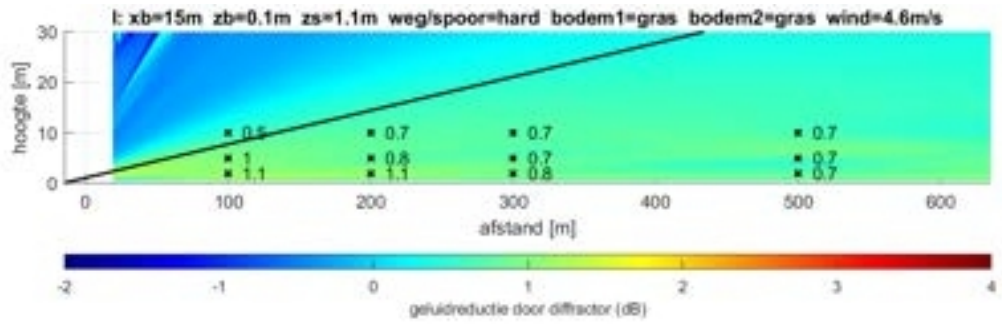
I: xb=15m zb=0.1m zs=1.1m weg/spoor=hard bodem1=gras bodem2=gras wind=4.6m/s
hoogte [m]
afstand [m]
geluidreductie door diffractor (dB)

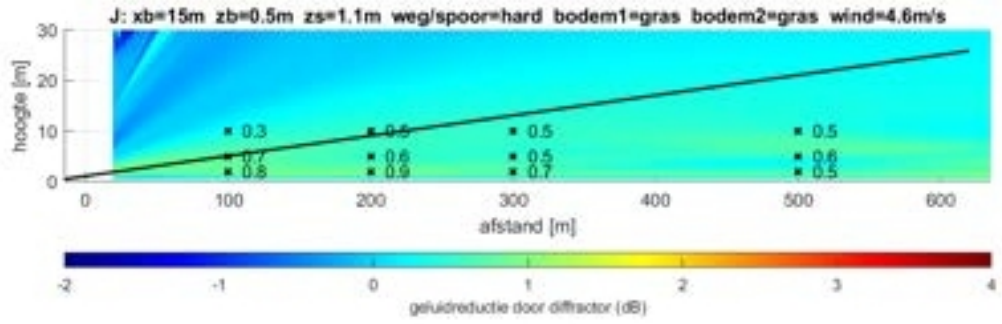
J: xb=15m zb=0.5m zs=1.1m weg/spoor=hard bodem1=gras bodem2=gras wind=4.6m/s
hoogte [m]
afstand [m]
geluidreductie door diffractor (dB)

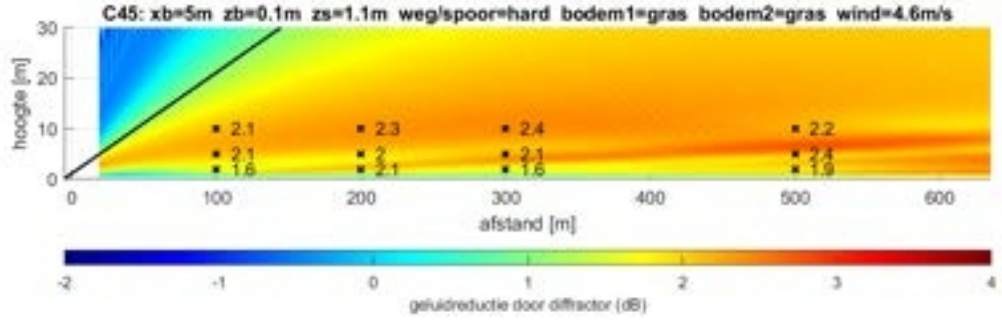
C45: xb=5m zb=0.1m zs=1.1m weg/spoor=hard bodem1=gras bodem2=gras wind=4.6m/s
hoogte [m]
afstand [m]
geluidreductie door diffractor (dB)

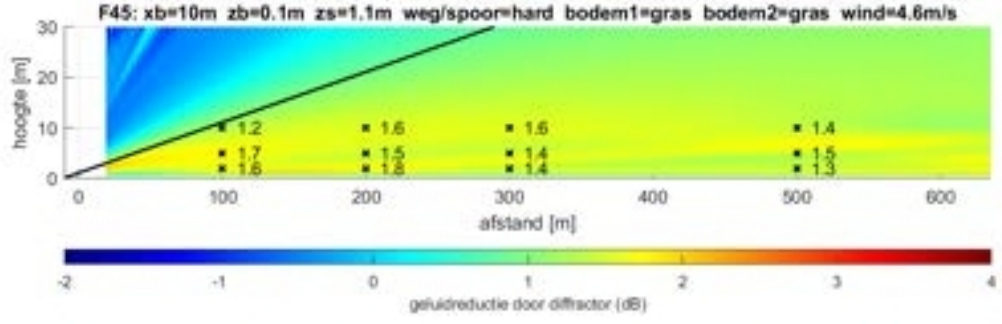
F45: xb=10m zb=0.1m zs=1.1m weg/spoor=hard bodem1=gras bodem2=gras wind=4.6m/s
hoogte [m]
afstand [m]
geluidreductie door diffractor (dB)

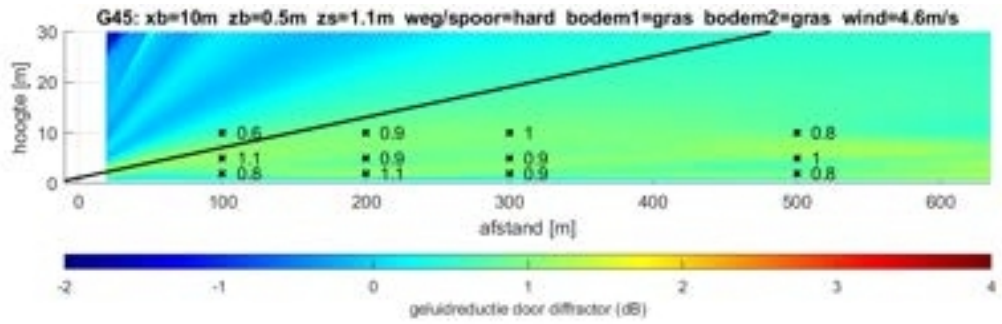
G45: xb=10m zb=0.5m zs=1.1m weg/spoor=hard bodem1=gras bodem2=gras wind=4.6m/s
hoogte [m]
afstand [m]
geluidreductie door diffractor (dB)

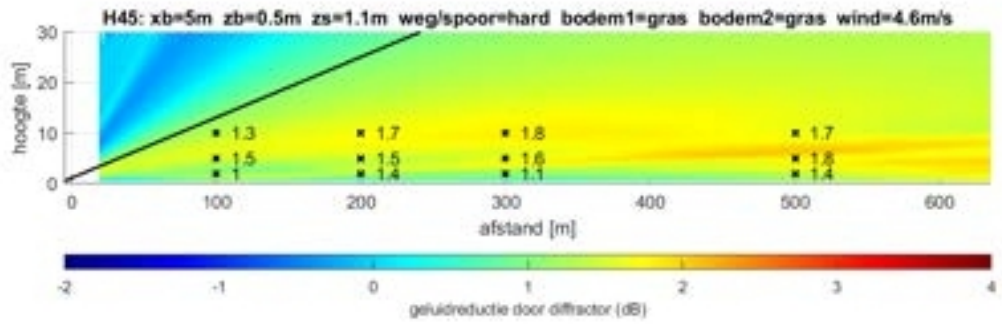
H45: xb=5m zb=0.5m zs=1.1m weg/spoor=hard bodem1=gras bodem2=gras wind=4.6m/s
hoogte [m]
afstand [m]
geluidreductie door diffractor (dB)

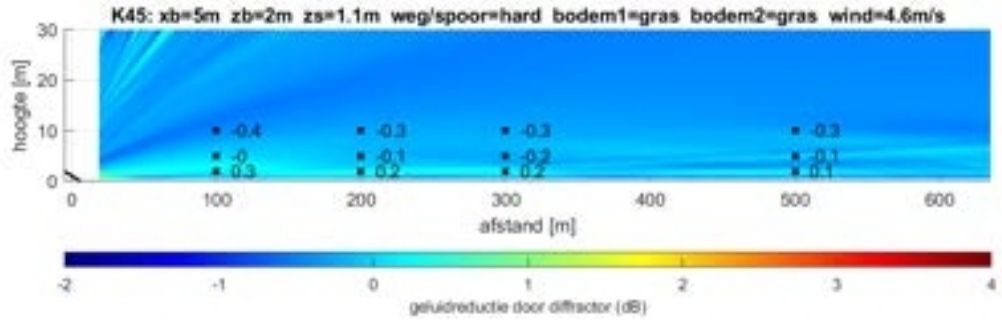
K45: xb=5m zb=2m zs=1.1m weg/spoor=hard bodem1=gras bodem2=gras wind=4.6m/s
hoogte [m]
afstand [m]
geluidreductie door diffractor (dB)

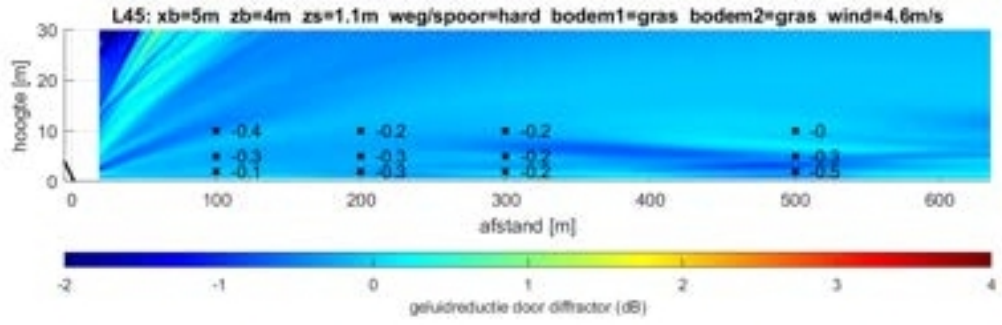
L45: xb=5m zb=4m zs=1.1m weg/spoor=hard bodem1=gras bodem2=gras wind=4.6m/s
hoogte [m]
afstand [m]
geluidreductie door diffractor (dB)

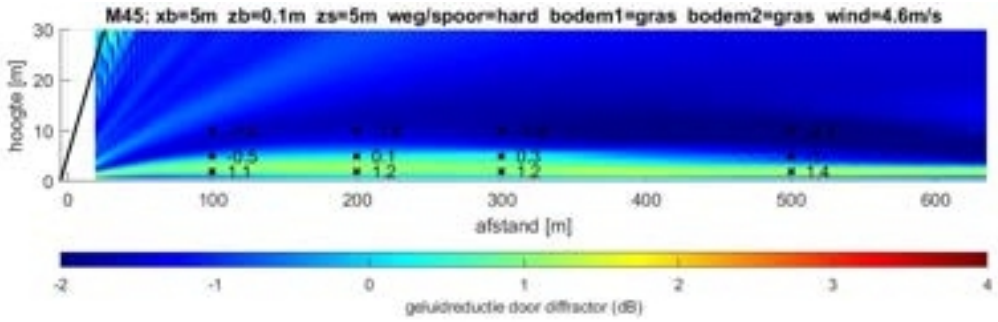
M45: xb=5m zb=0.1m zs=5m weg/spoor=hard bodem1=gras bodem2=gras wind=4.6m/s
hoogte [m]
afstand [m]
geluidreductie door diffractor (dB)

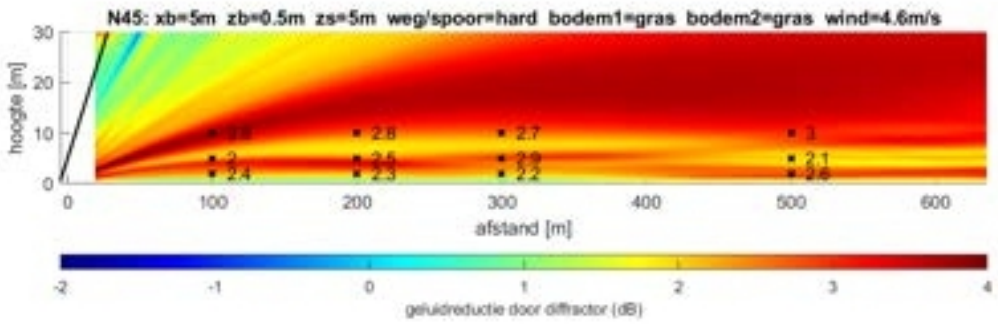
N45: xb=5m zb=0.5m zs=5m weg/spoor=hard bodem1=gras bodem2=gras wind=4.6m/s
hoogte [m]
afstand [m]
geluidreductie door diffractor (dB)

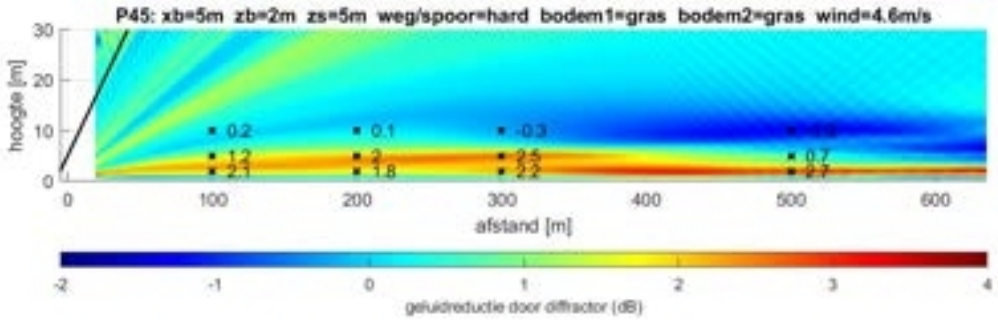
P45: xb=5m zb=2m zs=5m weg/spoor=hard bodem1=gras bodem2=gras wind=4.6m/s
hoogte [m]
afstand [m]
geluidreductie door diffractor (dB)

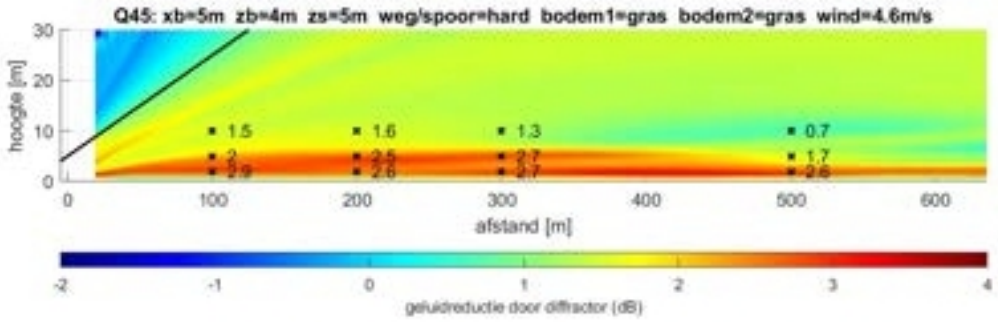
Q45: xb=5m zb=4m zs=5m weg/spoor=hard bodem1=gras bodem2=gras wind=4.6m/s
hoogte [m]
afstand [m]
geluidreductie door diffractor (dB)

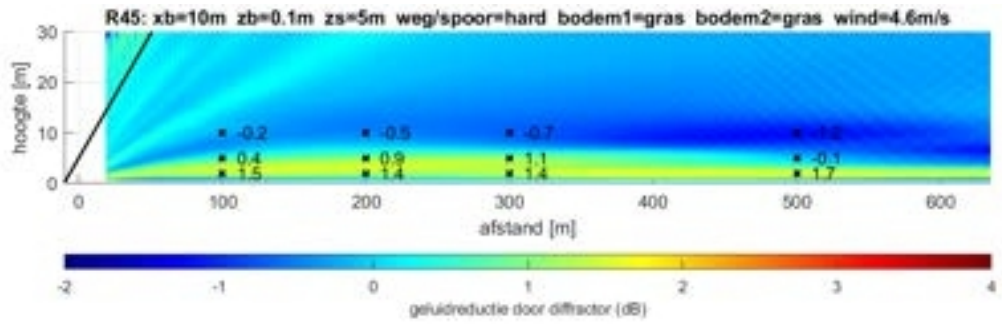
R45: xb=10m zb=0.1m zs=5m weg/spoor=hard bodem1=gras bodem2=gras wind=4.6m/s
hoogte [m]
afstand [m]
geluidreductie door diffractor (dB)

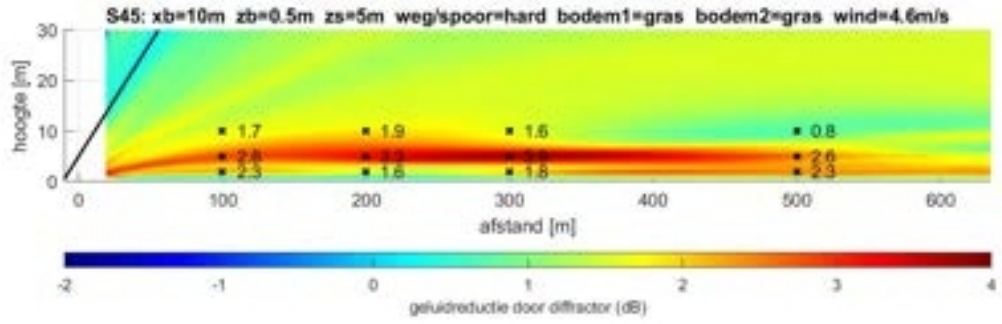
S45: xb=10m zb=0.5m zs=5m weg/spoor=hard bodem1=gras bodem2=gras wind=4.6m/s
hoogte [m]
afstand [m]
geluidreductie door diffractor (dB)

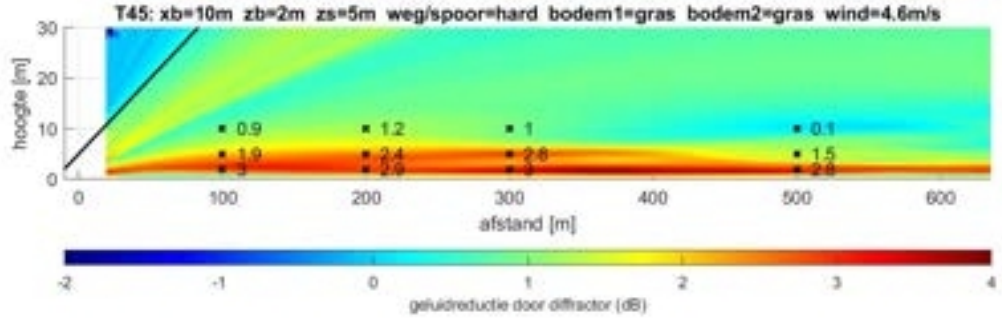
T45: xb=10m zb=2m zs=5m weg/spoor=hard bodem1=gras bodem2=gras wind=4.6m/s
hoogte [m]
afstand [m]
geluidreductie door diffractor (dB)

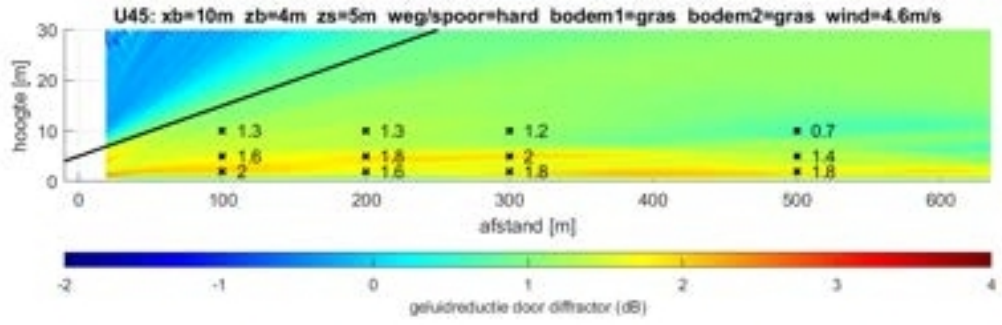
U45: xb=10m zb=4m zs=5m weg/spoor=hard bodem1=gras bodem2=gras wind=4.6m/s
hoogte [m]
afstand [m]
geluidreductie door diffractor (dB)

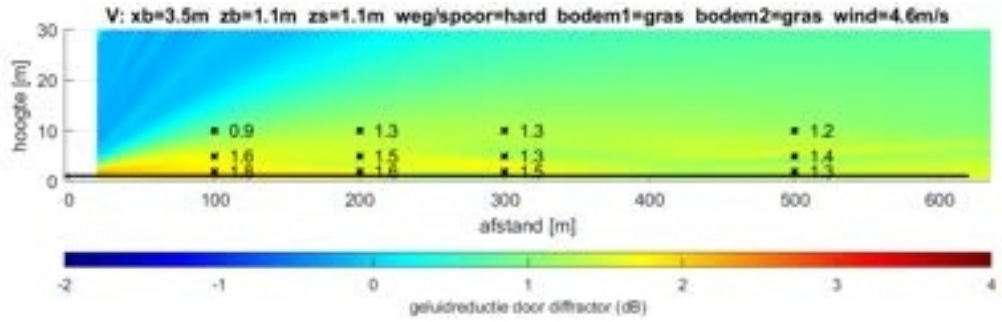
V: xb=3.5m zb=1.1m zs=1.1m weg/spoor=hard bodem1=gras bodem2=gras wind=4.6m/s
hoogte [m]
afstand [m]
geluidreductie door diffractor (dB)

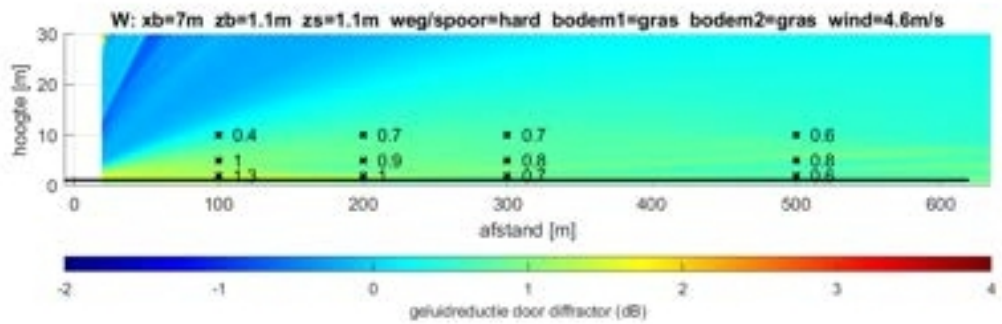
W: xb=7m zb=1.1m zs=1.1m weg/spoor=hard bodem1=gras bodem2=gras wind=4.6m/s
hoogte [m]
afstand [m]
geluidreductie door diffractor (dB)

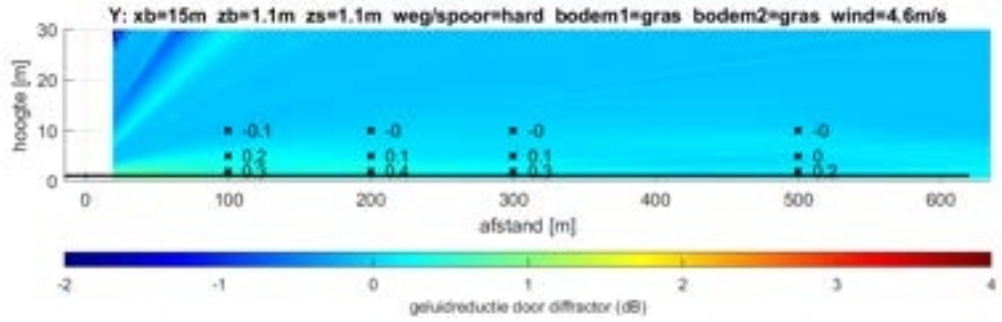
Y: xb=15m zb=1.1m zs=1.1m weg/spoor=hard bodem1=gras bodem2=gras wind=4.6m/s
hoogte [m]
afstand [m]
geluidreductie door diffractor (dB)

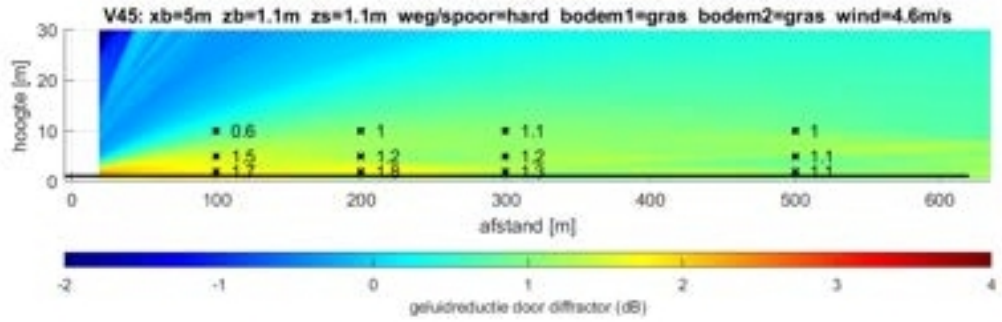
V45: xb=5m zb=1.1m zs=1.1m weg/spoor=hard bodem1=gras bodem2=gras wind=4.6m/s
hoogte [m]
afstand [m]
geluidreductie door diffractor (dB)

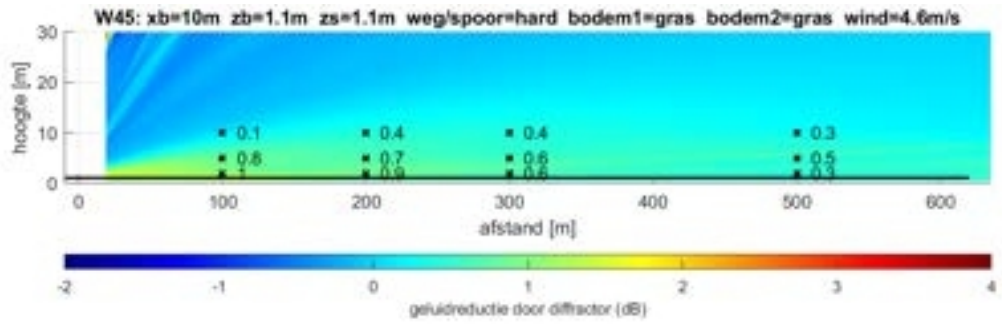
W45: xb=10m zb=1.1m zs=1.1m weg/spoor=hard bodem1=gras bodem2=gras wind=4.6m/s
hoogte [m]
afstand [m]
geluidreductie door diffractor (dB)

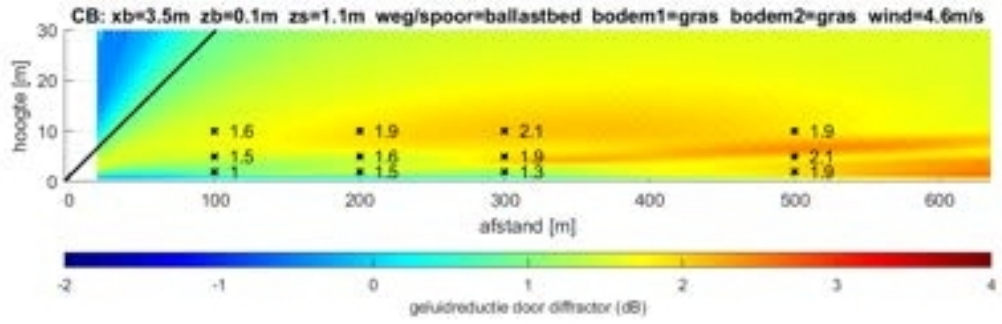
CB: xb=3.5m zb=0.1m zs=1.1m weg/spoor=ballastbed bodem1=gras bodem2=gras wind=4.6m/s
hoogte [m]
afstand [m]
geluidreductie door diffractor (dB)

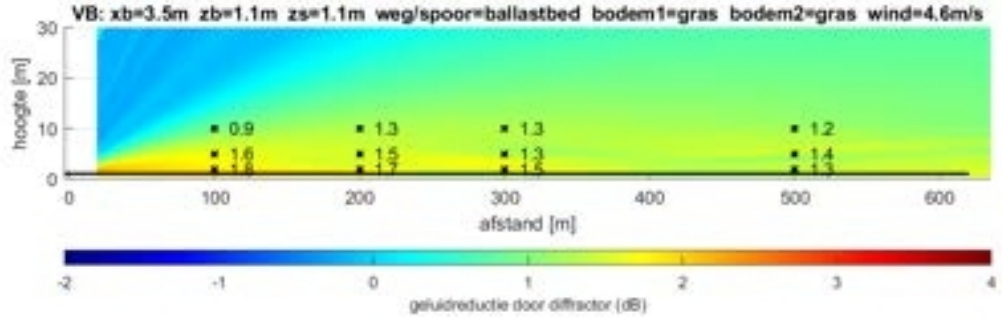
VB: xb=3.5m zb=1.1m zs=1.1m weg/spoor=ballastbed bodem1=gras bodem2=gras wind=4.6m/s
hoogte [m]
afstand [m]
geluidreductie door diffractor (dB)

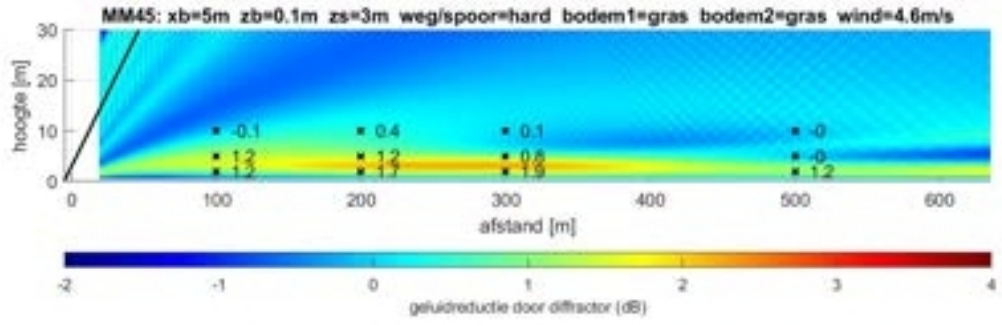
MM45: xb=5m zb=0.1m zs=3m weg/spoor=hard bodem1=gras bodem2=gras wind=4.6m/s
hoogte [m]
afstand [m]
geluidreductie door diffractor (dB)

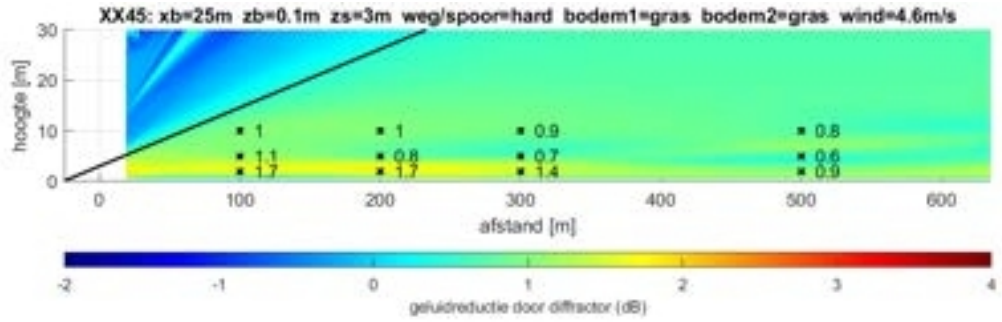
XX45: xb=25m zb=0.1m zs=3m weg/spoor=hard bodem1=gras bodem2=gras wind=4.6m/s
hoogte [m]
afstand [m]
geluidreductie door diffractor (dB)

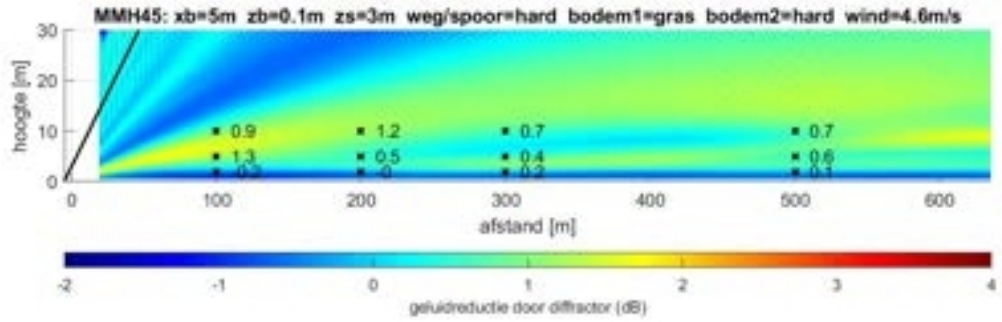
MMH45: xb=5m zb=0.1m zs=3m weg/spoor=hard bodem1=gras bodem2=hard wind=4.6m/s
hoogte [m]
afstand [m]
geluidreductie door diffractor (dB)

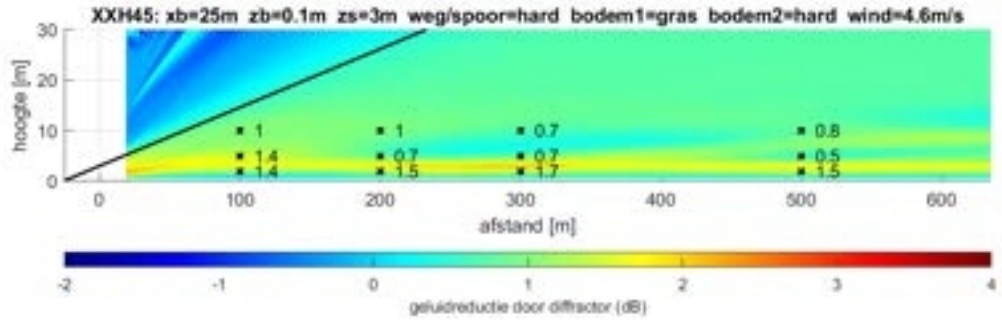
XXH45: xb=25m zb=0.1m zs=3m weg/spoor=hard bodem1=gras bodem2=hard wind=4.6m/s
hoogte [m]
afstand [m]
geluidreductie door diffractor (dB)

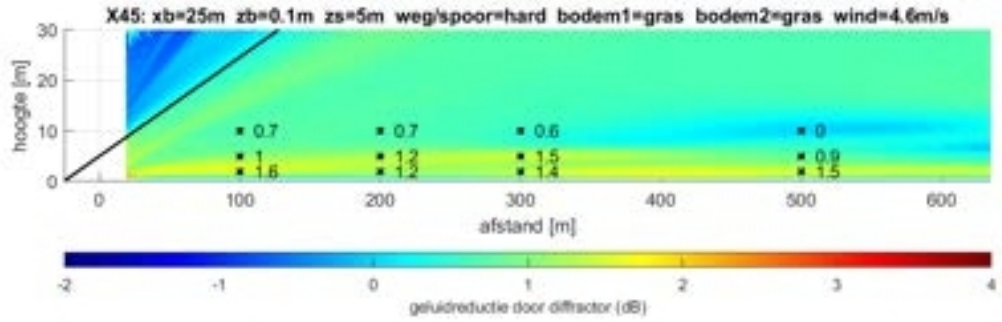
X45: xb=25m zb=0.1m zs=5m weg/spoor=hard bodem1=gras bodem2=gras wind=4.6m/s
hoogte [m]
afstand [m]
geluidreductie door diffractor (dB)

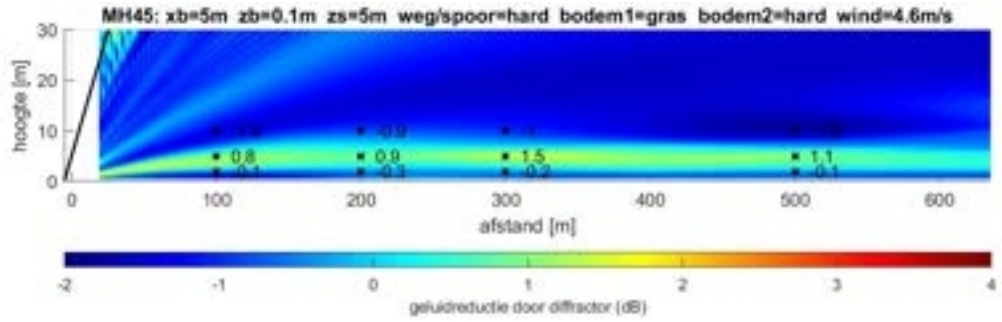
MH45: xb=5m zb=0.1m zs=5m weg/spoor=hard bodem1=gras bodem2=hard wind=4.6m/s
hoogte [m]
afstand [m]
geluidreductie door diffractor (dB)

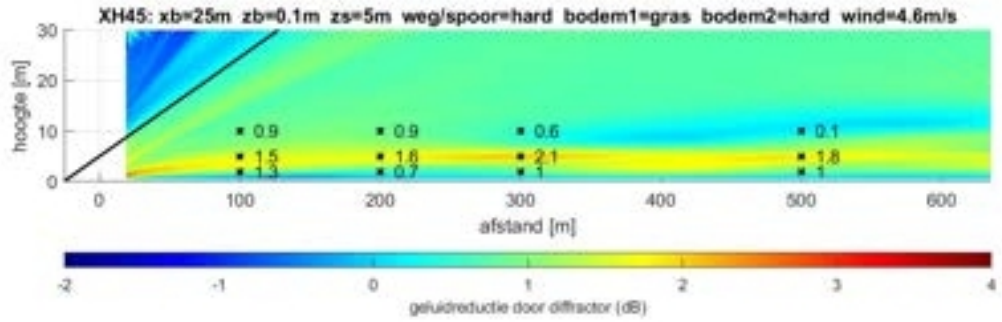
XH45: xb=25m zb=0.1m zs=5m weg/spoor=hard bodem1=gras bodem2=hard wind=4.6m/s
hoogte [m]
afstand [m]
geluidreductie door diffractor (dB)

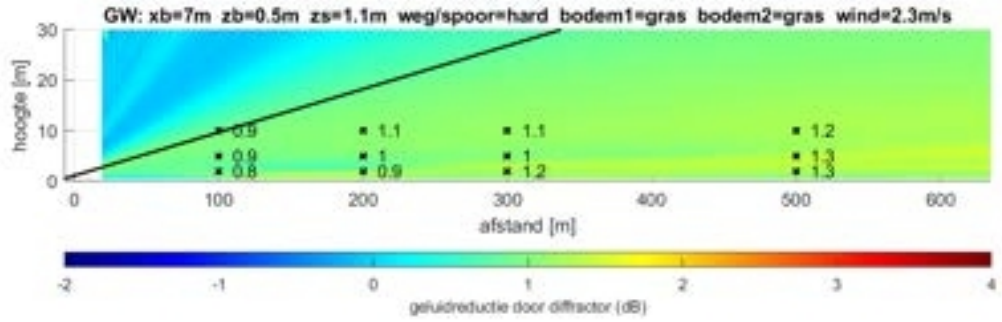
GW: xb=7m zb=0.5m zs=1.1m weg/spoor=hard bodem1=gras bodem2=gras wind=2.3m/s
hoogte [m]
afstand [m]
geluidreductie door diffractor (dB)

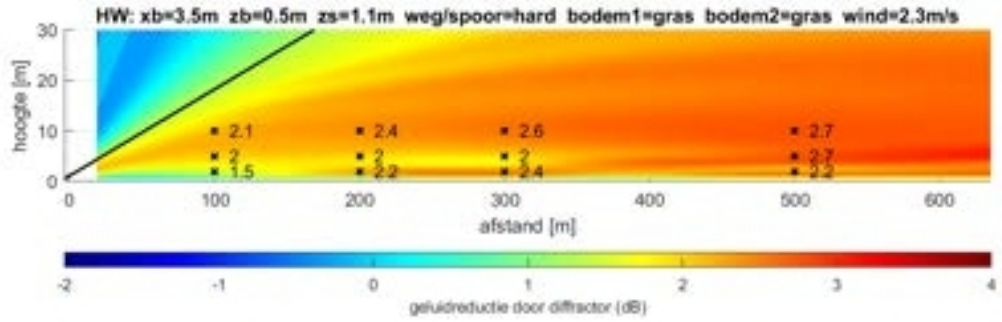
HW: xb=3.5m zb=0.5m zs=1.1m weg/spoor=hard bodem1=gras bodem2=gras wind=2.3m/s
hoogte [m]
afstand [m]
geluidreductie door diffractor (dB)

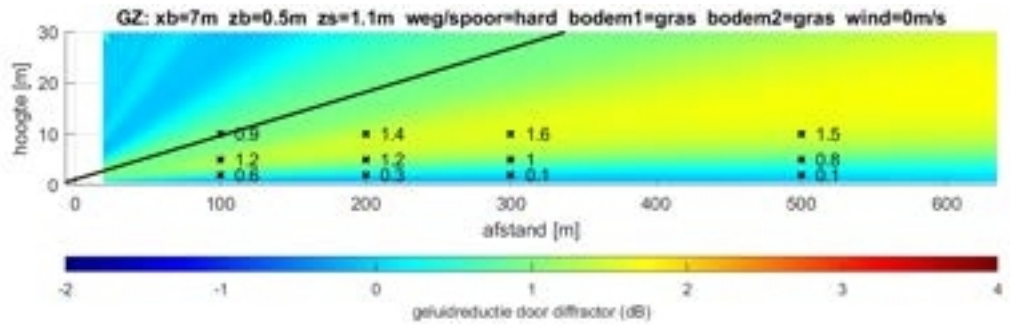
GZ: xb=7m zb=0.5m zs=1.1m weg/spoor=hard bodem1=gras bodem2=gras wind=0m/s
hoogte [m]
afstand [m]
geluidreductie door diffractor (dB)

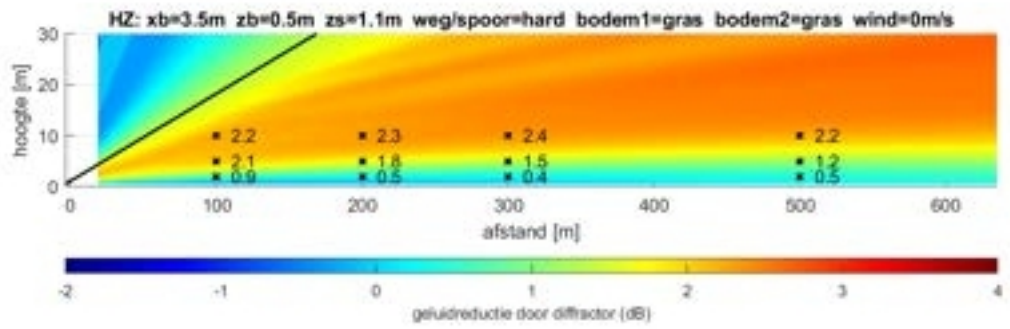
HZ: xb=3.5m zb=0.5m zs=1.1m weg/spoor=hard bodem1=gras bodem2=gras wind=0m/s
hoogte [m]
afstand [m]
geluidreductie door diffractor (dB)

# D Additional graphs for version 3 of the calculation rule

This appendix presents graphs results from FEM-PE with results from version 3 of the computational rule.

The graphs in Figure D.1 show the point clouds from Figure 3.26 in an alternative way. The noise reduction due to the diffractor is now not plotted against the Fresnel number, but the result of FEM-PE is plotted against the result of version 3 of the computational rule. The points for the 42 scenarios and 12 observer positions are around the diagonal (for 125-2000 Hz). This means that there is good agreement between FEM-PE and the computational rule.

Figures D.2-D.4 are also similar to Figure 3.26, only now the results are not shown for the 12 observer positions from Figure 3.15:

- $_{Rw}$= 100, 200, 300, 500m (distance Whiswall observer; $_{Rw=xw+15}$),
- $_{sw}$= 2, 5, 10 m (observer height),

but five other groups of observer positions were chosen:

a) $_{Rw}$= 30, 40, 50 m, $_{zw=2}$, 5, 10 m (Figure D.2),
b) $_{Rw}$= 75, 100, 125 m, $_{zw=2}$, 5, 10 m (Figure D.2),
c) $_{Rw}$= 175, 200, 225 m, $_{zw=2}$, 5, 10 m (Figure D.3),
d) $_{Rw}$= 275, 300, 325 m, $_{zw=2}$, 5, 10 m Figure D.3),
e) $_{Rw}$= 475, 500, 525 m, $_{zw=2}$, 5, 10 m Figure D.4).

The idea here is to determine in this way whether adding a distance-dependent correction term to the calculation rule leads to better agreement with FEM-PE. This turns out not to be the case. The agreement between FEM-PE and the computational rule without such a correction term is good for all five groups of observer distances.

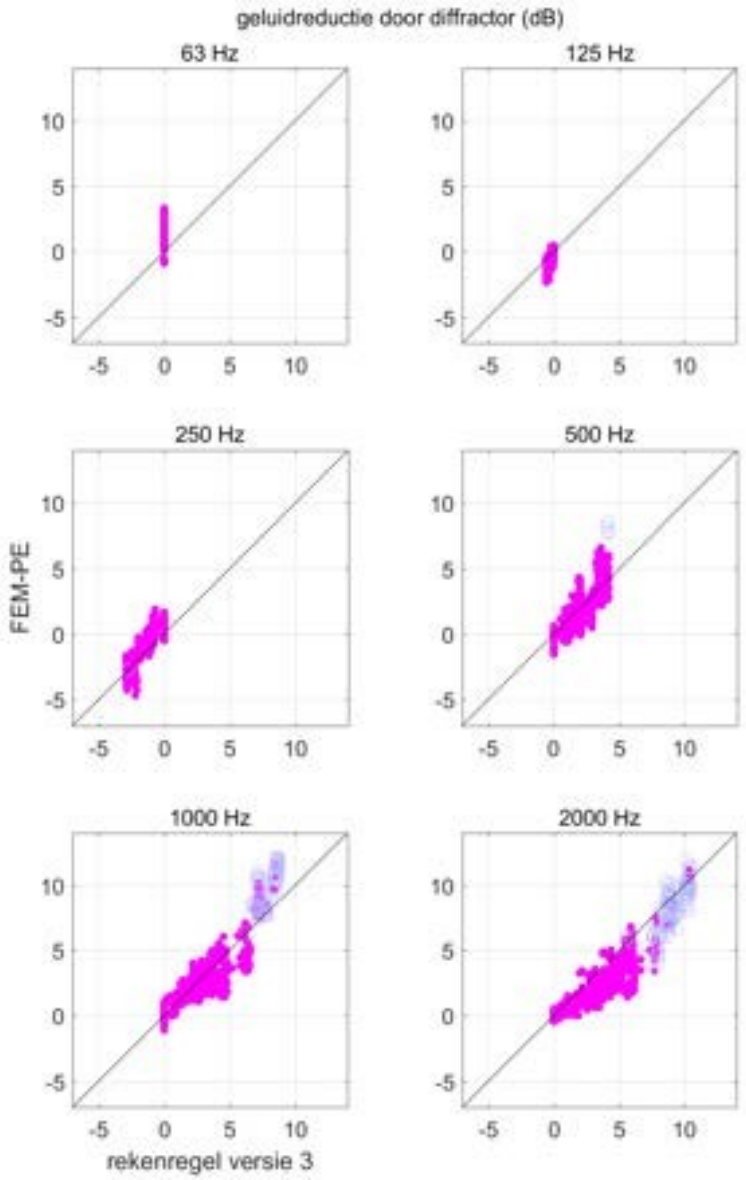


Figure D.1 Results of FEM-PE versus results of version 3 of the calculation rule, for the 42 scenarios and 12 observer positions. The symbols are as in Figure 3.26.

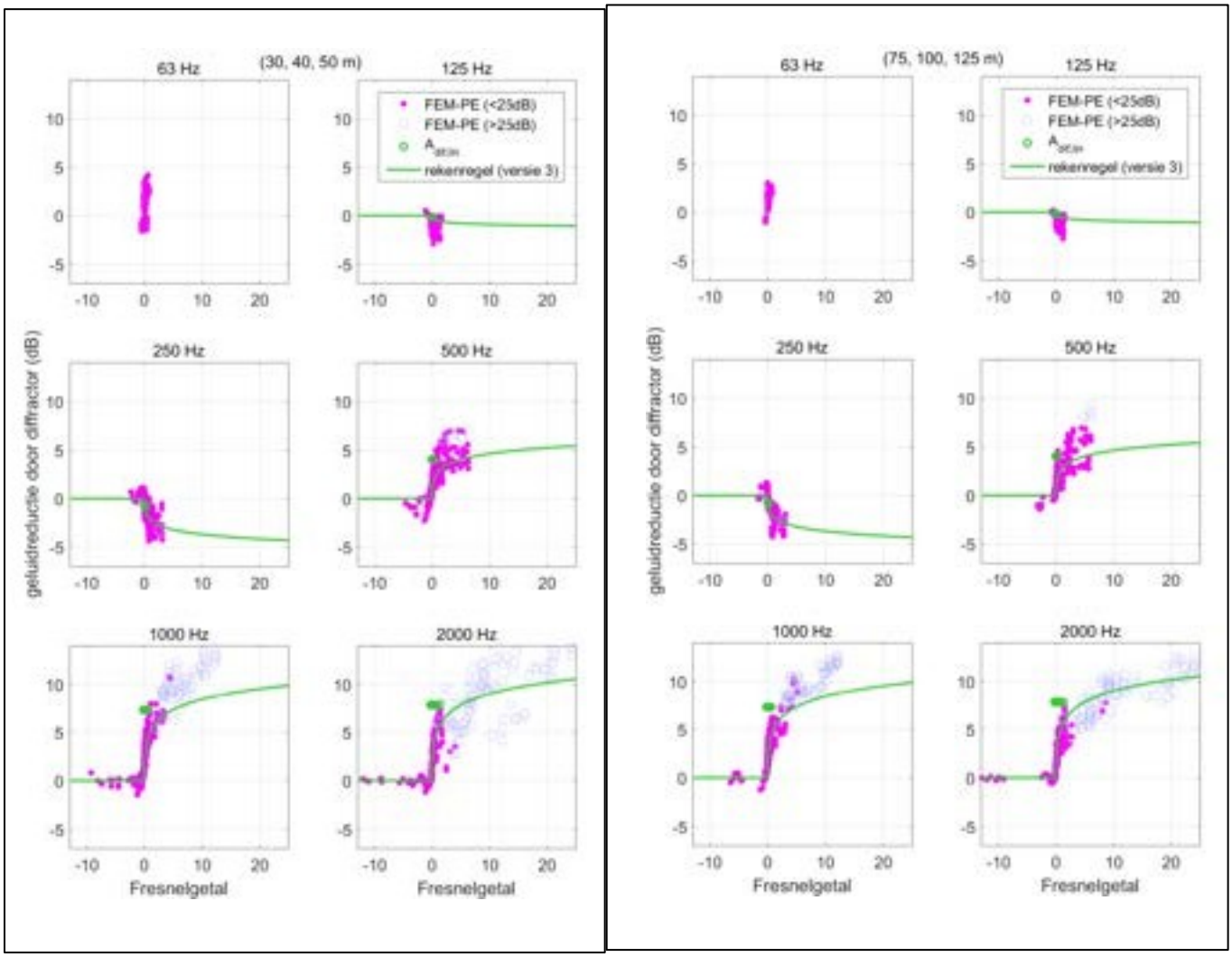


Figure D.2 As Figure 3.26, but now for 9 observer positions with Rw=30-50 m (left) and Rw=75-125 m (right).

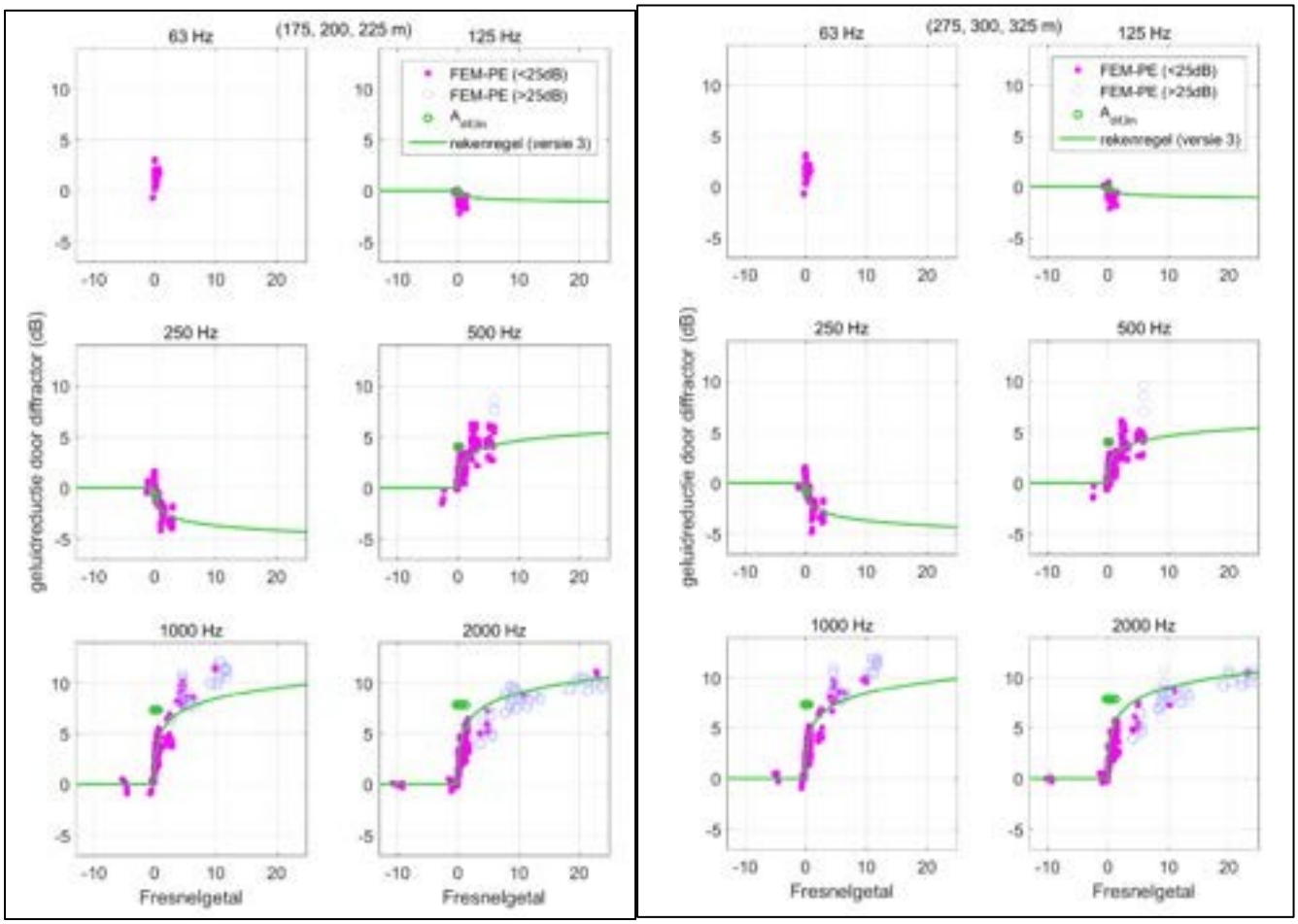


Figure D.3 As Figure 3.26, but now for 9 observer positions with Rw=175-225 m left) and Rw=275-325 m (right).

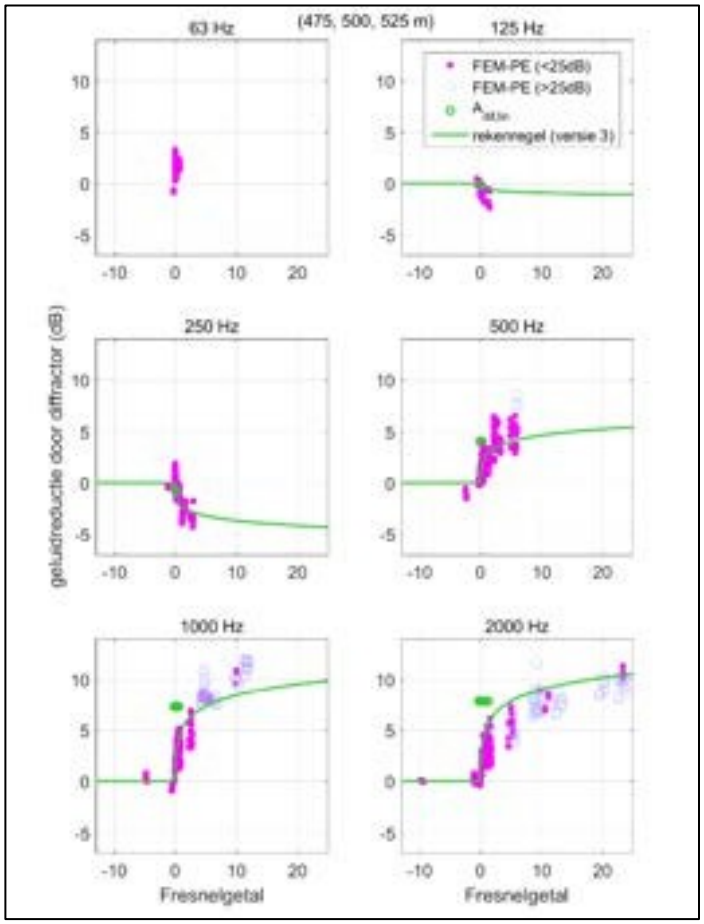


Figure D.4 As Figure 3.26, but now for 9 observer positions with Rw=475-525 m.

# E Graphs for analysis in chapter 4: screen effect

This appendix contains graphs for an analysis of noise reduction by the screen (without diffractor). These graphs give an impression of the spread of results of FEM-PE around the prediction according to Maekawa and SRM2. With Maekawa, only the screen effect is determined. With SRM2, the intermediate attenuation is determined, including the influence of the soil.

Figure E.1 shows the screen effect according to Maekawa and according to FEM-PE for the 42 scenarios, with 12 receivers at distances 100, 200, 300, 500 m, and two choices for the three heights: i) 2, 5, 10 m, and ii) 5, 10, 15 m. The idea was that with the second choice the dispersion might be smaller than with the first choice. This turns out not to be the case. The spread is represented by Maekawa's deviation, in two ways:

- $\delta_{rms}$= the rms value of the difference in noise reduction between FEM-PE and Maekawa,
- $\delta$= the noise reduction according to Maekawa minus the noise reduction according to FEM-PE.

The values of $\delta_{rms}$ and $\delta$ are given in the graphs.

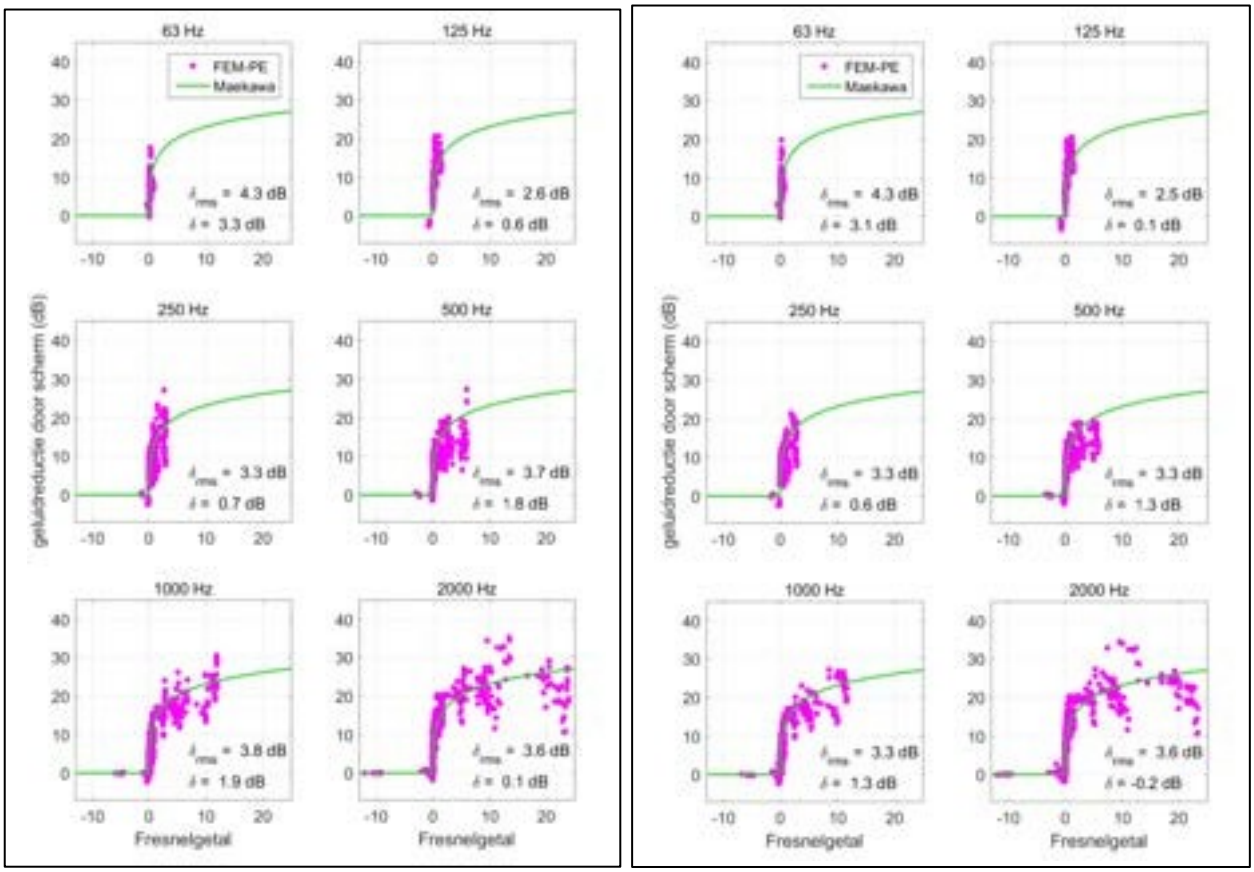


Figure E.1 Screen effects according to Maekawa and according to FEM-PE for the 42 scenarios, with 12 receivers at distances 100, 200, 300, 500 m, and heights 2, 5, 10 m (left) or 5, 10, 15 m right).

Figure E.2 shows the results from Figure E1 in a different , with horizontally the value according to Maekawa and vertically the value according to FEM-PE.

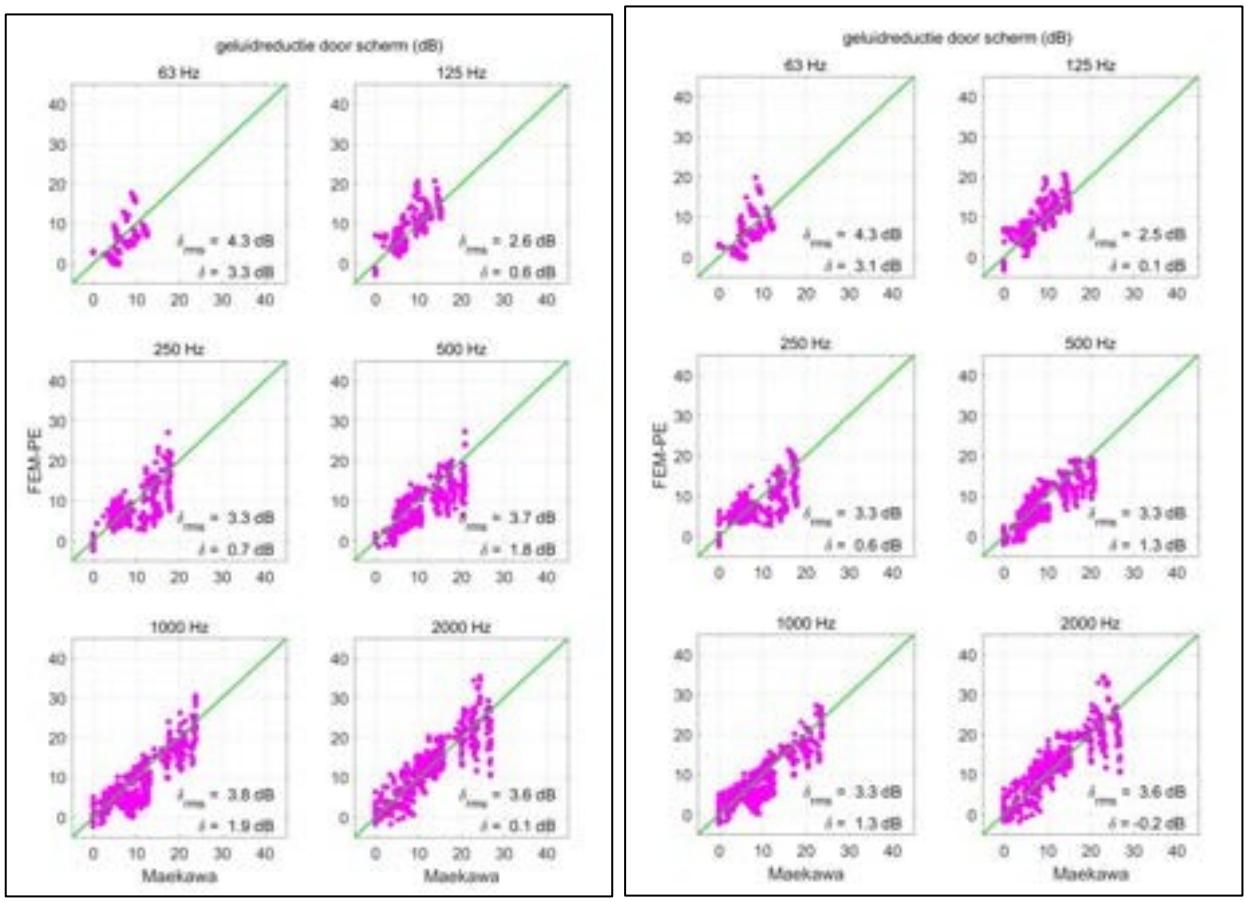


Figure E.2 Alternative representation of the results from Figure E1, with horizontally the value according to Maekawa and vertically the value according to FEM-PE. Left for receiver heights 2, 5, 10 m. Right for receiver heights 5, 10, 15 m.

Finally, we have repeated the equation in Figure E.2 where the screen effect according to Maekawa has been replaced by the value of noise reduction according to SRM2. The noise reduction according to SRM2 consists of two contributions: i) the screen effect according to a formula that is an approximation of Maekawa's formula, and ii) a change in the influence of soil on noise propagation. Thus, the value according to SRM2 is an intermediate attenuation.

The result is shown in Figure E.3. The spread is not really smaller than Figure E.2. Apparently, SRM2 does not give a significant improvement by taking into account the change in soil effect.

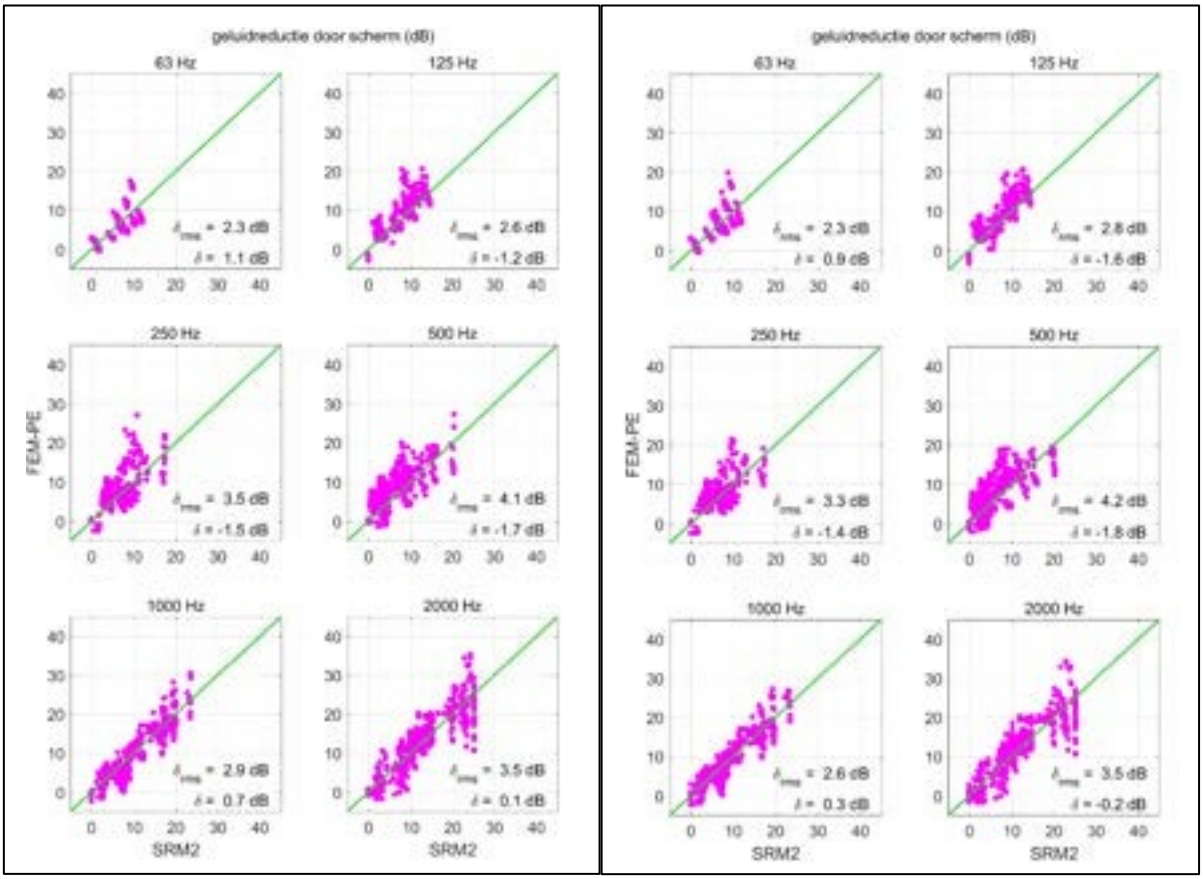


Figure E.3 As Figure E.2 but now showing horizontally the intermediate attenuation according to SRM2. Left for receiver heights 2, 5, 10 m. Right for receiver heights 5, 10, 15 m.

# F Graphs for analysis in chapter 4: effect of diffractor

In this appendix, we present graphs for an analysis of noise reduction by the diffractor, both the original diffractor and the LF diffractor. As in Appendix E, we have assumed the two choices for receiver heights: i) 2, 5, 10 m, and ii) 5, 10, 15 m. In each case, the graphs also show the prediction of the calculation rule for the diffractor effect, as green lines (the "diffractor effect" is the noise reduction due to the diffractor).

We initially assumed version 3 of the calculation rule, with fixed values of 0.2 and 0.05 for the coefficient. The coefficient is denoted by the symbol F. So for version 3 applies:

- F= 0.2 for $_{Adif,lin}< 0$
- F= 0.05 for $_{Adif,lin}\geq 0$

We compared the FEM-PE results with the computational rule both for third-band and octave bands. We have represented the deviation from the computational rule in two ways:

- $_{\delta rms}$= the rms value of the difference in diffractor effect between FEM-PE and the computational rule,
- δ= the diffractor effect according to the calculation rule minus the diffractor effect according to FEM-PE.

The values of $_{\delta rms}$ and δ are given in the graphs.

Figure F.1 shows the comparison between FEM-PE and the computational rule in thirds bands. Here we have thus assumed fixed values of 0.2 and 0.05 for the coefficient F for the computational rule.

Figure F.2 is as Figure F.1, but now we have optimized the coefficients F of the arithmetic rule for each third band, such that the value of $_{\delta rms}$ is minimal. The optimized values of F are shown in the graphs, and are also shown separately in Table F.1.

Figures F4-F6 are as Figures F.1-F.3, but now for the LF diffractor. The values of F, $_{\delta rms}$ and δ from Figures F.3 and F.6 are also given in Tables F.1-F.4.

Figures F7-F10 show the equation between FEM-PE and the calculation rule in octaves instead of thirds, for the original diffractor. Figures F.11-F.14 show the same equation for the LF diffractor.

We conclude that the choice between receiver heights 2, 5, 10 m and 5, 10, 15 m gives no significant difference for accuracy. Furthermore, the advantage of computing via the terces appears to be nil. The increase in accuracy due to optimization of F is also quite limited.

Figures F.15-F.22 are analogous to Figures F7-F14, but now for receivers at distances 30, 40, 50 instead of 100, 200, 300, 500 m (as in Appendix D). Also for 30-50 m we find a good agreement between FEM-PE and the computational rule. Here, for the calculation rule with optimization of F, the interval 100-500 m is assumed for optimization.

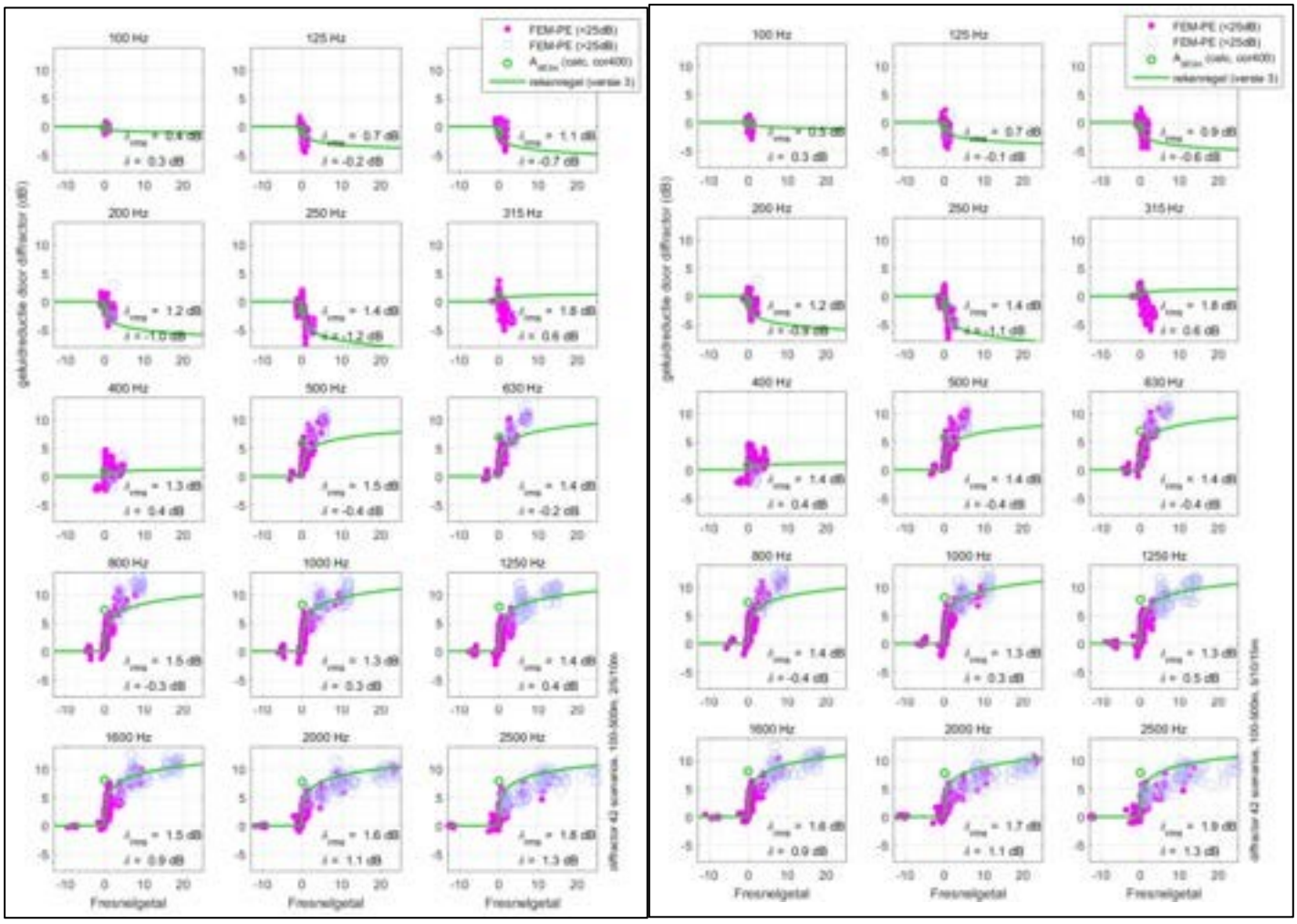


Figure F.1 Comparison of FEM-PE results in thirds with the computational rule (version 3) for the diffractor effect. The FEM-PE results were determined for 42 scenarios, with 12 receiver positions, at distances 100, 200, 300, and 500 m, and three heights: 2, 5, 10 m (left) or 5, 10, 15 m right).

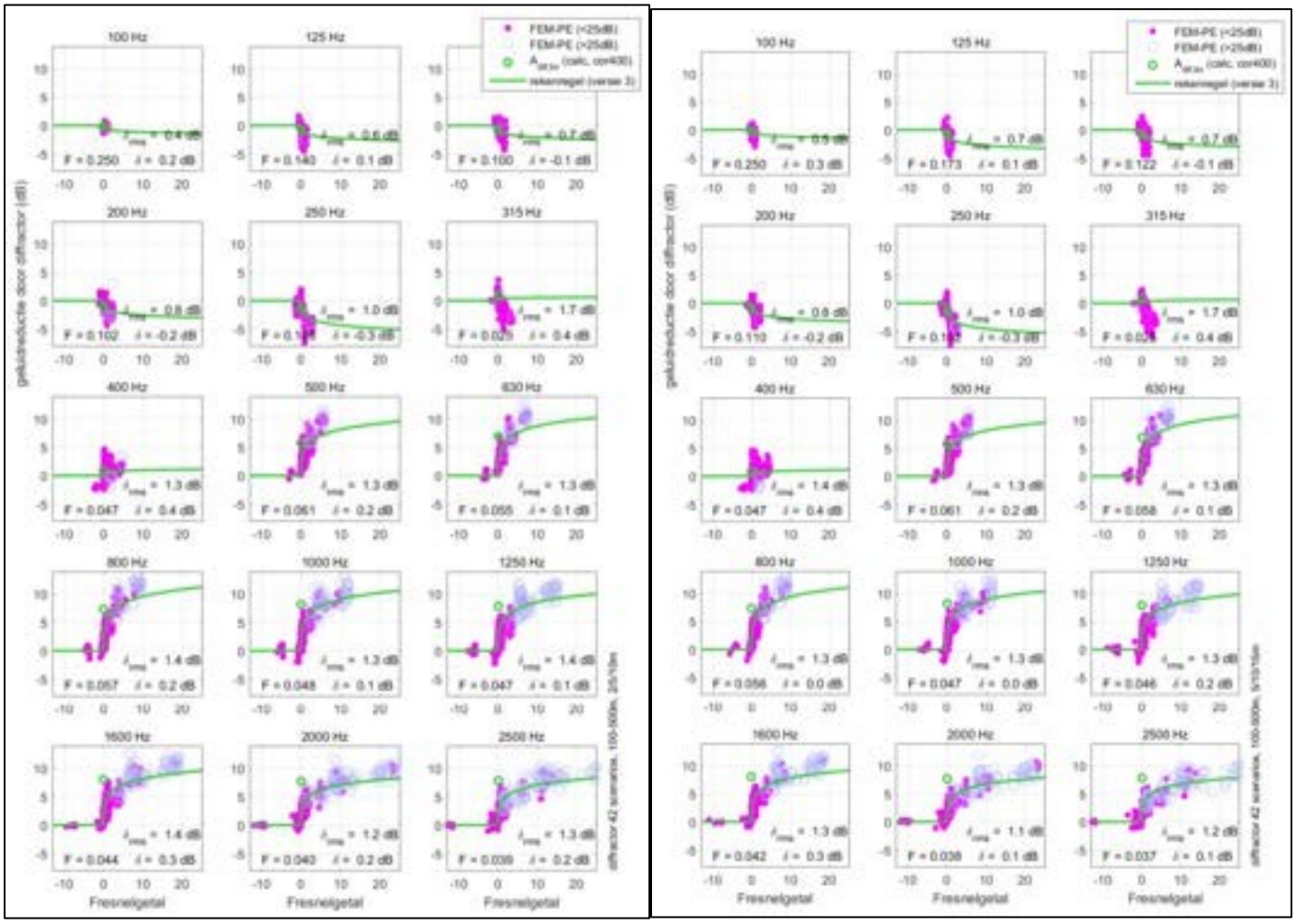

Figure F.2 As Figure F.1, but now with optimization of the coefficients F of the computational rule. The values of F are shown in the graphs.

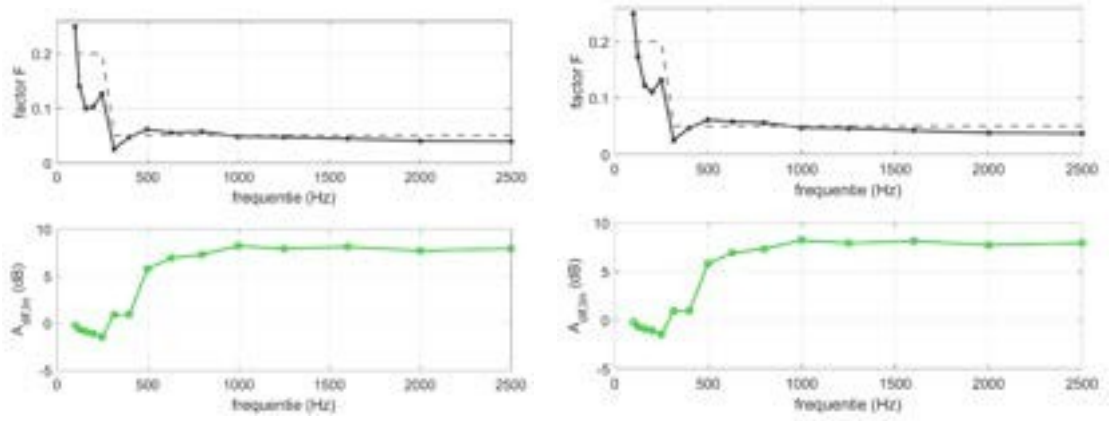

Figure F.3 Values of the coefficients F from Figure F.2, with heights 2, 5, 10 m left) and 5, 10, 15 m (right). The broken lines represent the values 0.2 and 0.05 from Chapter 3. Also shown, with the green line, are the corresponding values of $A_{dif,lin}$.

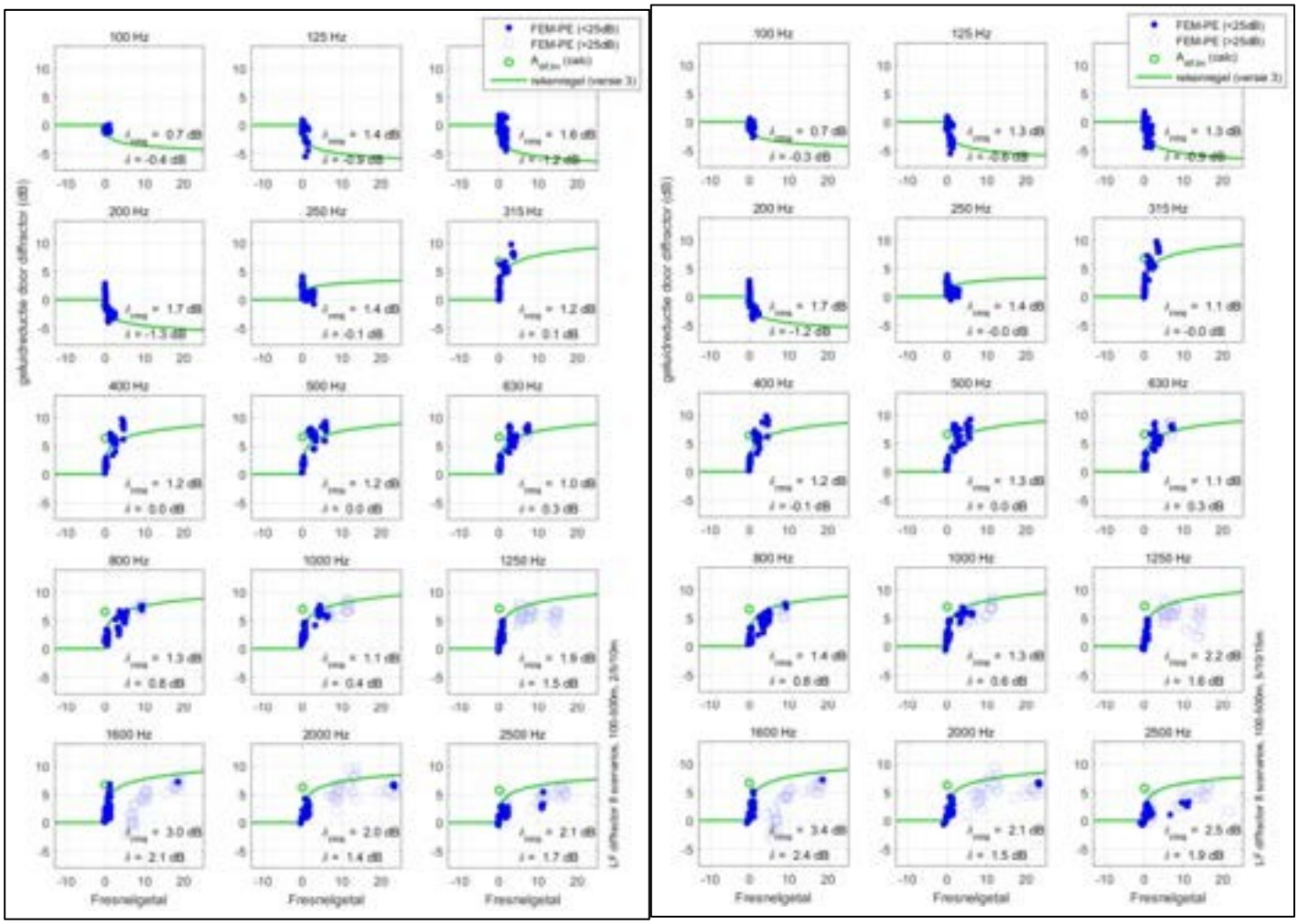


Figure F.4 As Figure F.1 (with fixed coefficients F), for the LF diffractor.

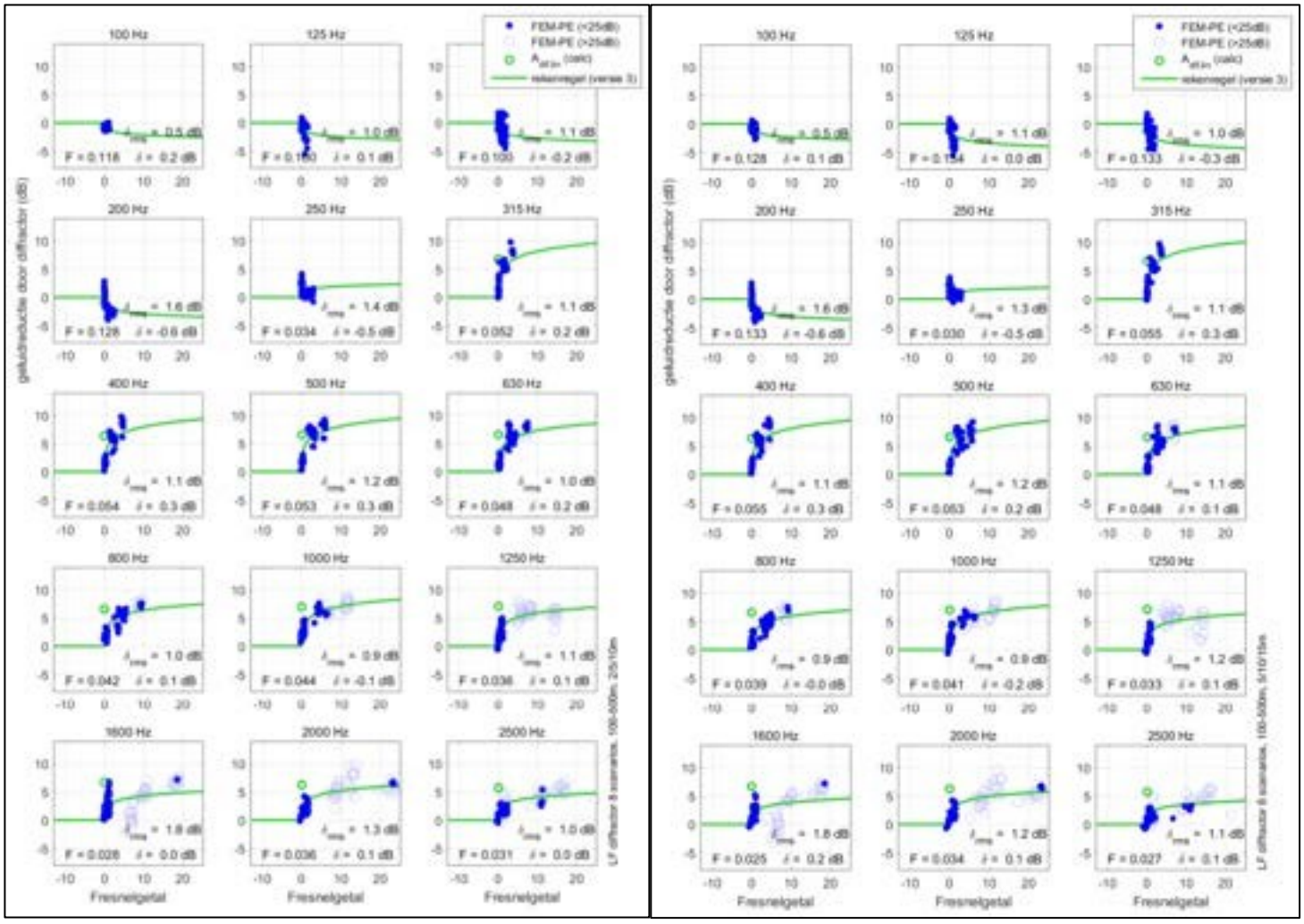


Figure F.5 As Figure F.2 (with optimization of the coefficients F), for the LF diffractor.

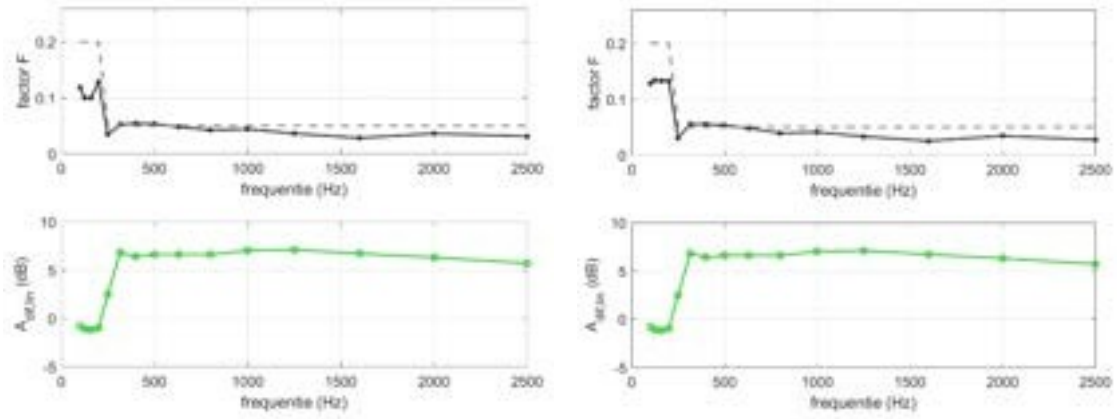


Figure F.6 As Figure F.3, for the LF diffractor.

Table F.1 Values of coefficient F and $_{\delta rms}$ and δ, for the original diffractor (receiver heights 2, 5, 10 m).

| f (Hz) | $_{Adiflin}$ (dB) | F | $_{drms}$ (dB) | d (dB) | F | $_{drms}$ (dB) | d (dB) |
|---|---|---|---|---|---|---|---|
| 100 | -0.2 | 0.20 | 0.4 | 0.3 | 0.250 | 0.4 | 0.2 |
| 125 | -0.7 | 0.20 | 0.7 | -0.2 | 0.140 | 0.6 | 0.1 |
| 160 | -0.9 | 0.20 | 1.1 | -0.7 | 0.100 | 0.7 | -0.1 |
| 200 | -1.1 | 0.20 | 1.2 | -1.0 | 0.102 | 0.8 | -0.2 |
| 250 | -1.5 | 0.20 | 1.4 | -1.2 | 0.126 | 1.0 | -0.3 |
| 315 | 0.9 | 0.05 | 1.8 | 0.6 | 0.025 | 1.7 | 0.4 |
| 400 | 0.9 | 0.05 | 1.3 | 0.4 | 0.047 | 1.3 | 0.4 |
| 500 | 5.8 | 0.05 | 1.5 | -0.4 | 0.061 | 1.3 | 0.2 |
| 630 | 6.9 | 0.05 | 1.4 | -0.2 | 0.055 | 1.3 | 0.1 |
| 800 | 7.3 | 0.05 | 1.5 | -0.3 | 0.057 | 1.4 | 0.2 |
| 1000 | 8.2 | 0.05 | 1.3 | 0.3 | 0.048 | 1.3 | 0.1 |
| 1250 | 7.9 | 0.05 | 1.4 | 0.4 | 0.047 | 1.4 | 0.1 |
| 1600 | 8.1 | 0.05 | 1.5 | 0.9 | 0.044 | 1.4 | 0.3 |
| 2000 | 7.7 | 0.05 | 1.6 | 1.1 | 0.040 | 1.2 | 0.2 |
| 2500 | 7.9 | 0.05 | 1.8 | 1.3 | 0.039 | 1.3 | 0.2 |

Table F.2 Values of coefficient F and $_{\delta rms}$ and δ, for the original diffractor (receiver heights 5, 10, 15 m).

| f (Hz) | $_{Adiflin}$ (dB) | F | $_{drms}$ (dB) | d (dB) | F | $_{drms}$ (dB) | d (dB) |
|---|---|---|---|---|---|---|---|
| 100 | -0.2 | 0.20 | 0.5 | 0.3 | 0.250 | 0.5 | 0.3 |
| 125 | -0.7 | 0.20 | 0.7 | -0.1 | 0.173 | 0.7 | 0.1 |
| 160 | -0.9 | 0.20 | 0.9 | -0.6 | 0.122 | 0.7 | -0.1 |
| 200 | -1.1 | 0.20 | 1.2 | -0.9 | 0.110 | 0.8 | -0.2 |
| 250 | -1.5 | 0.20 | 1.4 | -1.1 | 0.132 | 1.0 | -0.3 |
| 315 | 0.9 | 0.05 | 1.8 | 0.6 | 0.025 | 1.7 | 0.4 |
| 400 | 0.9 | 0.05 | 1.4 | 0.4 | 0.047 | 1.4 | 0.4 |
| 500 | 5.8 | 0.05 | 1.4 | -0.4 | 0.061 | 1.3 | 0.2 |
| 630 | 6.9 | 0.05 | 1.4 | -0.4 | 0.058 | 1.3 | 0.1 |
| 800 | 7.3 | 0.05 | 1.4 | -0.4 | 0.056 | 1.3 | 0.0 |
| 1000 | 8.2 | 0.05 | 1.3 | 0.3 | 0.047 | 1.3 | 0.0 |
| 1250 | 7.9 | 0.05 | 1.3 | 0.5 | 0.046 | 1.3 | 0.2 |
| 1600 | 8.1 | 0.05 | 1.6 | 0.9 | 0.042 | 1.3 | 0.3 |
| 2000 | 7.7 | 0.05 | 1.7 | 1.1 | 0.038 | 1.1 | 0.1 |
| 2500 | 7.9 | 0.05 | 1.9 | 1.3 | 0.037 | 1.2 | 0.1 |

Table F.3 Values of coefficient F and $_{\delta rms}$ and δ, for the LF diffractor (receiver heights 2, 5, 10 m).

| f (Hz) | $_{Adiflin}$ (dB) | F | $_{drms}$ (dB) | d (dB) | F | $_{drms}$ (dB) | d (dB) |
|---|---|---|---|---|---|---|---|
| 100 | -0.8 | 0.20 | 0.7 | -0.4 | 0.118 | 0.5 | 0.2 |
| 125 | -1.1 | 0.20 | 1.4 | -0.9 | 0.100 | 1.0 | 0.1 |
| 160 | -1.2 | 0.20 | 1.6 | -1.2 | 0.100 | 1.1 | -0.2 |
| 200 | -1.0 | 0.20 | 1.7 | -1.3 | 0.128 | 1.6 | -0.6 |
| 250 | 2.5 | 0.05 | 1.4 | -0.1 | 0.034 | 1.4 | -0.5 |
| 315 | 6.8 | 0.05 | 1.2 | 0.1 | 0.052 | 1.1 | 0.2 |
| 400 | 6.4 | 0.05 | 1.2 | 0.0 | 0.054 | 1.1 | 0.3 |
| 500 | 6.6 | 0.05 | 1.2 | 0.0 | 0.053 | 1.2 | 0.3 |
| 630 | 6.6 | 0.05 | 1.0 | 0.3 | 0.048 | 1.0 | 0.2 |
| 800 | 6.6 | 0.05 | 1.3 | 0.8 | 0.042 | 1.0 | 0.1 |
| 1000 | 7.0 | 0.05 | 1.1 | 0.4 | 0.044 | 0.9 | -0.1 |
| 1250 | 7.1 | 0.05 | 1.9 | 1.5 | 0.036 | 1.1 | 0.1 |
| 1600 | 6.7 | 0.05 | 3.0 | 2.1 | 0.028 | 1.8 | 0.0 |
| 2000 | 6.3 | 0.05 | 2.0 | 1.4 | 0.036 | 1.3 | 0.1 |
| 2500 | 5.7 | 0.05 | 2.1 | 1.7 | 0.031 | 1.0 | 0.0 |

Table F.4 Values of coefficient F and $_{\delta rms}$ and δ, for the LF diffractor (receiver heights 5, 10, 15 m).

| f (Hz) | $_{Adiflin}$ (dB) | F | $_{drms}$ (dB) | d (dB) | F | $_{drms}$ (dB) | d (dB) |
|---|---|---|---|---|---|---|---|
| 100 | -0.8 | 0.20 | 0.7 | -0.3 | 0.128 | 0.5 | 0.1 |
| 125 | -1.1 | 0.20 | 1.3 | -0.6 | 0.134 | 1.1 | 0.0 |
| 160 | -1.2 | 0.20 | 1.3 | -0.9 | 0.133 | 1.0 | -0.3 |
| 200 | -1.0 | 0.20 | 1.7 | -1.2 | 0.133 | 1.6 | -0.6 |
| 250 | 2.5 | 0.05 | 1.4 | -0.0 | 0.030 | 1.3 | -0.5 |
| 315 | 6.8 | 0.05 | 1.1 | -0.0 | 0.055 | 1.1 | 0.3 |
| 400 | 6.4 | 0.05 | 1.2 | -0.1 | 0.055 | 1.1 | 0.3 |
| 500 | 6.6 | 0.05 | 1.3 | 0.0 | 0.053 | 1.2 | 0.2 |
| 630 | 6.6 | 0.05 | 1.1 | 0.3 | 0.048 | 1.1 | 0.1 |
| 800 | 6.6 | 0.05 | 1.4 | 0.8 | 0.039 | 0.9 | -0.0 |
| 1000 | 7.0 | 0.05 | 1.3 | 0.6 | 0.041 | 0.9 | -0.2 |
| 1250 | 7.1 | 0.05 | 2.2 | 1.6 | 0.033 | 1.2 | 0.1 |
| 1600 | 6.7 | 0.05 | 3.4 | 2.4 | 0.025 | 1.8 | 0.2 |
| 2000 | 6.3 | 0.05 | 2.1 | 1.5 | 0.034 | 1.2 | 0.1 |
| 2500 | 5.7 | 0.05 | 2.5 | 1.9 | 0.027 | 1.1 | 0.1 |

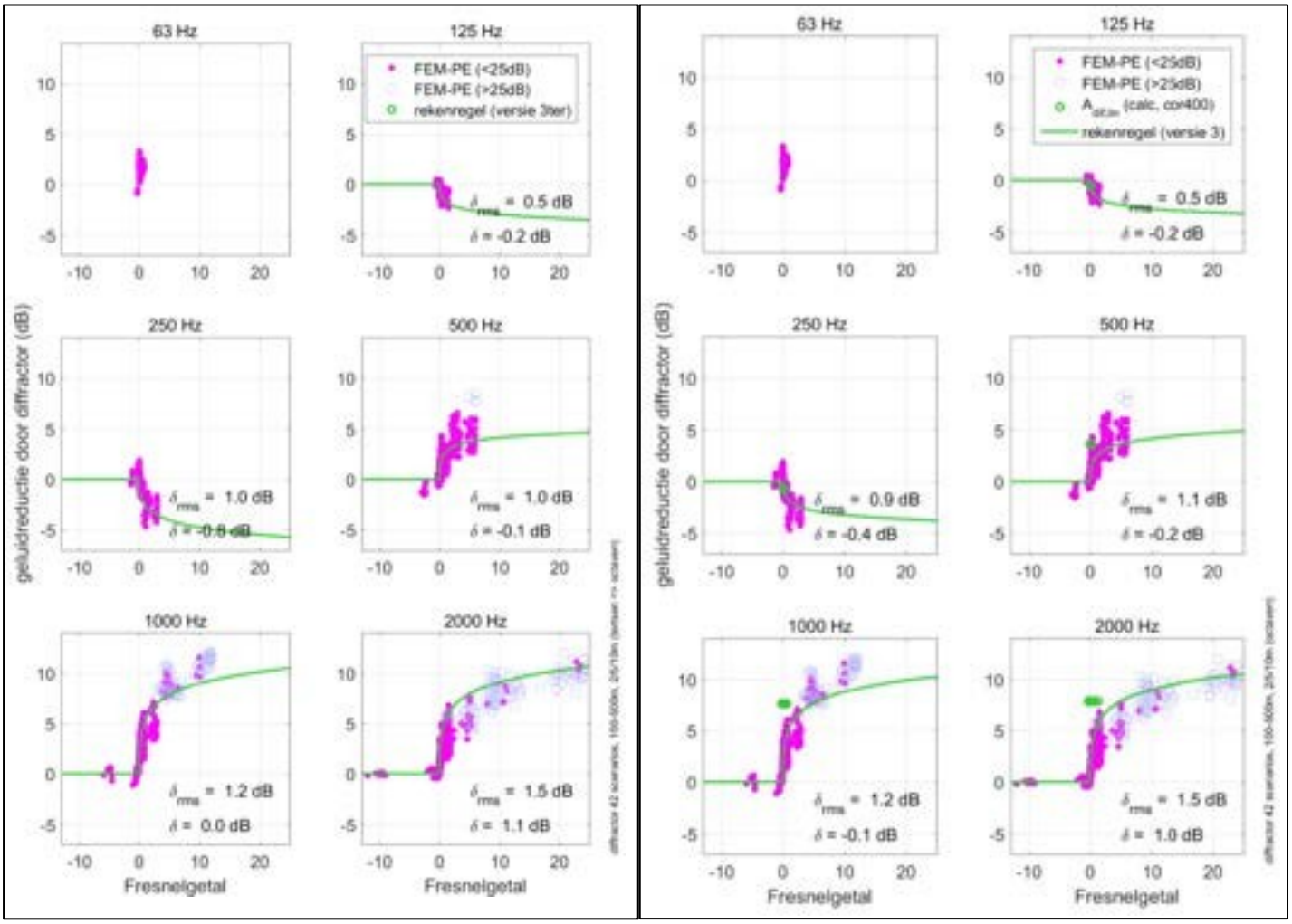


Figure F.7 FEM-PE versus calculation rule for the original diffractor, in octaves, with receiver heights 2, 5, 10 m, and fixed coefficients F of 0.2 and 0.05. Left: computational rule applied at the third-band level and then converted to . Right: directly in octaves.

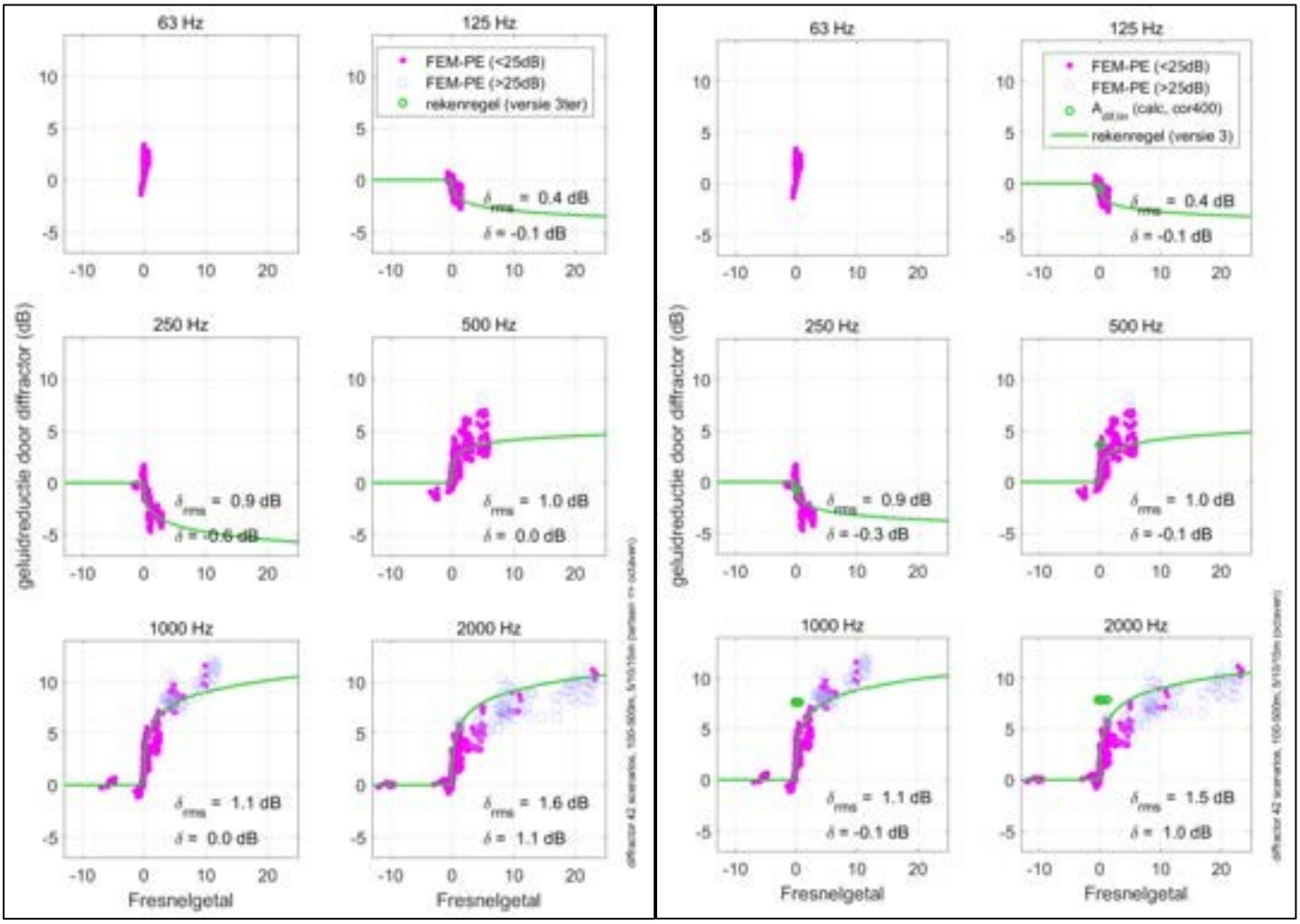


Figure F.8 As Figure F.7, for receiver heights 5, 10, 15 m.

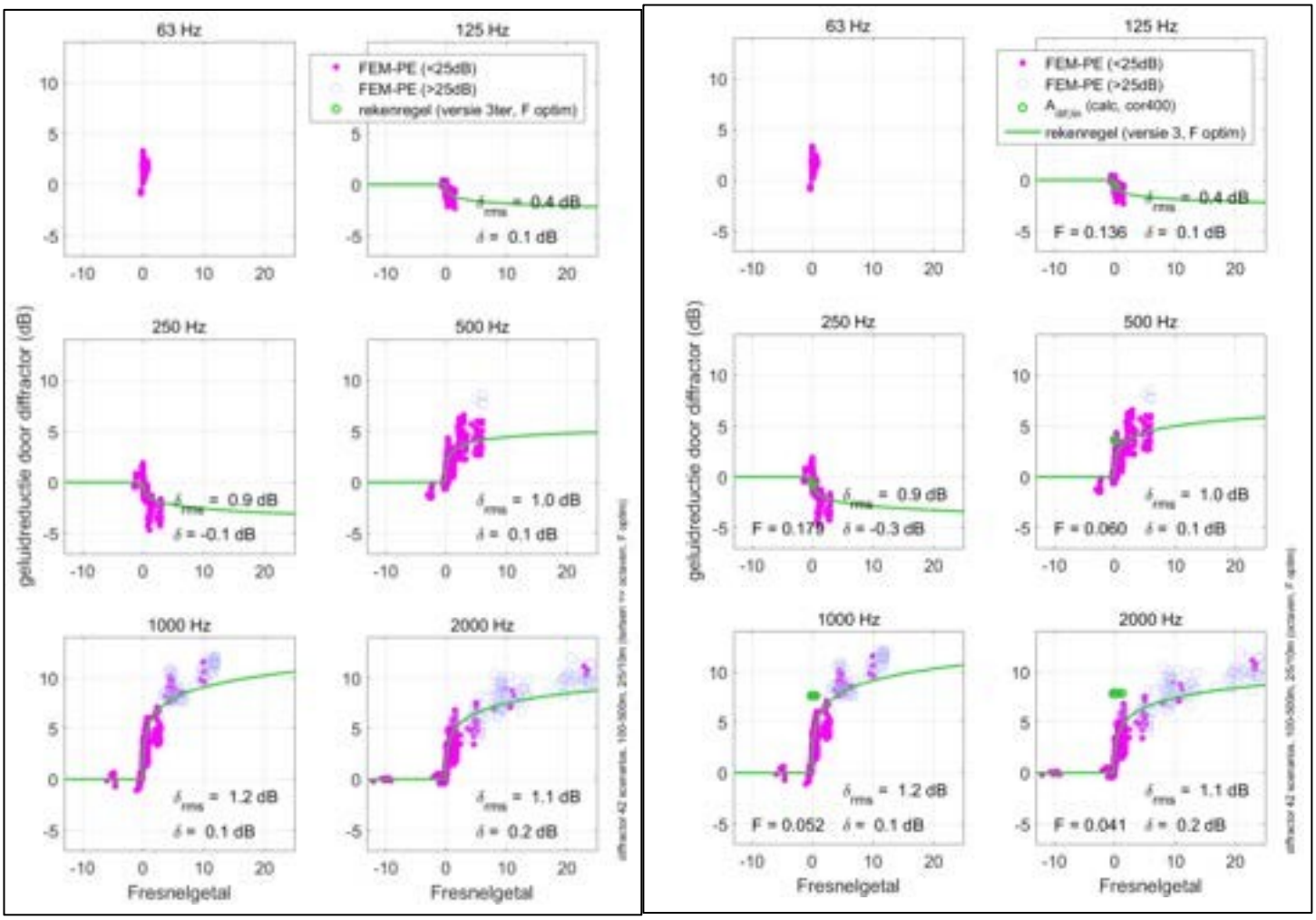


Figure F.9 As Figure F.7, with optimization of F.

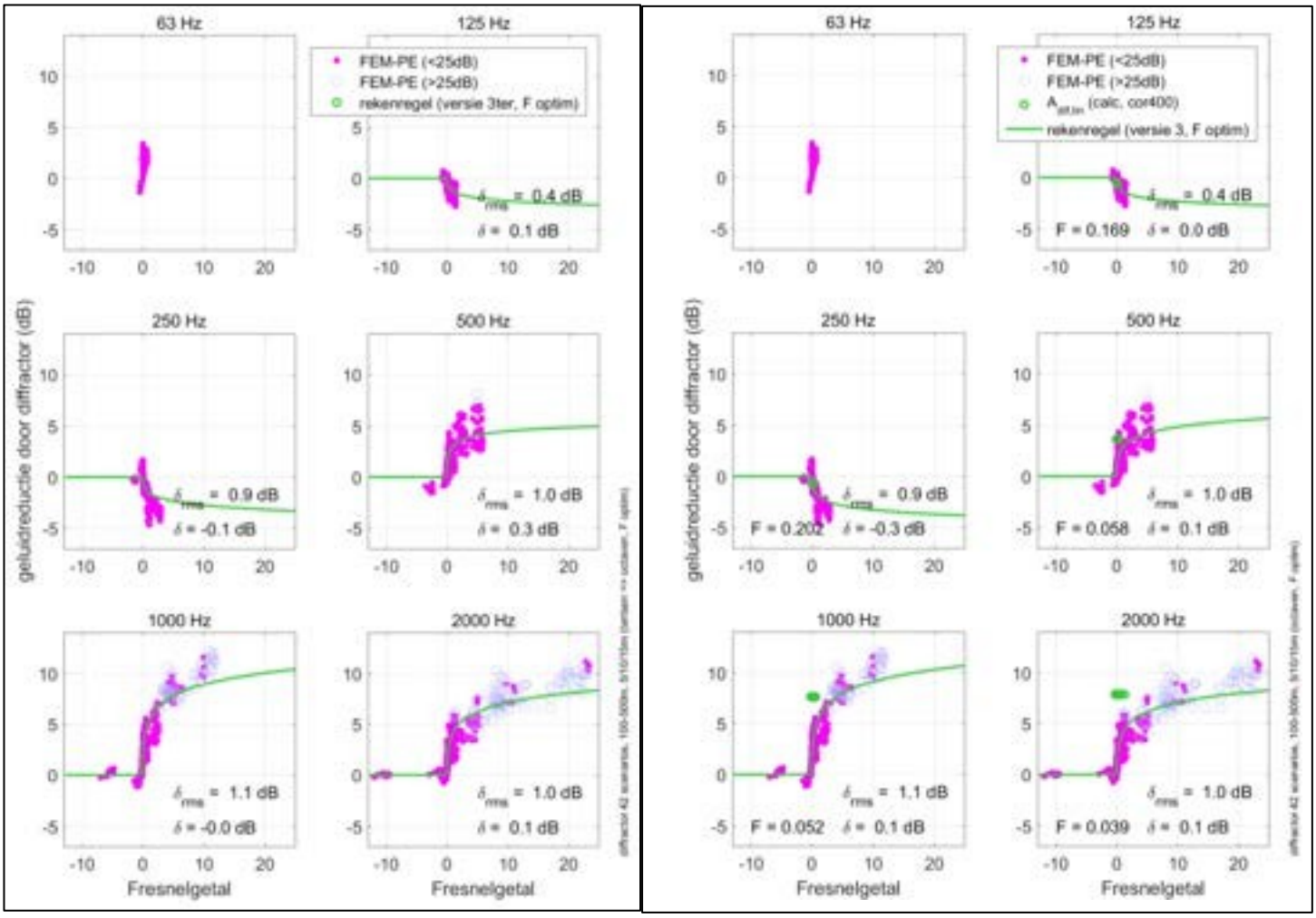


Figure F.10 As Figure F.8, with optimization of F.

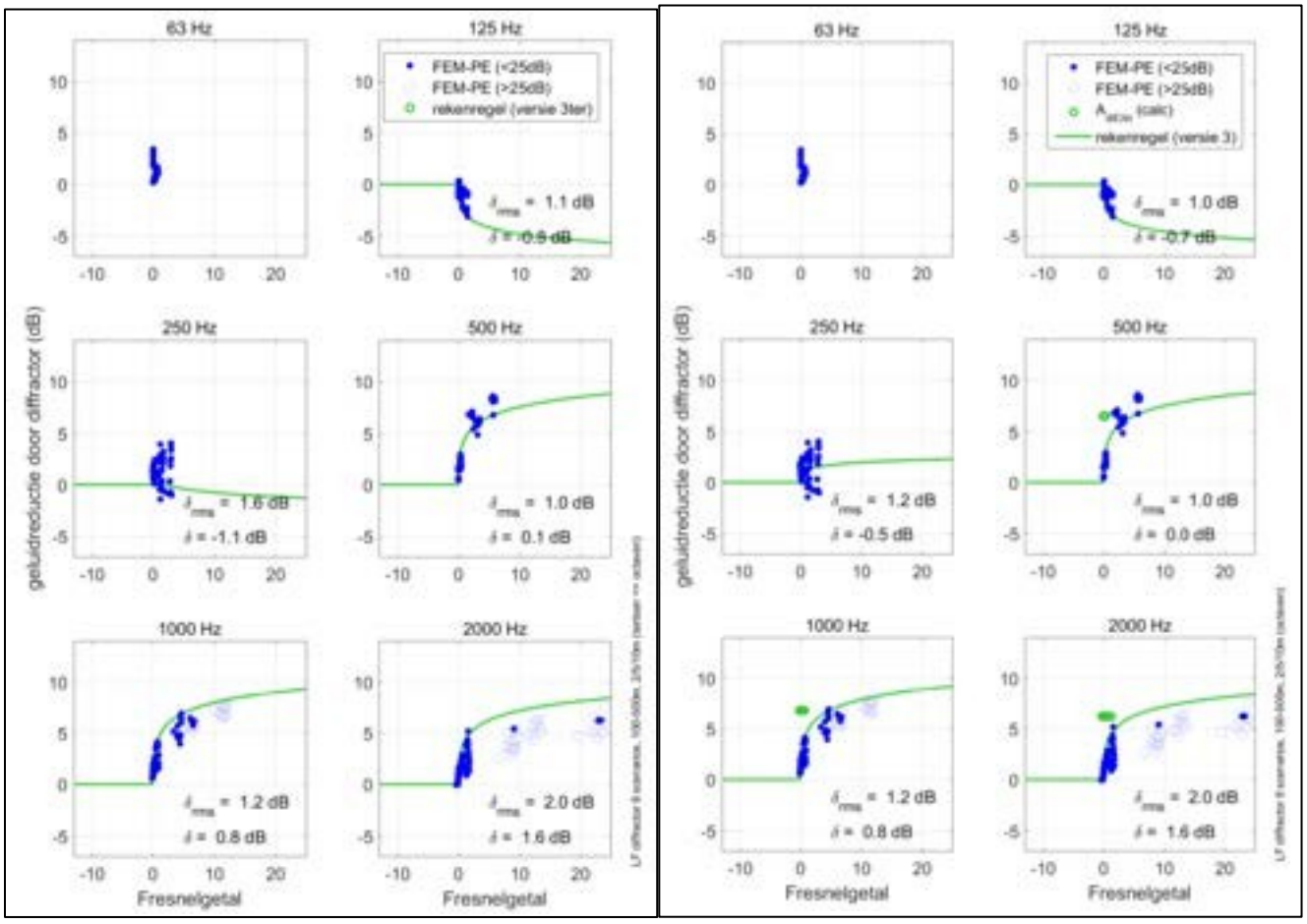


Figure F.11 FEM-PE versus computational rule for the LF diffractor, in octaves, with receiver heights 2, 5, 10 m, and fixed coefficients F of 0.2 and 0.05. Left: computational rule applied at the third-band level and then converted to octaves. Right: directly in octaves.

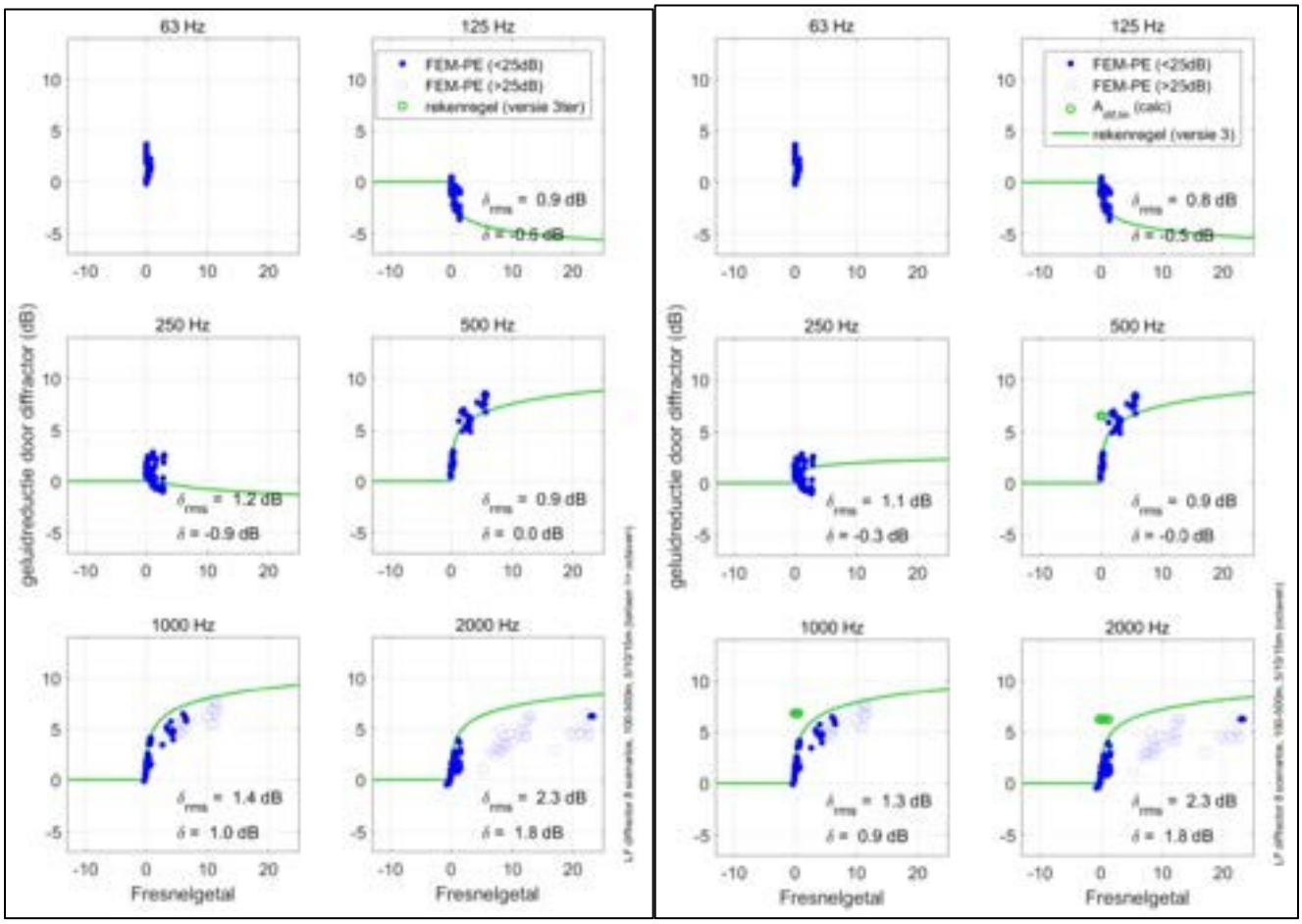


Figure F.12 As Figure F.11, for receiver heights 5, 10, 15 m.

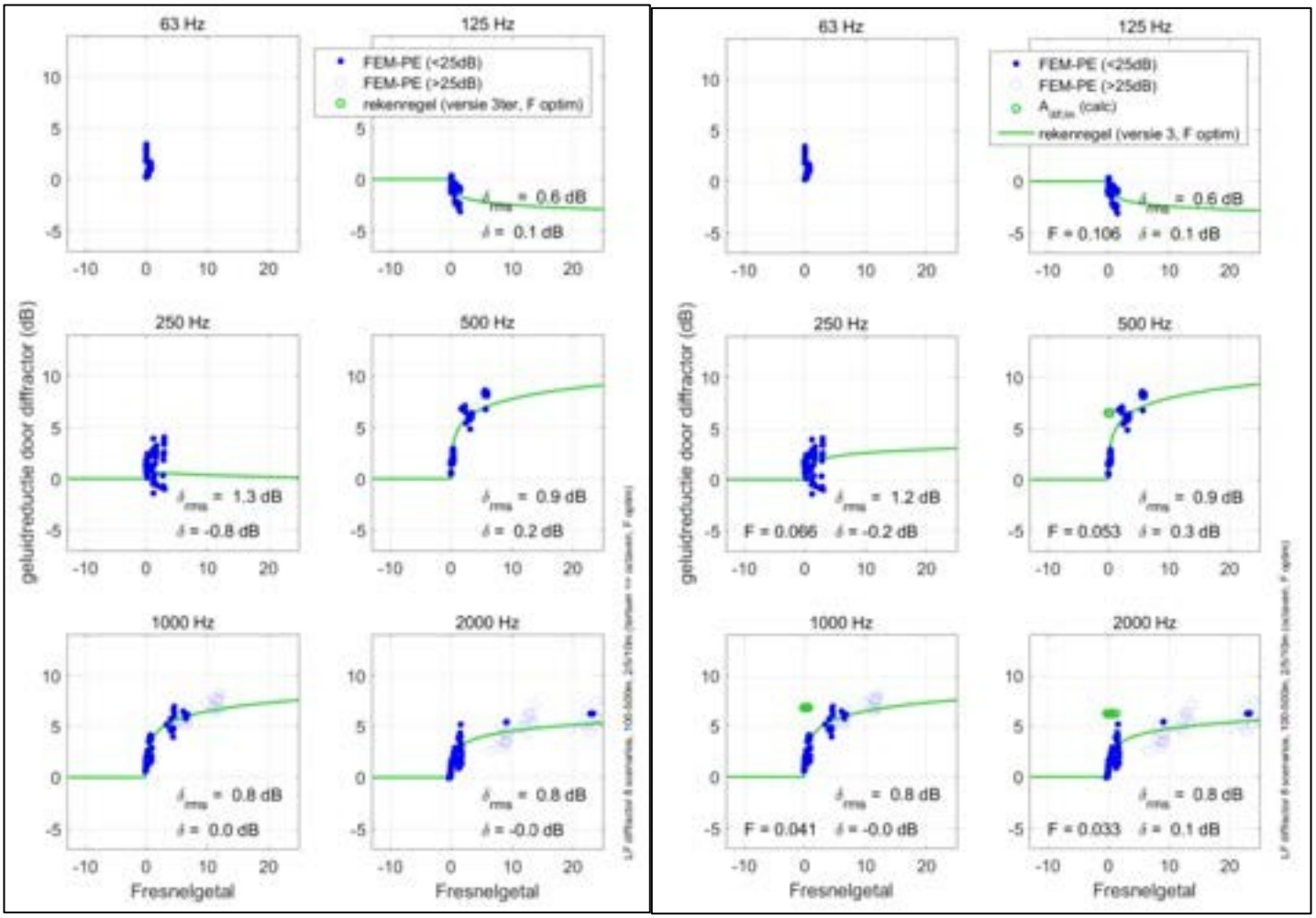


Figure F.13 As Figure F.11, with optimization of F.

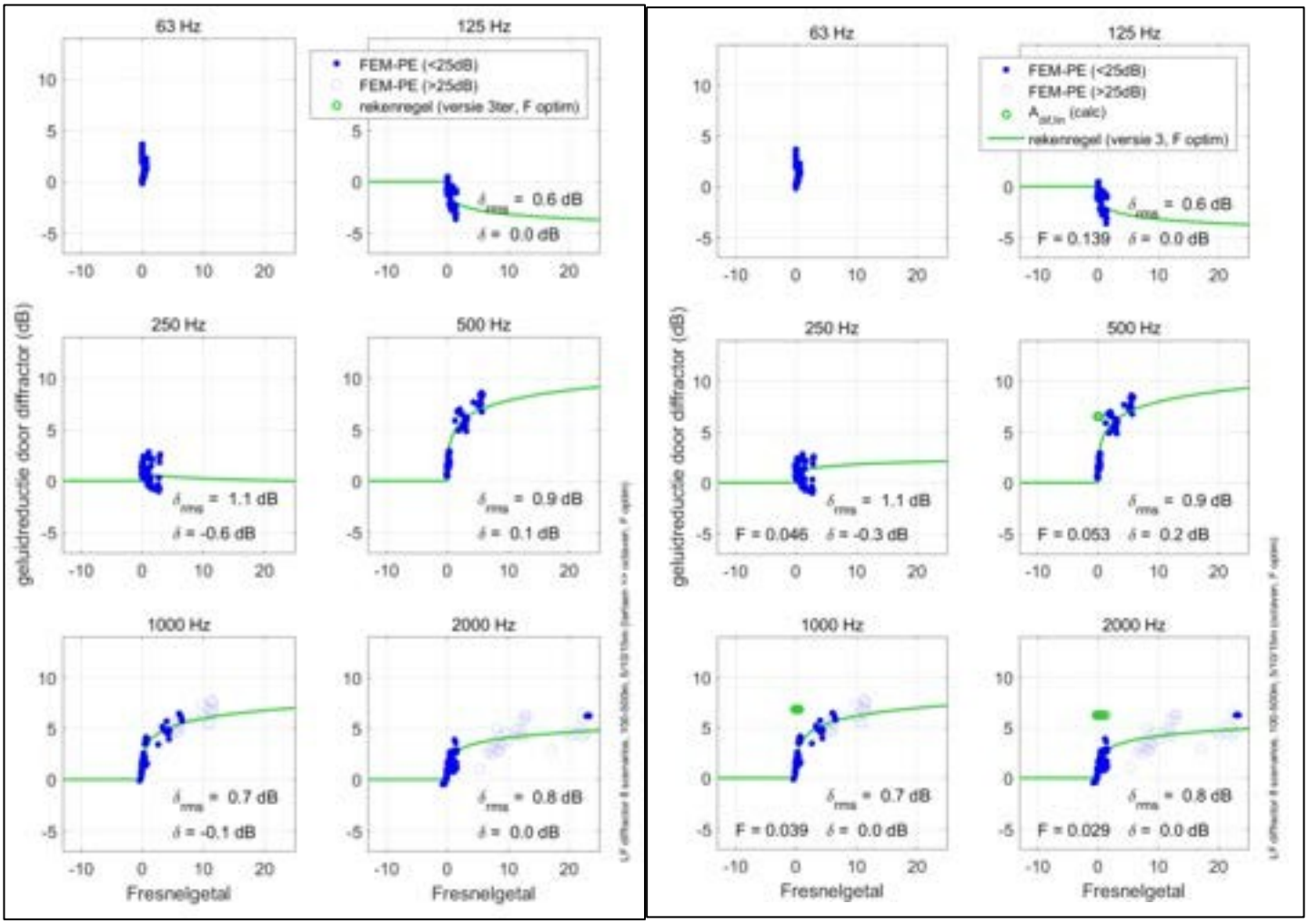


Figure F.14 As Figure F.12, with optimization of F.

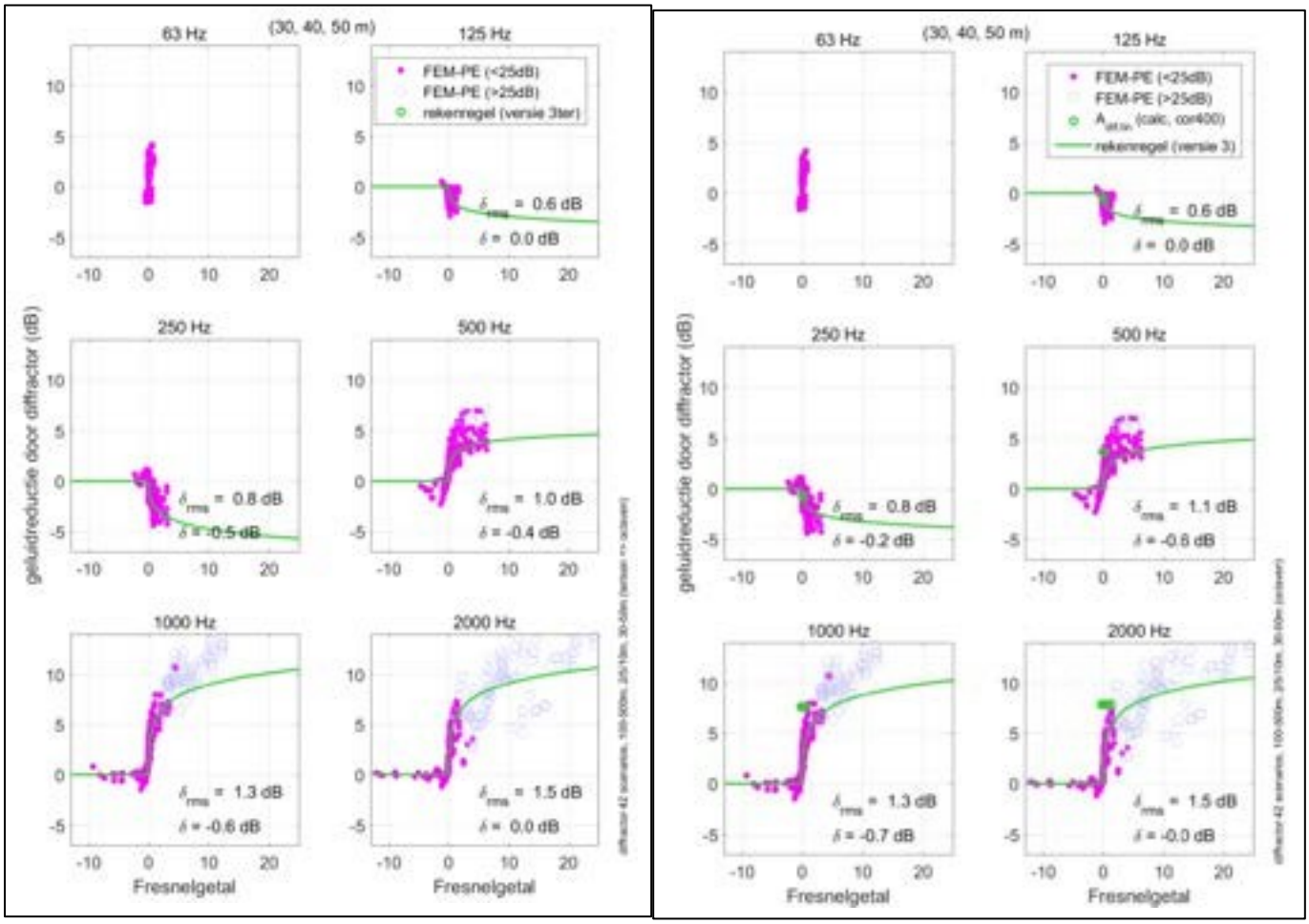


Figure F.15 As Figure F.7, for receivers at distances 30-50 m instead of 100-500 m.

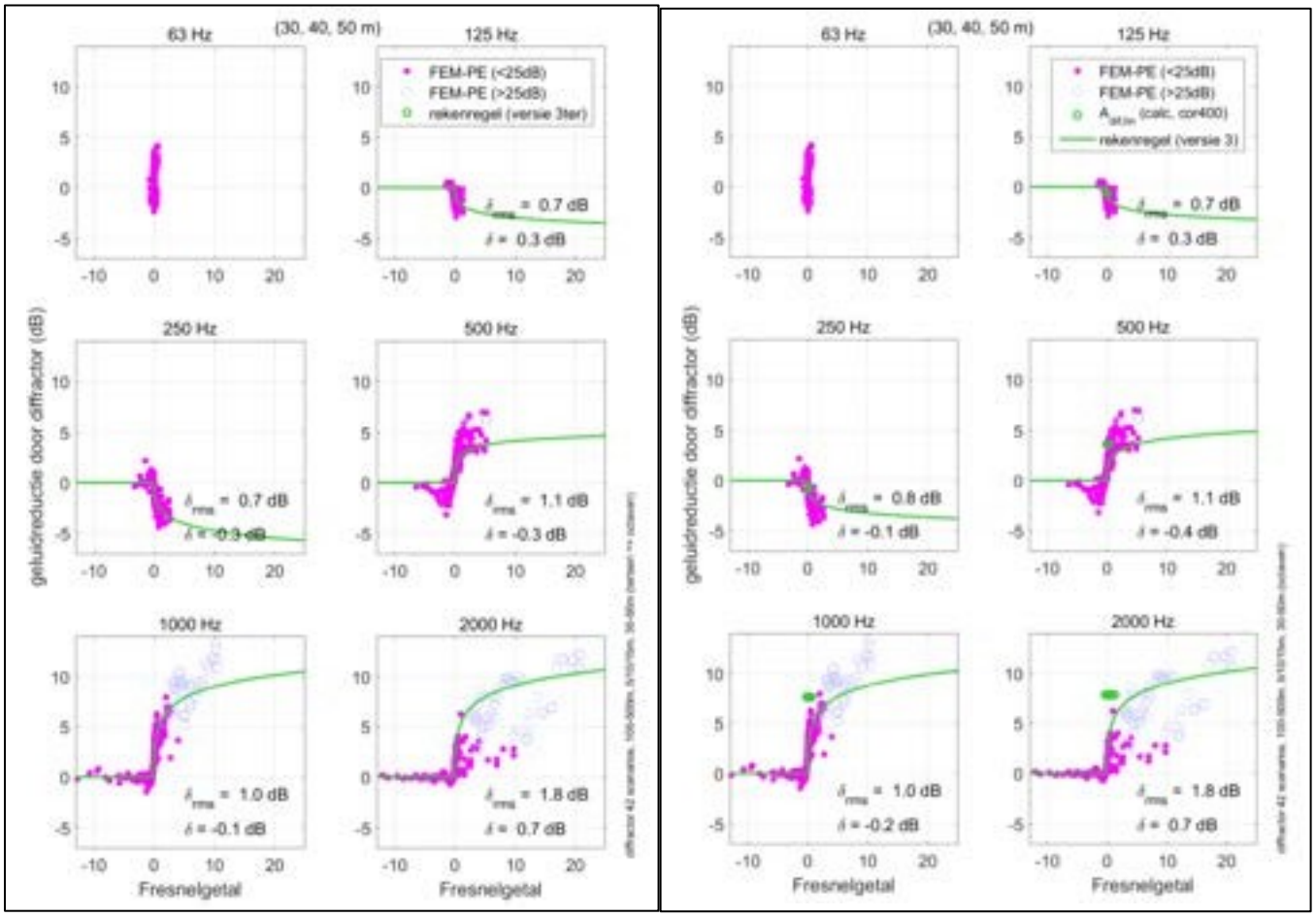


Figure F.16 As Figure F.8, for receivers at distances 30-50 m instead of 100-500 m.

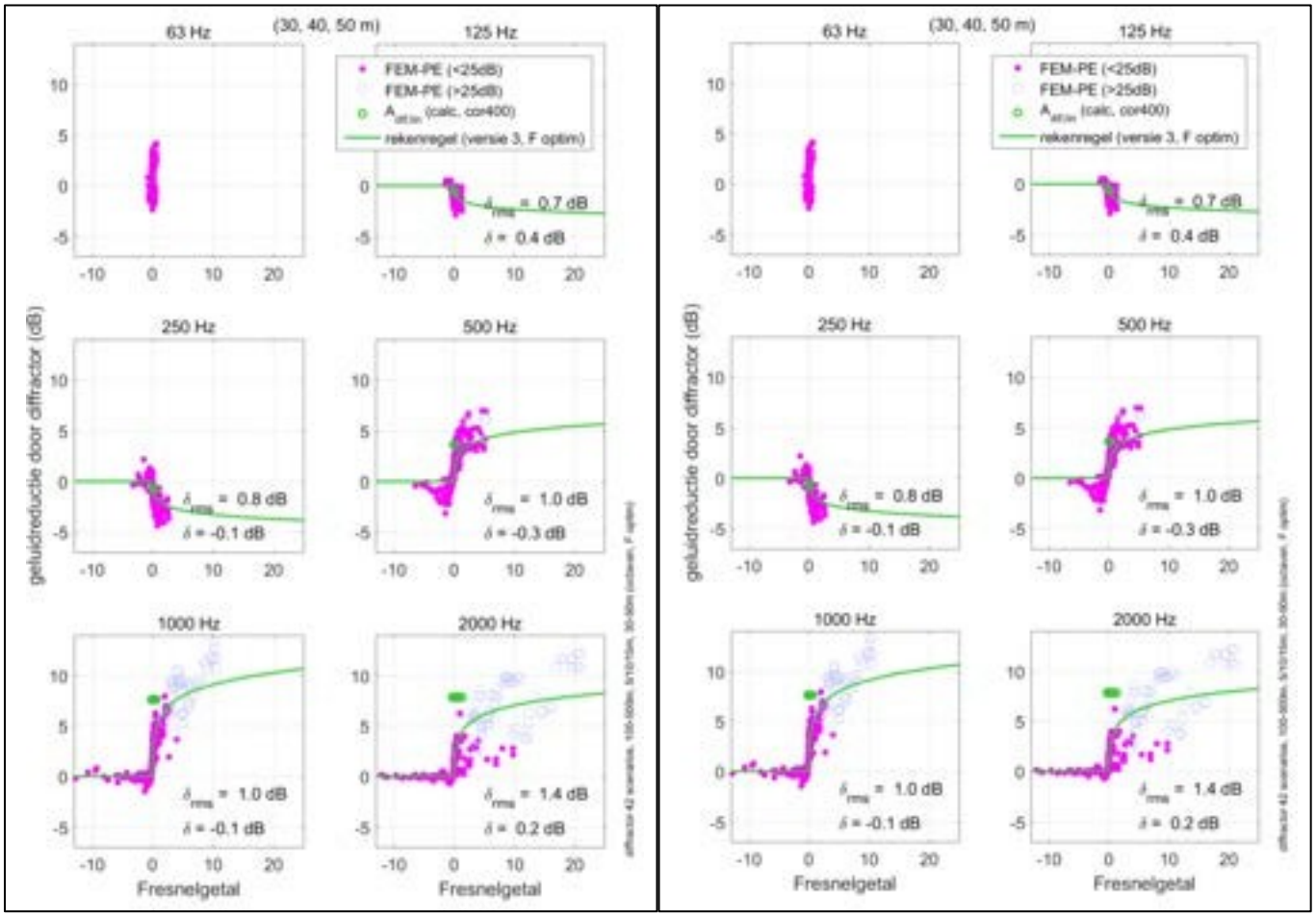


Figure F.17 As Figure F.9, for receivers at distances 30-50 m instead of 100-500 m.

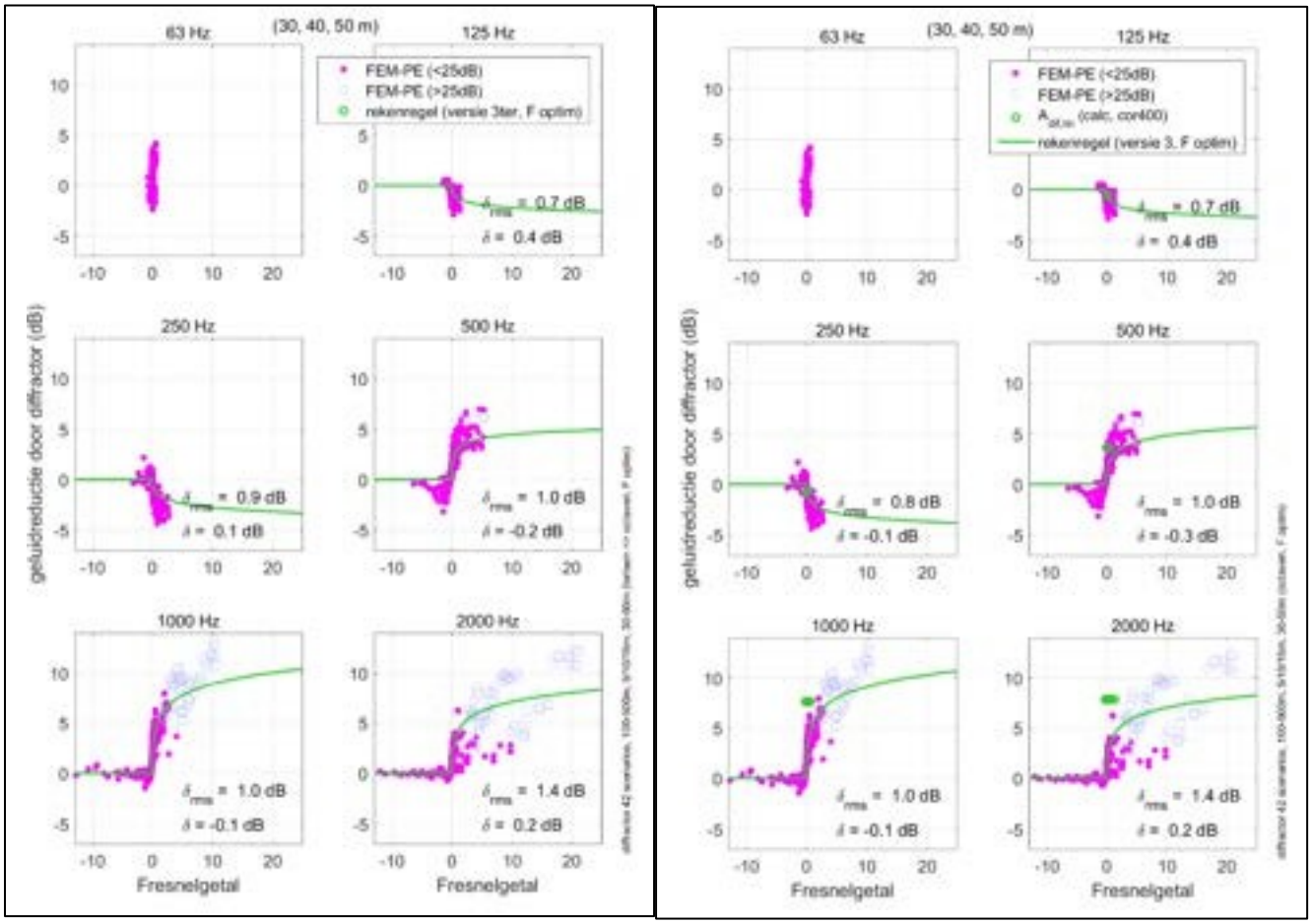


Figure F.18 As Figure F.10, for receivers at distances 30-50 m instead of 100-500 m.

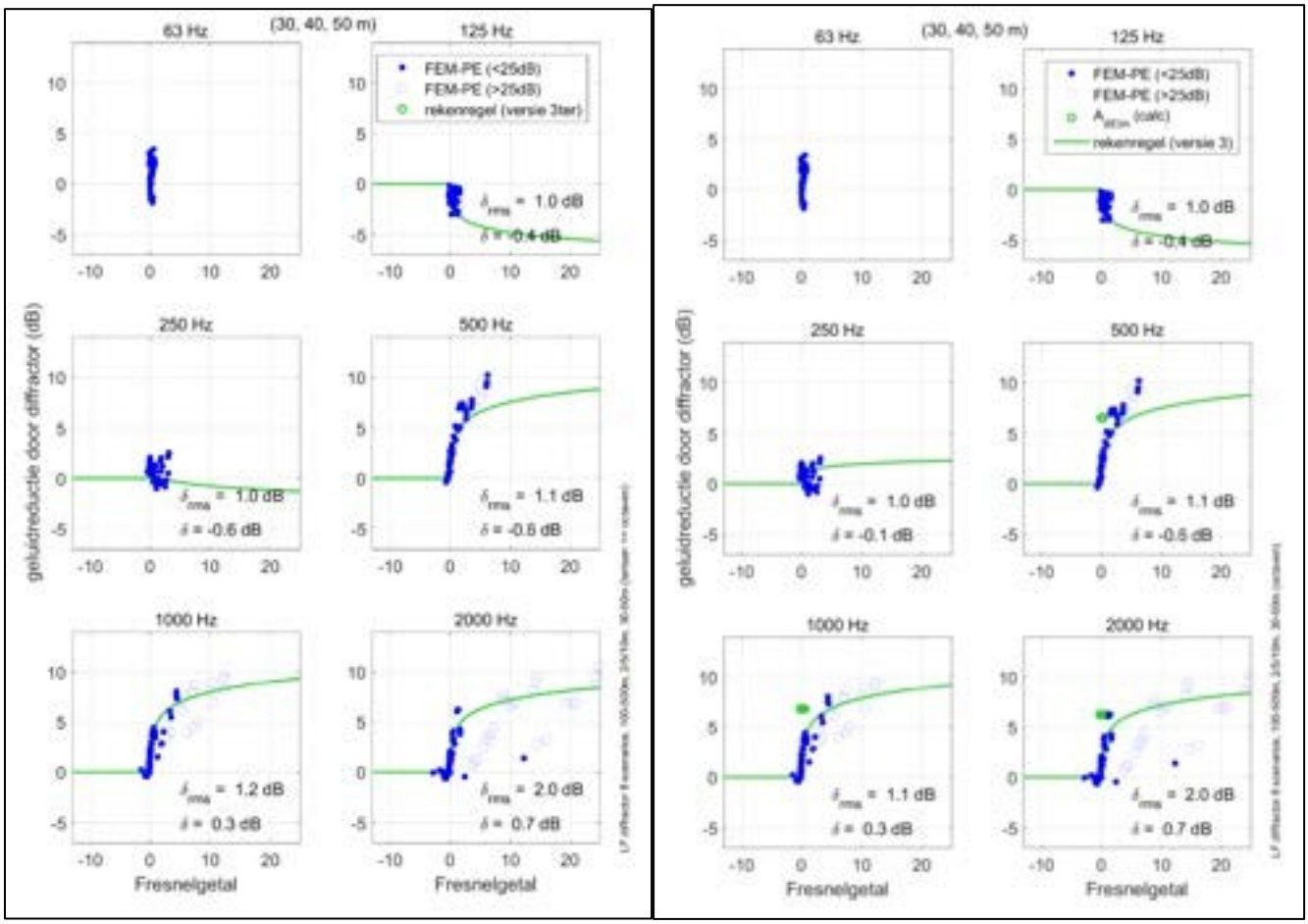


Figure F.19 As Figure F.11, for receivers at distances 30-50 m instead of 100-500 m.

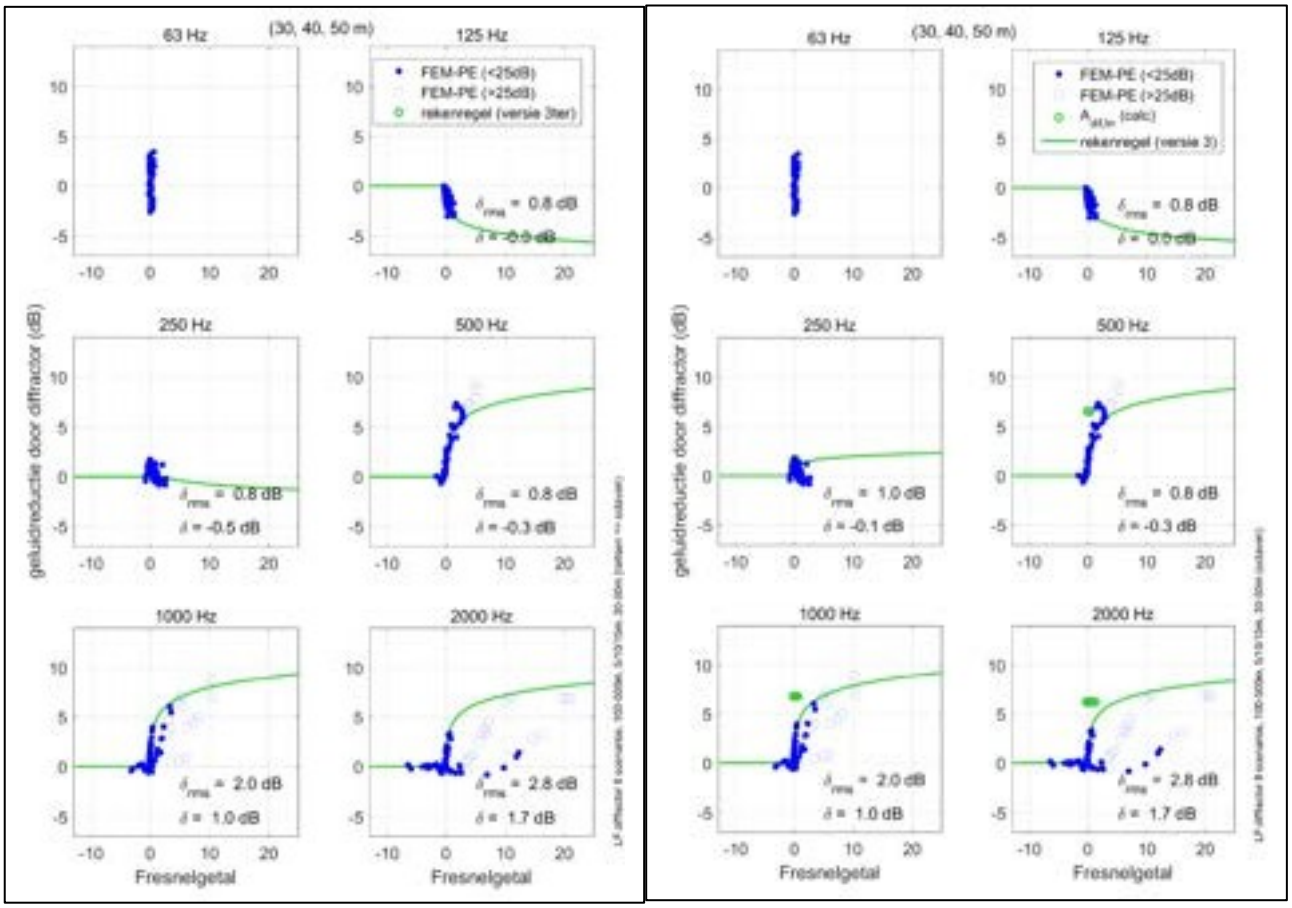


Figure F.20 As Figure F.12, for receivers at distances 30-50 m instead of 100-500 m.

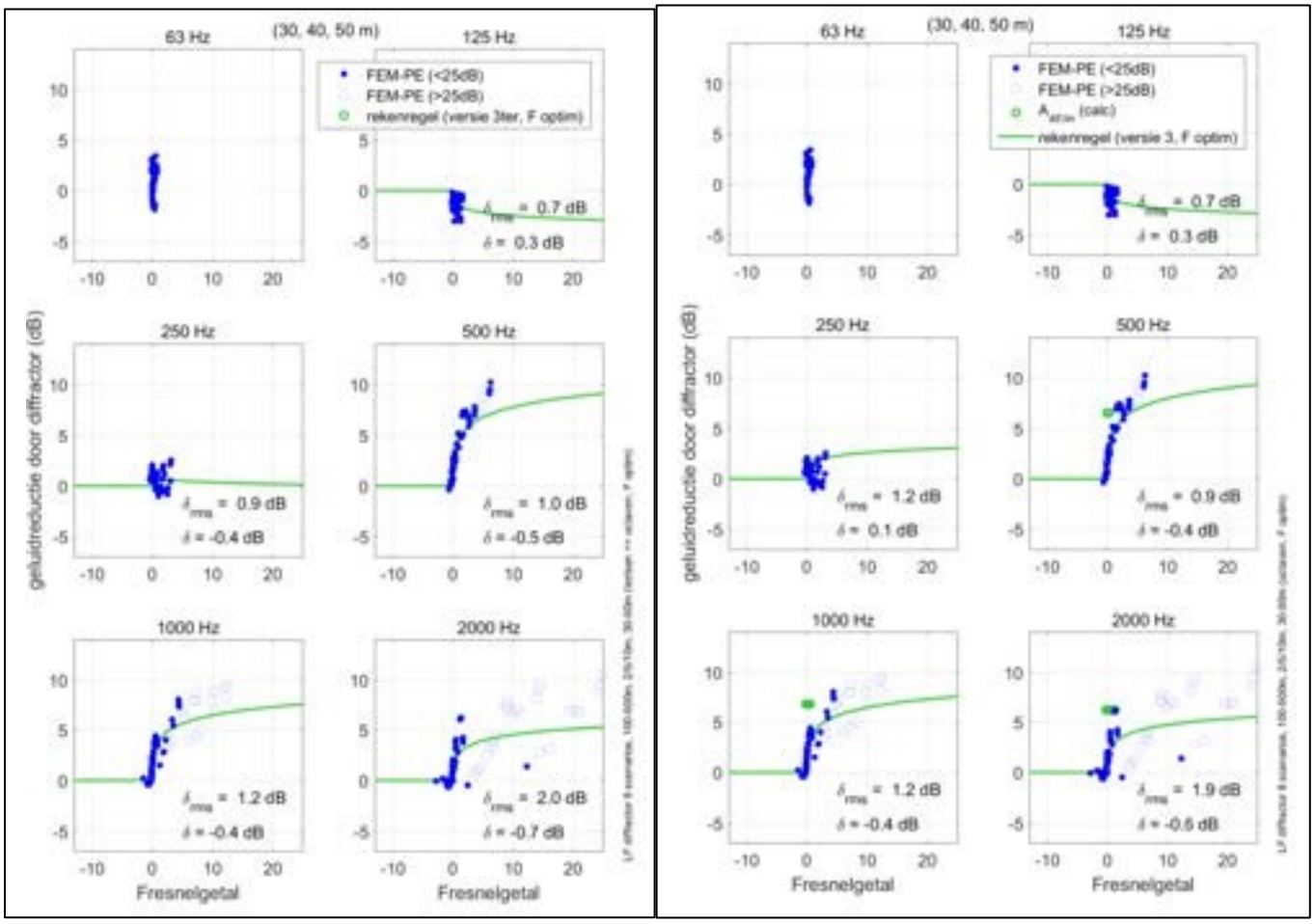


Figure F.21 As Figure F.13, for receivers at distances 30-50 m instead of 100-500 m.

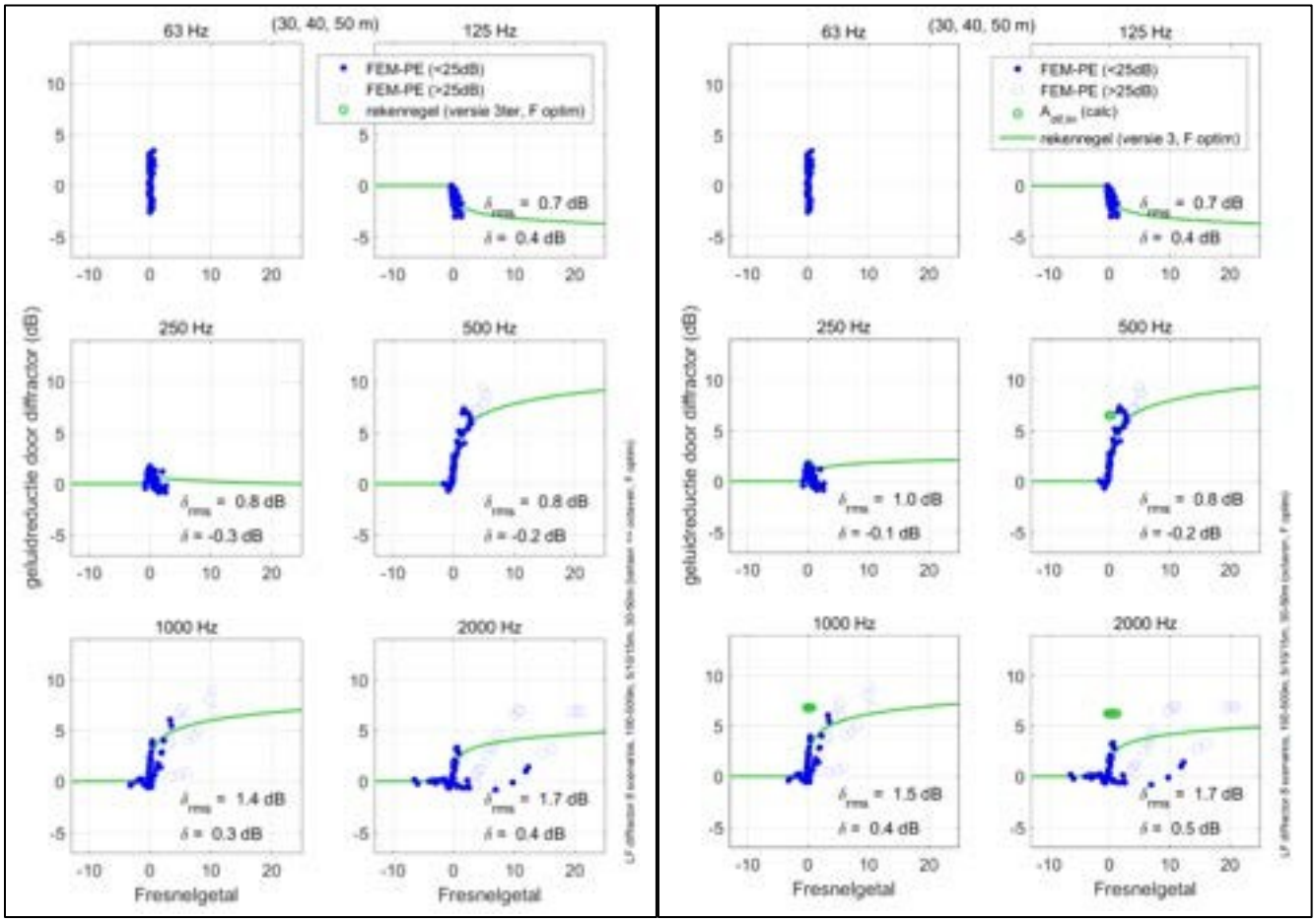


Figure F.22 As Figure F.14, for receivers at distances 30-50 m instead of 100-500 m.